Seismic Behaviour of Existing Reinforced Concrete Buildings with Thin Walls

(Final report for *Stiftung zur Förderung der Denkmalpflege*, Zürich)

João Pacheco de Almeida

Postdoctoral Researcher
Earthquake Engineering and Structural Dynamics (EESD)
École Polytechnique Fédérale de Lausanne (EPFL)

Katrin Beyer

Assistenzprofessorin
Leiterin der Gruppe Earthquake Engineering and Structural Dynamics (EESD)
École Polytechnique Fédérale de Lausanne (EPFL)

Lausanne, September 2014

Preface

The seismic assessment of an existing structure calls for a deep understanding of the type of failure mechanisms that can influence the behaviour of the building. The project that is presented in this report addresses the seismic behaviour of reinforced concrete wall buildings that were constructed 1950-1970 in Switzerland. A number of these buildings belong to the Swiss cultural heritage. For such valued structures seismic retrofit interventions need often be kept to an absolute minimum. The project aims therefore at understanding the performance of these structures in their original state through large-scale testing and at exploring advanced computer simulation procedures to predict their seismic response. Findings of these tests and recommendations for the analysis of such buildings are described in detail in chapter 2 and 3 of the report and summarised in chapter 4.

Katrin Beyer, Lausanne, September 2014

Table of Contents

1. MOTIVATION AND FRAMEWORK

1.1. Introduction

The goal of this project is to investigate experimentally and numerically the deficiencies in the seismic behaviour of a building typology that was constructed in Switzerland until the 1970s without consideration for earthquake loads: reinforced concrete (RC) structures with thin walls. The latter were commonly used for apartment buildings but can also be found in special-purpose facilities which are now part of the Swiss cultural heritage, e.g. the theatre of Basel.

Earthquake damage is often associated to a life safety hazard in countries of high seismicity – such as New Zealand, Japan, California, and Chile. However, also in regions of low to moderate seismicity seismic risks related to economic, social and cultural/heritage impairment can be very harmful in the long term. In Switzerland, which is precisely known on a global scale as having a low to moderate seismicity, the Federal Office for the Environment (FOEN) estimates that earthquakes account for about half of all risks due to natural hazards (BABS, 2004). The seismic risk is not only dependent on the frequency and magnitude of earthquakes, but also on the vulnerability of the exposed structures and their content, as it will be discussed hereinafter. Such content includes the non-structural components of the building, as well as their occupants.

Literature review (Steinmann, 1974) and consultation of existing archives (ACM, 2013; AVL, 2013) show that, even before the appearance of the first national seismic regulations, Swiss engineers were concerned with the influence of the seismic loads in the performance of man-made structures. As a matter of fact, it is documented that, for very few special or important structures, experimental techniques were sought (see Figure 1) in order to supplement the very limited knowledge on the nonlinear behaviour of buildings with the aim of getting additional insight into the behaviour of the structure during earthquake loads. Unfortunately, only in very particular cases was the earthquake action considered, and always with a high degree of approximation.

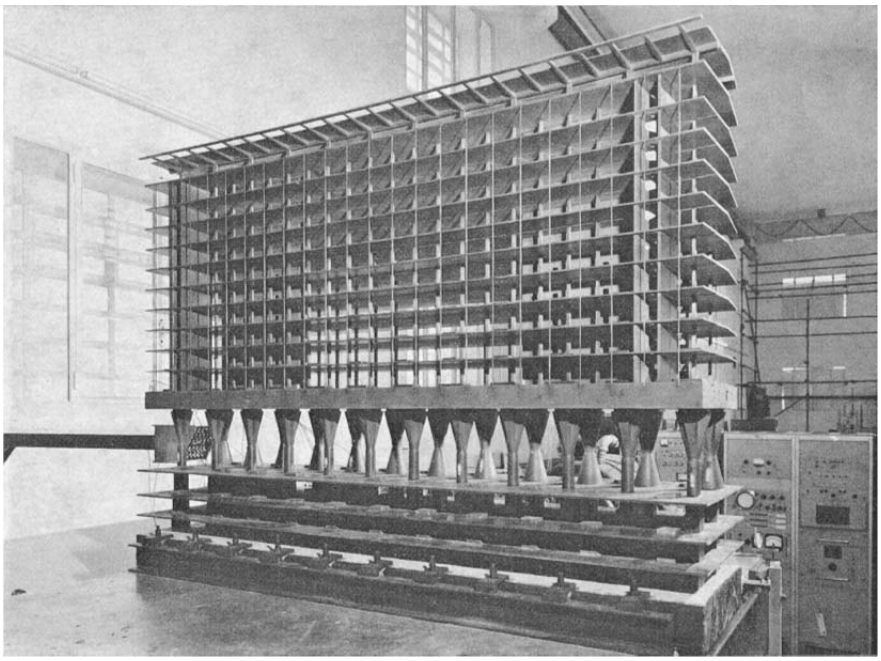

Figure 1. Model in synthetic resin at scale 1:40 of the *Bureau International du Travail*, built to study the effects of the seismic action (Steinmann, 1974).

In Switzerland, first seismic loads were introduced in the design standard in 1970 but at this time seismic loads were defined as a fixed fraction of the selfweight, which varied between 2-5% (Wenk, 2008). Modern earthquake standards were first introduced in 1989and capacity design principles in 2003. Therefore, buildings from the 1950s-1970s (which are targeted in the present study) were not designed for earthquake loading. The only horizontal forces considered in the design calculations were hence the wind forces, which for many residential buildings represent but a fraction of present prescribed seismic forces (Wenk, 2008). This non-compliance with today's regulations needs to be addressed in the risk assessment framework that was developed by Kölz and Schneider (2005) as it will be the basis of the new seismic code for existing structures (SIA 269/8, 2014; Wenk, 2014). In particular, monuments deserve special attention for reasons of historical preservation, and also because their architectural design often brings them closer to the limits of construction engineering (BABS, 2004), making them potentially more vulnerable to damage from earthquakes.

1.2. Seismic Risk and National Maps

The natural *risk* of a region is the product of a number of factors: (i) *hazard*, the natural phenomenon – such as earthquakes – that has potential to cause harm and which remains constant throughout time in the same region, (ii) *exposed value*, and (iii) *vulnerability*:

$$\textit{Seismic risk} = \textit{Hazard} \times \textit{Earthquake exposed value} \times \textit{Vulnerability}$$

The only variable that can be controlled without compromising on the society's standards is the *vulnerability*. A reduction of the vulnerability with a limited amount of resources requires a well-planned management process. How do the current national standards tackle this? Figure 2 shows the seismic hazard zones defined for the Confederation (Zone Z3b being the most critical) according to the Swiss code SIA 261 (Société Suisse des Ingénieurs et des Architectes, 2003). The importance of the structure is considered by a coefficient on the seismic loads that varies between 1.0 (class I, regular buildings) and 1.4 (class III, crucial facilities or those representing a potentially important danger for the environment). The risk-based framework for the retrofit of existing structures will be provided in SIA 269/8 (2014). A framework for cultural heritage structures is currently developed (Wenk and Beyer, 2014).

1.3. The Role of RC Walls in Swiss Construction

The historical role of reinforced concrete in the evolution of Swiss construction practices, architecture, and culture, is indelible. Reinforced concrete constructions spread faster in Switzerland than in any other country thanks to structural engineer Wilhelm Ritter (1847-1906) and businessmen like Edmund Züblin and Robert Maillart (1872-1940). The latter, in particular, revolutionized the use of structural RC with designs such as beamless floor slabs, mushroom ceilings for industrial buildings, bridges with three-hinged combining deck and arch ribs, etc.

From the end of the 40s until the 1973 oil crisis – i.e., during "the glorious thirty [years]" (*Trente Glorieuses*, as the French economist Jean Fourastié named them), the soar in construction is dominated by an elated feeling of confidence in the future, spurred by the full employment status (Hebdo, 2007). The speedy increase in population became a real challenge: additional 700 000 inhabitants during the 50s, and 900 000 in the following decade (Hebdo, 2007). Such state of affairs pushed the development of cities and the construction of satellite towns; for example, in Lignon (Genève), housing for 10 000 people was constructed all at once, which represents an unimaginable scenario nowadays (Hebdo, 2007).

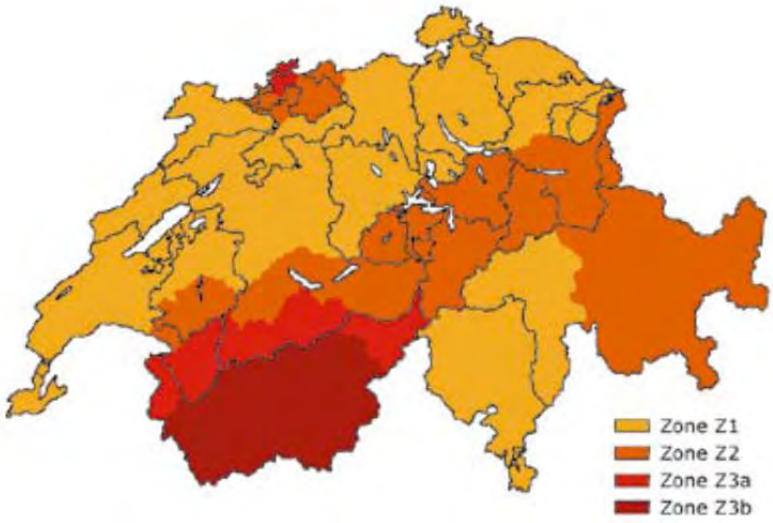

Figure 2. 'Seismic risk' (*seismic hazard*) zones according to SIA 261 (Société Suisse des Ingénieurs et des Architectes, 2003).

It is therefore apparent that reinforced concrete has accompanied and fuelled the boom of national housing stock, which has roughly doubled during the XX century (Marchand et al., 2012); a significant part of these RC constructions make use of thin walls (thickness up to 20 cm) as the backbone of the structure (Allenspach, 1999), which justifies the fundamental interest in their assessment.

The global lateral (seismic) strength of RC wall buildings depends primarily on the resistance of those vertical members, which can be used either as stand-alone elements, coupled with spandrel members, or combined in order to form more complex shapes accommodating elevators or staircases. RC walls are frequently used to brace mid- to high-rise buildings against earthquakes. They are often preferred to frames since they tend to lead to smaller inter-storey drifts and therefore smaller non-structural damage.

The research work carried out by the authors to characterize thin RC walls in Swiss construction practice involved: (i) review of existing literature, (ii) personal interaction with experienced researchers and practitioners[1], (iii) consultation of libraries, institutes, and archives (ACM, 2013; AVL, 2013) regarding the construction practice between 1950 and 1970[2], and (iv) examination of construction drawings and blueprints of a number of projects, obtained from different sources (*fonds d'architects*, professors, practitioners, etc).

Overall, the analysed buildings showed a rather strong regularity regarding geometry and detailing of thin shear walls. This observation is backed up by observations from other sources (Greifenhagen & Lestuzzi, 2005; Greifenhagen, Papas, & Lestuzzi, 2005; Greifenhagen, 2006; Peter, 2000). The uniformness concerns the wall thicknesses (between 15 and 20 cm), longitudinal/transversal reinforcement ratios (roughly between 0.3 and 0.8%), and detailing (uniformly distributed, with transversal stirrups placed on the inside of longitudinal rebars). Wall lengths were typically very large, between 4 m and 9 m, while the concrete cover was quite thin, as low as 10 mm. All walls feature lap splices at the wall base. The current code forbids lap splices in ductile walls, but for many decades the construction practice was to execute lap splices using lengths of only around 30-35 times the diameter (Lestuzzi, 2013; personal communication). This calls for an assessment of the lap splice length on the seismic behaviour.

[1] The authors are grateful for the continuous assistance of Dr. Thomas Wenk and Dr. Pierino Lestuzzi.
[2] In particular, the assistance of Mme Joëlle Feihl and M. Jean-Daniel Chavan is acknowledged.

The aforementioned remarkable similarity of Swiss design and detailing practices which can be found amongst distinct projects of thin RC wall buildings reflects, to a certain extent, the substantial protection that has been granted to Swiss architects and engineers in their own country. As a matter of fact, only in the last years of the XX century have foreign architects started to be invited to participate in Swiss project calls. The exception has been, for a long time, the building blocks in Lucerne-Schönbühl (1965-68) designed by Finnish architect Alvar Aalto (Allenspach, 1999). The observed regularity in construction practices of thin RC wall structures in Switzerland greatly facilitates the design and detailing of the test specimens used for the present study, as well as the general validity of the conclusions herein obtained, as it will be discussed in Chapter 2.

1.4. Performance of Thin RC Walls in Recent Earthquakes

Historically, the seismic performance of structural wall buildings has been regarded as generally good (Priestley, Calvi, & Kowalsky, 2007), since complete collapse under even extreme seismic excitation remained rare. However, a series of recent earthquakes have cast a new light on the actual behaviour of wall buildings, in particular slender wall structures.

The large earthquakes in Chile (2010) and New Zealand (2011) revealed new types of failure mechanisms in RC walls that were subjected to large axial load ratios (Figure 3), namely bending-compression failures. The corresponding mechanism of collapse is at present poorly understood and not addressed in seismic design codes. The authors think that it could be related with the reduction of the compressive strength of the wall due to stress concentration from bending crack offsets resulting from the application of cyclic (seismic) loading. This failure takes place at the wall boundary and is potentially dangerous for walls subjected to large axial forces, i.e. typically in multi-storey buildings. Missing stirrups will favour this type of collapse mechanism (photo on the right side of Figure 3).

Thin RC walls are also prone to other modes of failure, namely out-of-plane buckling, see Figure 4 (a). The mechanics of this phenomenon can be summarised as follows, for a wall with double layer reinforcement. At large in-plane curvature demands, the wall edge region develops large tensile strains that cause wide near-horizontal cracks across the width of the section. That leads to longitudinal reinforcement yielding in tension and eventual strain-hardening. Upon unloading, an elastic strain recovery takes place, although the cracks remain wide due to the plastic tensile strains previously accumulated in the rebars. During reloading in compression, and until crack closure, the compression force must be resisted solely by the two layers of vertical reinforcement. This stage is typically accompanied by an incipient out-of-plane displacement, which occurs due to an unavoidable eccentricity of the axial force C acting in this region, and construction misalignments in the position of the longitudinal reinforcements – see Figure 4 (b). While the rebars retain their significant axial stiffness before yielding in compression, the out-of-plane displacement tends to remain small. However, as compression increases the longitudinal rebar near the concave side will yield, originating an abrupt reduction in stiffness and a consequent increase in the out-of-plane displacement. It is noted that, at this point, the second layer of longitudinal reinforcement—which has not yet yielded in compression—is the main source of out-of-plane stiffness. Depending on the magnitude of the tensile strain previously attained (i.e., before unloading), different scenarios can then take place as compression progresses. The cracks may close, re-establishing compressive concrete contact, or they may remain open leading to compression yielding of the second layer of reinforcement. In the latter case, out-of-plane displacements will abruptly increase, leading to wall buckling failure. Intermediate conditions, wherein the second layer of reinforcement yields but cracks still close, at least partially, are also possible.

Figure 3. Poor performance of structural walls during the 2010 Chile Earthquake.

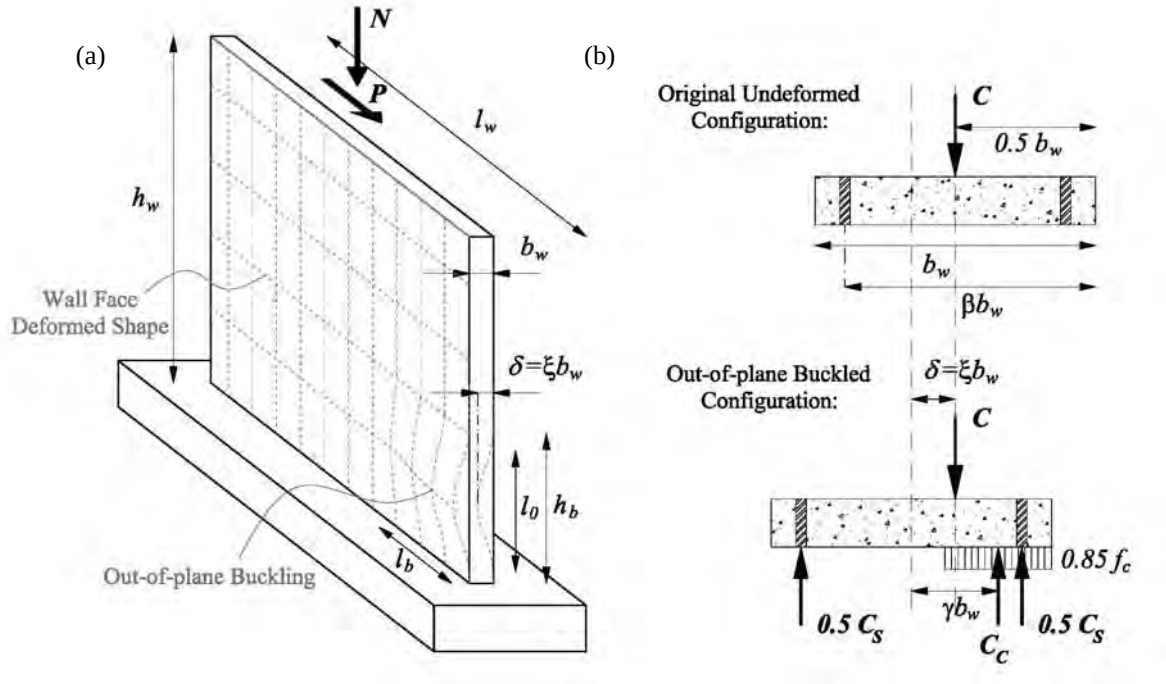

Figure 4. (a) Geometrical characteristics of the wall and out-of-plane buckling; (b) Equilibrium of external and internal forces at mid-height of the buckling region, adapted from Paulay & Priestley (1993).

Figure 5. Out-of-plane bucking of walls during the 2011 New Zealand Earthquake (from Sritharan et al. (2014)).

Independently of the scenario that effectively takes place, the occurrence of out-of-plane displacements and second-order moments will affect the in-plane wall response and should therefore be taken into account. Field observations from recent earthquakes (Sritharan et al., 2014) have concluded that this phenomenon has contributed to the failure of structural wall members, as depicted in Figure 5.

The smaller earthquakes in Italy (L'Aquila, 2009, Emilia, 2012) also exposed some known and new wall failure modes. Of particular relevance for the present project were the issues of diagonal concrete compression and out-of-plane instability with buckling of longitudinal reinforcement for slender RC walls.

The application of current Swiss RC standards (SIA, 2003) will avoid most of the previous failure modes through empirical rules regarding minimum wall thicknesses and maximum axial forces, as well as design rules regarding transverse reinforcement. Unfortunately, pre-1989 designed RC wall buildings with thin walls can be vulnerable to shear, stability and bending-compression failure induced by earthquake loading.

1.5. Performance-Based Earthquake Engineering

The idea that a structure should be able to resist minor seismic shaking without damage, withstand a moderate earthquake possibly experiencing some non-structural damage, and survive a major event without collapse, was born in the late 1950s (SEAOC, 1959). Such statement embodies the concept of *performance-based earthquake engineering* (PBEE), which builds on the definition of desired performance targets (Bozorgnia & Bertero, 2004). Until the early 1970s, these targets were quantified by empirical criteria, e.g. for use in equations estimating the base shear (SEAOC, 1980). As research progressed, such empirical relations were replaced by equations founded upon physical principles, and uncertainties were also progressively considered (ATC-3-06, 1978). At the beginning of the XXI century, PBEE found its way in assessment (ASCE, 2006; ATC-40, 1996; EN1998-3, 2005; FEMA 356, 2000; FEMA, 2012a, 2012b; SEAOC, 1995) and design codes (ASCE 7-02, 2002; EN1998-1, 2002; FEMA 368, 2001). All these guidelines share a common feature: for each desired performance objective, they prescribe discrete, document-specific, performance levels—ranging from fully operational to collapse prevention—and discrete hazard levels.

Characterising these performance levels requires the definition of a set of engineering demand parameters (EDPs) on which performance assessment can be based. The values of this set of EDPs needs to be estimated from numerical simulations. It should be noted that within a formal theoretical setting of performance-based assessment, a distinction exists between EDPs and damage measures: Damage measures describe the damage and its consequences to structural or non-structural components while EDPs include all engineering parameters based on which such damage can be

estimated. In reinforced concrete (RC) structures, examples of damage measures are maximum crack width, spalling of cover concrete, buckling or fracture of longitudinal steel, damage to core concrete, while EDPs are, for example, member forces, inter-story drift values or maximum tensile and compressive strains. Floor accelerations and velocities, residual displacements, displacement ductility, and cumulative measures like hysteretic energy dissipation, are further examples of EDPs that can be suitable to describe the building performance.

Until the 90s, traditional EDPs were limited to member forces and inter-story drifts, obtained from equivalent lateral force and/or response-spectrum analysis. These analysis methods are still the basis of many current design codes. From the early to mid-1990s, the development of nonlinear methods of analysis led to the introduction of deformation-based EDPs, such as member chord rotations (Romão, Delgado, & Costa, 2010) and inter-story drifts (Whittaker, Deierlein, Hooper, & Merovich, 2004). Many commercial software packages of structural analysis now include relatively advanced nonlinear modelling and analysis features, which are used by practitioners to estimate the aforementioned EDPs (e.g. Computers and Structures Inc. (Computers and Structures Inc., 2013a, 2013b)) and a number of research analysis softwares have been specifically developed for seismic analysis purposes (OpenSees, 2013; SeismoSoft, 2013; Wong, Vecchio, & Trommels, 2014).

EDPs such as member forces and inter-story displacements are ‘global-level’ parameters, i.e., quantities that refer to the member or structural level. However, the advancement of numerical simulation tools and new code and guidelines specifications are progressively promoting the supplementary use of local EDPs, e.g. quantities that refer to the material or sectional levels, which are considered to better and more directly correlate to damage (Berry, Lehman, & Lowes, 2008). They include, amongst others, rebar strains, cover and core concrete strains, maximum curvature, and curvature ductility (Mackie & Stojadinovic, 2001). For instance, the reinforcing steel tensile strain can be defined as the EDP to assess the maximum residual crack width, which can then be compared to a reference value to assess if the damage level is negligible or requires a certain repair method. Other examples are the cover and core concrete compressive strains, which can be related to a minor spalling of the cover (slight damage level) or a major spalling exposing the longitudinal reinforcement (moderate damage level).

PBEE demands therefore an accurate estimation of both global and local EDPs, which can be estimated from numerical analyses of different degrees of sophistication. In this report, the suitability of different modelling approaches for the seismic analysis of reinforced concrete (RC) walls will be assessed in chapter 3.

1.6. Objectives of the Study and Organization of the Report

Bearing in mind the framework presented in the previous sections, the first objective of this project was to plan and carry out an experimental program to better understand the expected performance of thin RC walls as they were typically designed and built during the 1950s-1970s in Switzerland. The importance of carrying out such tests is also proportional to the lack of knowledge regarding specific failure modes that are poorly understood, as discussed in section 1.4. These large-scale tests of entire walls, subjected to cyclic loading reproducing seismic excitation, will illustrate directly how Swiss walls will behave in the event of an earthquake. Measurements, photos and videos gathered during the tests will also be valuable material for research and educational purposes. These new tests, which are described in chapter 2, will therefore allow to close an important gap in the experimental international database on RC walls, which includes very few past tests on thin RC walls.

The data gathered during the tests with cutting-edge instrumentation and data-acquisition systems should then be used for validation of numerical models applied in consulting. In fact, the characterization of the seismic *vulnerability*, as discussed in the aforementioned chapters, depends on the engineer’s ability to predict and simulate structural damage. The second objective of this study was

thus to assess the capabilities of existing engineering models, typically used in practice, to simulate inelastic wall behaviour. It is carried out in chapter 3. Only a combination of sound mechanical models with advanced numerical tools will allow to simulate the expected seismic behaviour of existing buildings with a high degree of confidence and, consequently, to accurately determine if a particular structure should be subjected to a structural rehabilitation operation. If so required, such joint approach will further be able to identify the strengthening measures that minimize the intervention and optimize the response of the retrofitted building.

From the scientific viewpoint, estimation of damage relates directly to local member quantities such as strains, which underlines the fundamental need to efficiently establish a relation between these and global quantities (e.g., member forces), which can be in general simulated with more accuracy. The investigation of this often forgotten link is another objective of the present study. It comprises two phases. The first one, completed, consists of a comparison between local quantities as simulated by different modelling approaches. It was addressed in an extensive technical study that has been recently submitted for publication in the journal 'Archives of Computational Methods in Engineering' (Almeida, Tarquini, & Beyer, 2014). The second phase corresponds to a comparison between the aforementioned results of the mathematical models with those obtained from the experimental tests carried out in the laboratory. It is an ongoing effort that will soon also be submitted for publication in international peer-reviewed journals. The details of these two phases are not included in the current report as they represent a level of technical detail that was judged incompatible with the character of the document. If the reader is interested in the abovementioned reference the authors will gladly supply it.

The last objective of this report, explained in chapter 4, is to provide recommendations and guidance that can be used by practicing engineers with expertise in earthquake engineering, in order to improve the overall seismic assessment of RC wall buildings and therefore allow a more sustainable protection of the Swiss Heritage in the long term.

2. EXPERIMENTAL PROGRAMME

2.1. Introduction and Objectives

Whilst detailed assessment is done, in general, through computational simulations (as addressed to a greater extent in chapter 3), it can only be carried out with confidence if the numerical tools acceptably reproduce the real structural behaviour. In turn, the latter can only be fully understood through experimental tests of representative specimens that follow the design and detailing criteria used in common construction practice.

A review of experimentally tested specimens verifying conditions of (loose) similarity with the Swiss construction practice of the 1950s-1970s was carried out. Some of the most relevant characteristics that affect the seismic response of walls with uniform distribution of reinforcement include: wall thickness, length, vertical and horizontal reinforcement ratios. If the wall also includes boundary elements, their length (as a ratio of total wall length), and the corresponding partition of the longitudinal reinforcement ratio between boundaries and web regions is also relevant. With the above in mind, the database review fell on test units respecting the following requirements:

- Rectangular geometry.
- Absence of boundary elements or having boundary elements with a similar reinforcement ratio as the web.
- Relatively low vertical and horizontal reinforcement ratios (< 1.5 %).
- Shear span ratios between 1 and 3.

Unfortunately, the existing experimental results show that their applicability to further the knowledge on the performance of thin RC walls with Swiss construction practices, as described in Section 1.3, is extremely limited. Such fact pointed out to the need of carrying out specific experimental tests to bridge this gap.

Even very advanced numerical simulations are in general not sufficient to predict, accurately and without *a-posteriori* calibration, the inelastic response of a shear wall at the global and local levels. Hence, the only available option for a reliable and controlled acquisition of data consists of the execution of highly instrumented experimental tests.

Within the scope of this project it was decided to test two thin RC walls, denoted by TW2 and TW3[3]. The experimental program, which is being carried out at the GIS-GE Lab of EPFL, started in September 2013 and lasted until April 2014. The main objectives of the tests are:

- Evaluation, in terms of displacement and ductility capacity, of the wall performance under cyclic loading.
- Assessment of the governing failure mechanism.
- Estimation of the influence of lap splices in reducing the ductility and the capacity of the wall.
- Providing consistent and reliable modelling guidelines in order to predict, both at the global and local levels, the behaviour of structural elements with similar geometrical and mechanical characteristics.

2.2. Description of Experimental Campaign

The geometrical, mechanical, and reinforcement detailing regularity of RC walls in Swiss construction practice during the 50s-70s, discussed in section 1.3, makes it simpler to define representative RC wall

[3] The acronym TW stands for 'Thin Wall'. Actually, the complete test series included a total of three walls, but specimen TW1 represents a distinct design code and thus is not of direct interest to the present project.

members to be tested in the laboratory. Specimens TW2 and TW3 are thus intended to reproduce the features of RC walls that can be found in existing structures built during the referred time period.

Experimental simulation is restrained by laboratory limitations, which are of different sorts. In the present case, a full scale specimen could not be considered in view of the large length of typical walls. Although the construction of the latter would be too costly, laboratory conditions (capacity of the available actuators, physical volumetric features of the laboratory, etc) were the main limiting factor defining the upper bound for the scale factor. On the other hand, small scale factors will typically imply an untrustworthy reproduction of the scaled-down material behaviour (concrete and steel) and, consequently, of the wall response. In view of the above, a satisfactory scale factor of 2/3 was defined.

Both test units are models of the ground storey of a RC wall belonging to a 5-storey reference building, characteristic of typical Swiss construction practice during the 50s-70s. The influence of the part of the building wall comprised between its effective height and the height of the specimen (Figure 6) is taken into account by the specific load application enabled by the particular test setup.

2.2.1. Test Setup

Most monotonic and quasi-static cyclic wall tests are performed in specimens responding as either: (i) a cantilever, i.e., a wall subjected simultaneously to a top axial and lateral force, or (ii) as a double cantilever, in which case the upper end is restrained against rotation. The imposition of a specific (and controllable) top moment – which can more realistically simulate the boundary conditions of a storey wall – poses a number of experimental difficulties, and is therefore usually not pursued. The current test setup, depicted in Figure 7, Figure 8, and Figure 11, was devised precisely to overcome such problems.

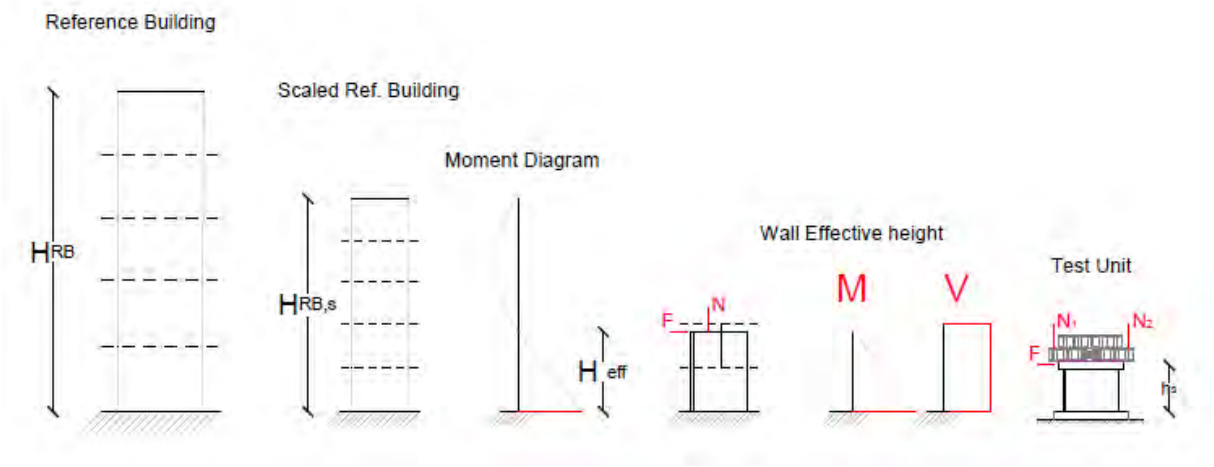

Figure 6. Definition of the test specimens TW so as to reproduce a realistic behaviour of the original wall of the reference building.

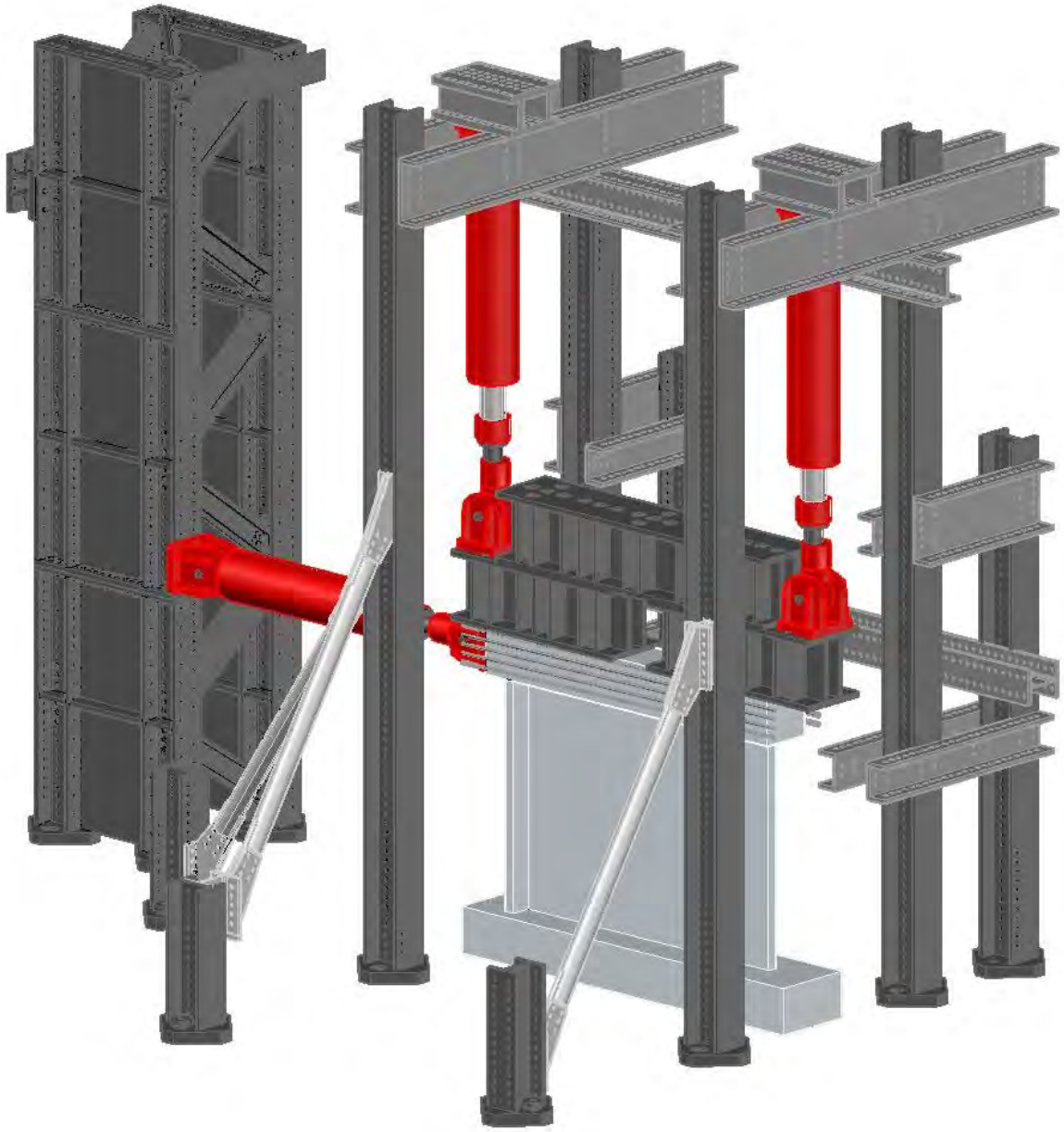

Figure 7. Three-dimensional view of the test setup (SW).

It can be observed that the test setup consists of a steel frame and reaction wall, designed to prevent tilting of the wall and to provide a support for the actuators and the measurement system. All the steel columns were clamped to the floor with tensioning rods. Three actuators are employed: two vertical ones apply the axial load and bending moment corresponding to a chosen shear span ratio through the actuators' lever arm, and the third actuator applies the cyclic horizontal displacement history to the top RC beam of the specimen (see also section 2.2.2). The actuators (*Walter+Bai* AG servo-hydraulic actuators with force capacity of ±1000 kN and total stroke of 1000 mm) are controlled in a fully coupled mode in such a way that the axial force and the height of zero moment remains constant throughout the test. The horizontal actuator is the master while the vertical actuators are slaved to the previous one. Each actuator is equipped with a load cell and a displacement transducer, used to control the deformation rate. Since small deformations are imposed in the horizontal direction and the hinges of the actuators have some backlash, which are both part of the deformation measured by the actuator's internal transducer, an external LVDT was used to measure and control the top displacement of the test unit.

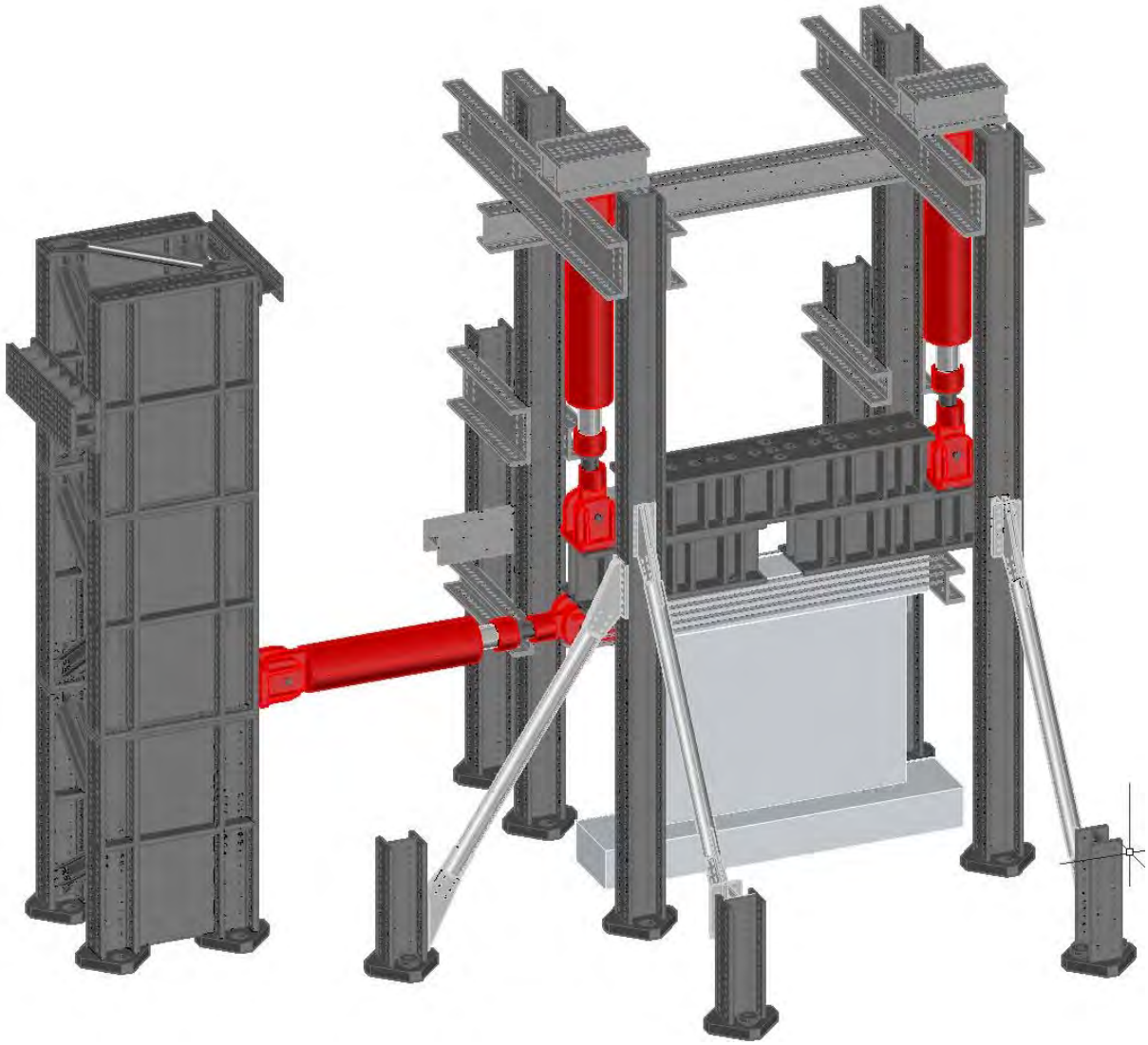

Figure 8. Three-dimensional view of the test setup (NW).

In test setups of cantilever and double-bending specimens, cracks can spread all over the specimen's height, which typically lacks physical meaning due to the realistic localized increase in stiffness and resistance provided by the slab at each storey level. The present loading conditions replicate the as-built status in a more realistic way, avoiding the much increased costs of constructing (and testing) a multi-storey test unit including slabs.

Three steel beams were placed over the top RC beam of the test unit, to warrant a distributed application of loads. Such steel loading beams have strength and stiffness of a much larger order than that of the wall. Again in order to reproduce *in-situ* conditions, the lateral stability of the specimen was guaranteed at the storey level by a bracing system consisting of four steel tubes that allow for free lateral displacements in the loading direction and restrict them in the out-of-plane direction. The force in these tubes was controlled by strain gage measurements. On the other hand, the possible development of lateral instability modes along the height of the wall, triggered by in-plane loading, was not avoided. The latter are an integral part of the potential realistic failure modes of walls in real buildings and should therefore be allowed to take place (see section 1.4).

The construction of the test setup in the structural engineering laboratory GIS-GE of EPFL started in the month of September 2013 (Figure 9, Figure 10) and lasted until November 2013 (Figure 11).

Figure 9. Overview of the testing space in the beginning of September 2013.

Figure 10. Overview of the test setup at the end of October 2013, close to completion.

Figure 11. Overview of the test setup upon completion.

2.2.2.Specimens TW2 and TW3

The overall geometrical characterization and reinforcement layout of the test units can be found in Figure 12. Each specimen consists of a foundation, the wall itself, and a top beam. A significant number of parameters (e.g., axial load ratio, shear span ratio, boundary conditions, geometrical or mechanical properties, detailing) could have been changed to differentiate the two tests. The one that was thought to potentially have a greater impact on the behaviour of the specimens was the presence / absence of lap-splices (see section 1.3), and it was thus decided to provide TW3 with lap splices according to past construction practice, i.e., between 30-35 times the diameter of the longitudinal rebars. In other words, the two specimens share the same geometry, reinforcement ratios, mechanical properties, boundary conditions, axial load ratio, shear span ratio, and are submitted to the same load protocol.

Both walls are 2 m high, 2.7 m long and 0.12 m thick, and include a small flange (0.44 m × 0.12 m) at one edge that simulates the presence of an orthogonal wall. The objective of the construction of such small flange is not to account for the increase in strength in that direction, but rather to check its influence on the concrete confinement, lateral stability of the wall, and eventual concentration of damage along the interface. The longitudinal and horizontal reinforcements are 6 mm diameter rebars spaced respectively at 95 mm and 130 mm, and concrete cover is 15 mm. In case of TW2, the vertical reinforcement is placed all the way down into the foundation, whilst for TW3 it stops at the wall-foundation interface. The lap spice length is of 215 mm, which corresponds to approximately 35 × diameter of the longitudinal bars. The reinforcement ratios characterizing both TW2 and TW3 are listed in Table 1.

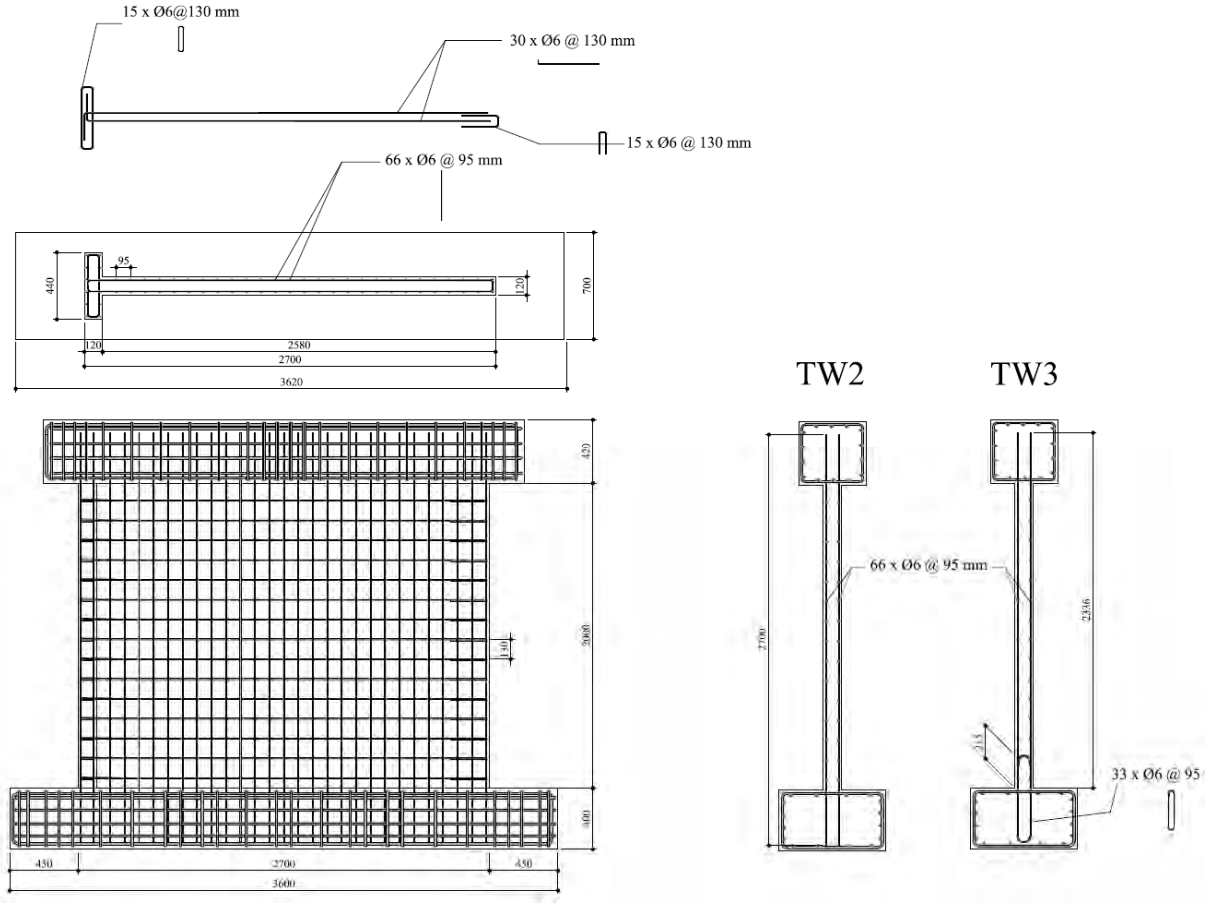

Figure 12. Geometry of RC specimens TW2 and TW3, and corresponding reinforcement detailing. All dimensions in [mm].

Table 1. Reinforcement ratios of test units TW2 and TW3.

REINFORCEMENT RATIOS			
	Vertical	**Horizontal**	**Orthogonal**
	ρ_v [%]	ρ_h [%]	ρ_{ort} [%]
Web	0.49	0.35	[-]
Flange	0.64	0.19	0.35

As it can be noted, the reinforcement layout lacks seismic detailing rules. No stirrups or hoops are present and the longitudinal reinforcement is placed externally to the transverse rebars. This detailing is quite rare in current design practice wherein, especially in seismic regions, providing the structural members with an adequate confinement is standard recommendation.

The construction of the specimens was commissioned to the company 'Proz Frères SA – Éléments en Béton' in September 2013. The walls arrived to the GIS-GE Lab in the month of December (Figure 13 and Figure 14) and were painted white. The test unit was then connected to the test setup and six tensioning rods passing though vertical openings in the foundation fastened it to the laboratory strong floor. Horizontal prestressing of the top RC beam was also applied and the wall was instrumented as described in section 2.2.5.

Figure 13. General view and close-up of the specimens after construction, upon arrival to the laboratory.

Figure 14. Transportation of the first specimen to the test setup.

2.2.3.Material Properties

A number of concrete compression tests and double punch tests were carried out in cylinder specimens to determine the modulus of elasticity, the compression strength, and the tensile strength for the concrete of both walls. The results, corresponding to averages of the tests, are summarised in Table 2.

The 6 mm diameter reinforcing steel employed in both test units TW2 and TW3 originates from the same production batch (it corresponds to a special order from the EESD Lab, wherein a more realistic ductile response was envisaged). In order to describe its mechanical behaviour, six bars were subjected to uniaxial tension tests. The corresponding stress-strain results are displayed in Figure 15 and summarized in Table 2.

2.2.4.Loading Protocol

The main guiding principle for the loading application was once again an as-close-as-possible reproduction of the expected loading conditions imposed by an earthquake on a storey wall of a real multi-storey building. A constant axial load $N = 690$ kN, equivalent to an axial load ratio of $\frac{N}{f_c' \cdot A_g} \cong 5\%$ (A_g is the gross sectional area), was applied to the top of the wall, which was considered to be representative of a building of approximately 5 to 6 storeys. It is a relatively low value, but it should be kept in mind that the thickness of the storey slabs used in Swiss construction was also typically very small (around 16-18 cm; Lestuzzi, 2013, personal communication).

The shear span was fixed at 3.15 m, which corresponds to a shear span ratio of 1.17. As described in section 2.2.1, the moment on the top of the wall was simulated by the lever arm between the forces N1 and N2 applied by the vertical actuators. They were calibrated so that their resultant is applied at the centroid of the wall section (Figure 16).

The test was a quasi-static cyclic experiment. The loading protocol consisted in a reversed cyclic history, which was applied in deformation control. The corner values of imposed (cyclic) drift were named load stages (LS), as shown in Figure 17 and Figure 18 respectively for walls TW2 and TW3. Numbering of the load stages started with LS00 (initial measurements), for the unloaded test unit, and LS01 corresponded to the application of the axial load. Each target (positive and negative) drift was thereafter numbered successively.

Table 2. Mechanical properties of the concrete for test units TW2 and TW3, and of the 6 mm diameter rebars.

MATERIAL PROPERTIES					
Concrete TW2	f'_c	ε_c	E_c	f'_t	
	[MPa]	[‰]	[MPa]	[MPa]	
	50.7	2	31750	2	
Concrete TW3	f'_c	ε_c	E_c	f'_t	
	[MPa]	[‰]	[MPa]	[MPa]	
	43.3	2	30200	2	
Steel	f_y	f_u	E_s	ε_{sy}	ε_{su}
	[MPa]	[MPa]	[MPa]	[‰]	[‰]
	460	625	200000	2.5	80

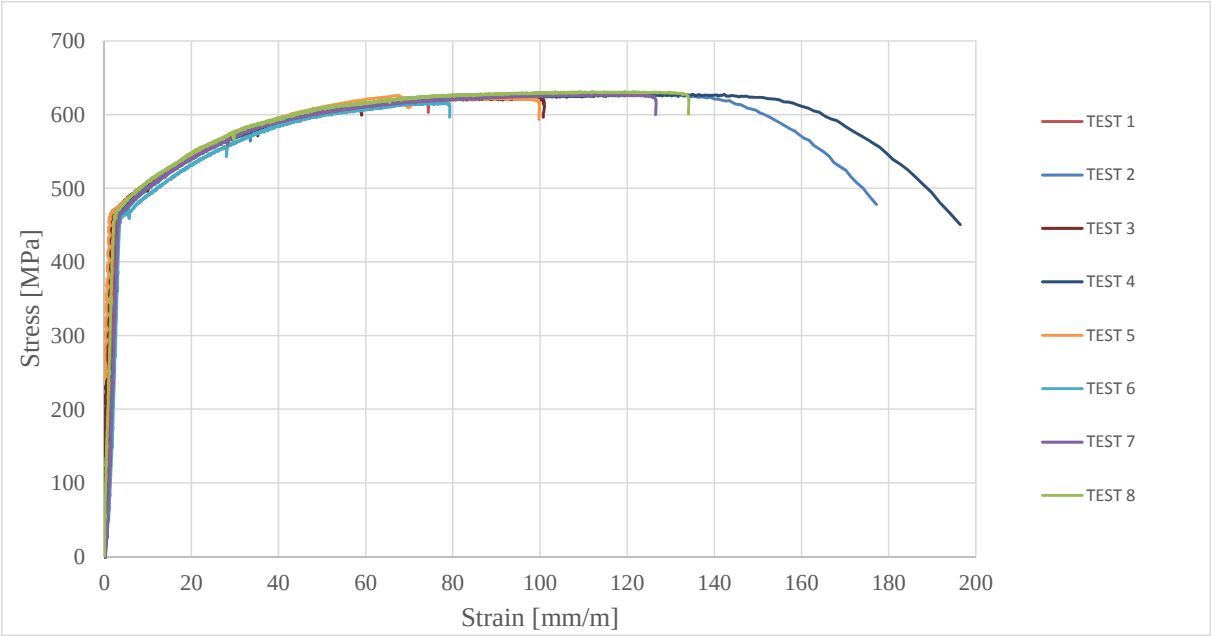

Figure 15. Steel stress-strain relationship as obtained from tension tests in 8 rebars with diameter = 6 mm.

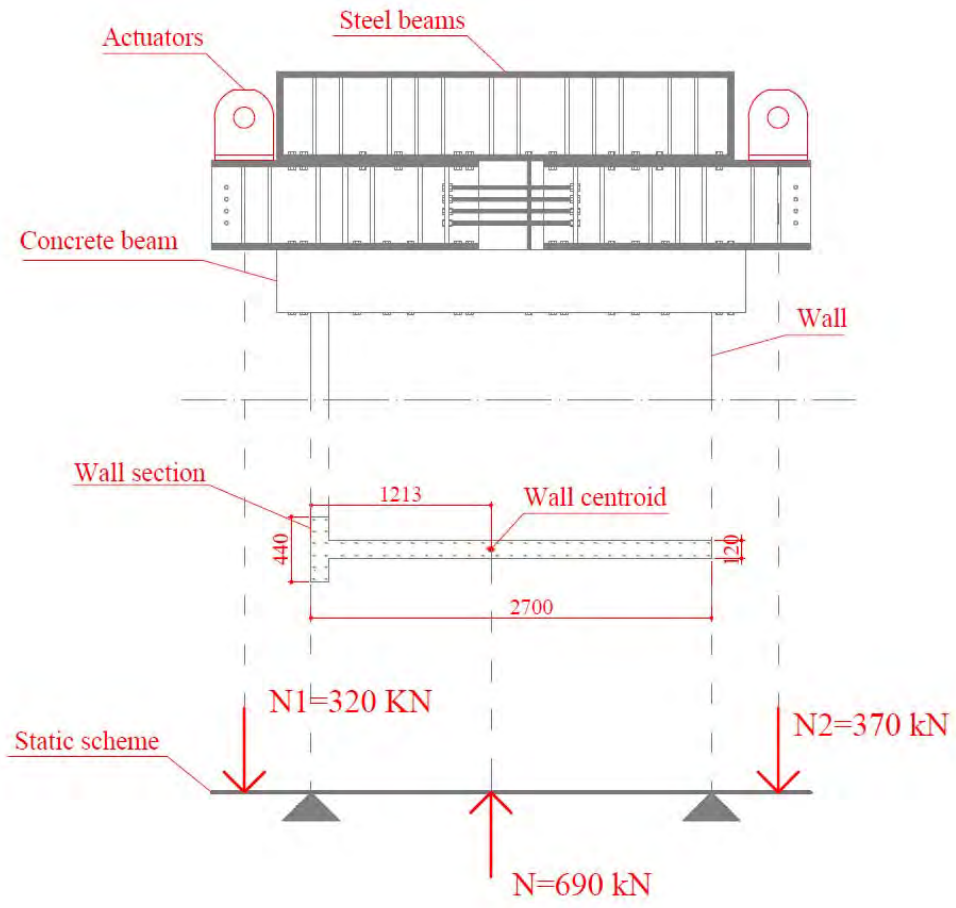

Figure 16. Forces N1 and N2 applied by the vertical actuators to simulate the self-weight of the structure.

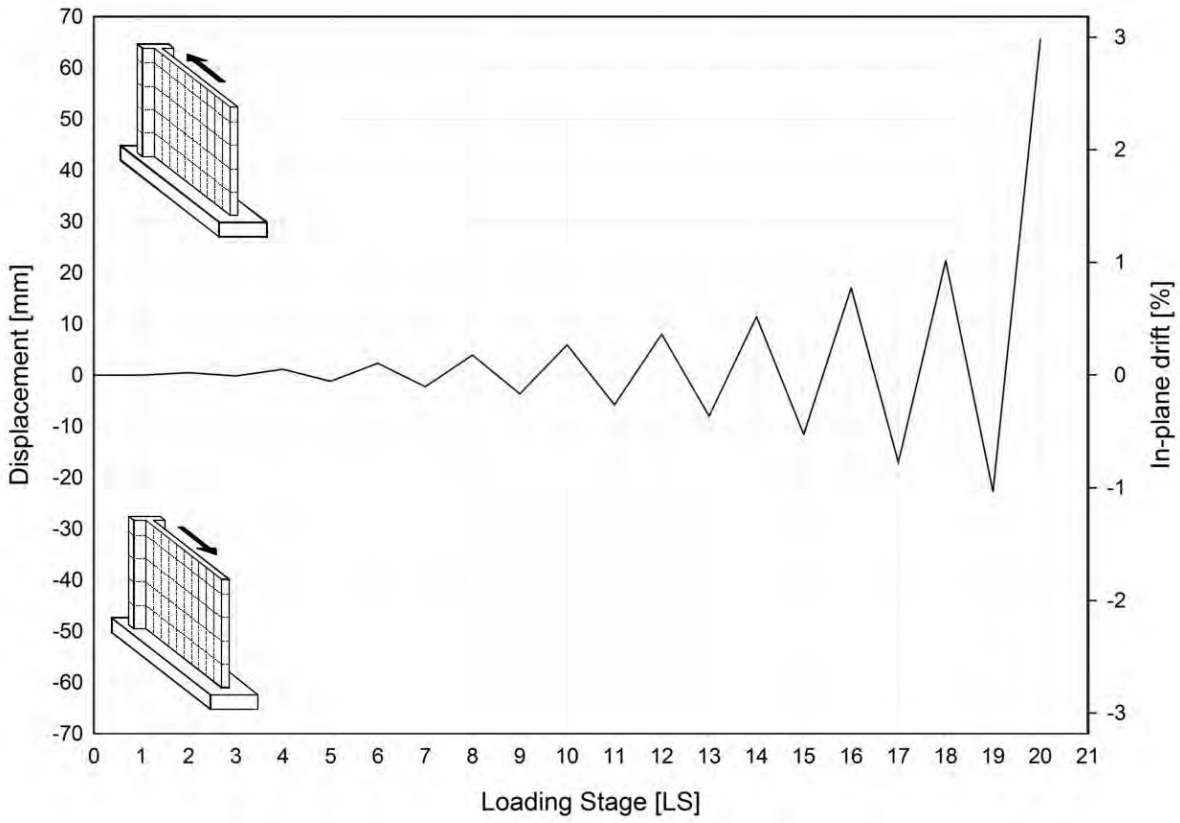

Figure 17. Applied drift history with loading stages (LS) for wall TW2.

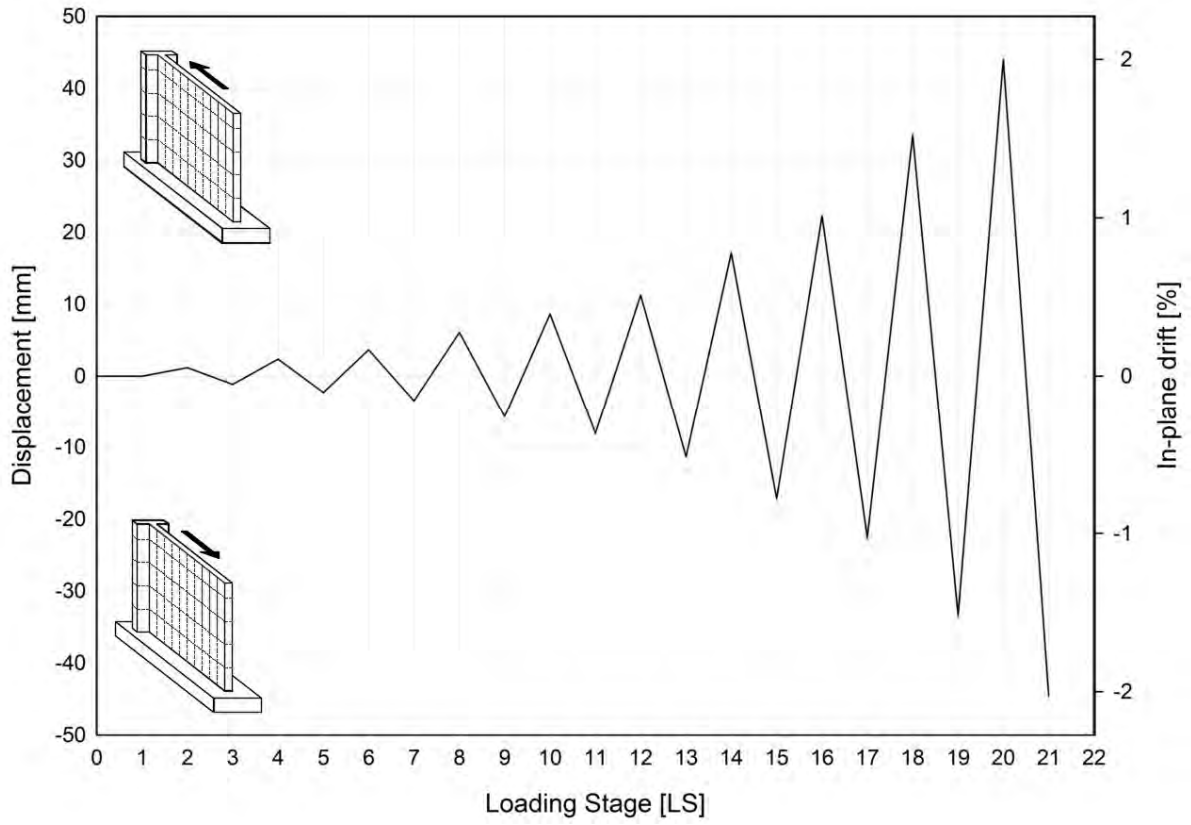

Figure 18. Applied drift history with loading stages (LS) for wall TW3.

2.2.5. Instrumentation and Measurements

The wall tests were instrumented with hard-wired LVDTs and strain gages, optical measurement devices, and digital image correlation systems.

Eight LVDTs with different displacement ranges were placed along both the North (flange) and South (web) sides of the wall, as shown respectively in Figure 19 (a) and (b). Two additional LVDTs, reacting against an external column independent of the test setup and covering a stroke range of ± 50 mm, were placed horizontally to measure the displacement of the top RC beam at the actuator height. The average of their measurements was used to control the test.

The forces in the four steel tubes restricting the out-of-plane displacement of the walls at the height of the top RC beam were derived from strain gage measurements (three per tube). Applied in-plane forces were registered with the internal load-cells of the actuators.

Deformations of the wall surface were measured along a grid of light emitting diodes (LEDs) over the entire wall surface using the optical measurement system *NDI Optotrak Certus HD* (NDI, 2009), as depicted in Figure 20. The LEDs, whose spatial position is tracked by a sensor during the test, were glued on small metal plates along the grid on the Eastern face of the wall. To measure the deformations with respect to the foundation and the top RC beam, L- and Z-shaped brackets instrumented with LEDs were glued to these elements. The LEDs were placed on a base grid of 29 columns × 18 rows (the top beam had slightly less sensors due to the system limitation of 511 channels). Each LED occupied the geometrical centre of the rectangle defined adjacent horizontal and vertical rebars.

The optical measurement data were collected during loading between LSs, as well as during two-minute slots at each load stage (i.e., at constant horizontal displacement). The measured x-, y- and z-coordinates of all LEDs were stored and then post-processed to check the reliability of the measurements during the all test.

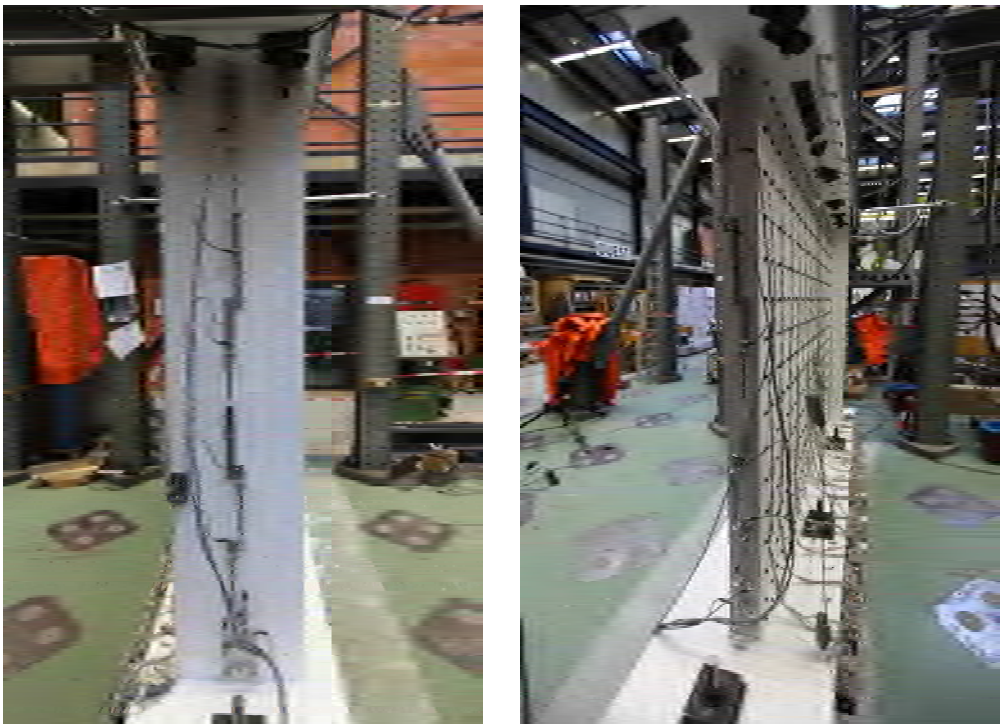

(a) (b)

Figure 19. View of vertical LVDTs: (a) North (flange) side; (b) South (web) side.

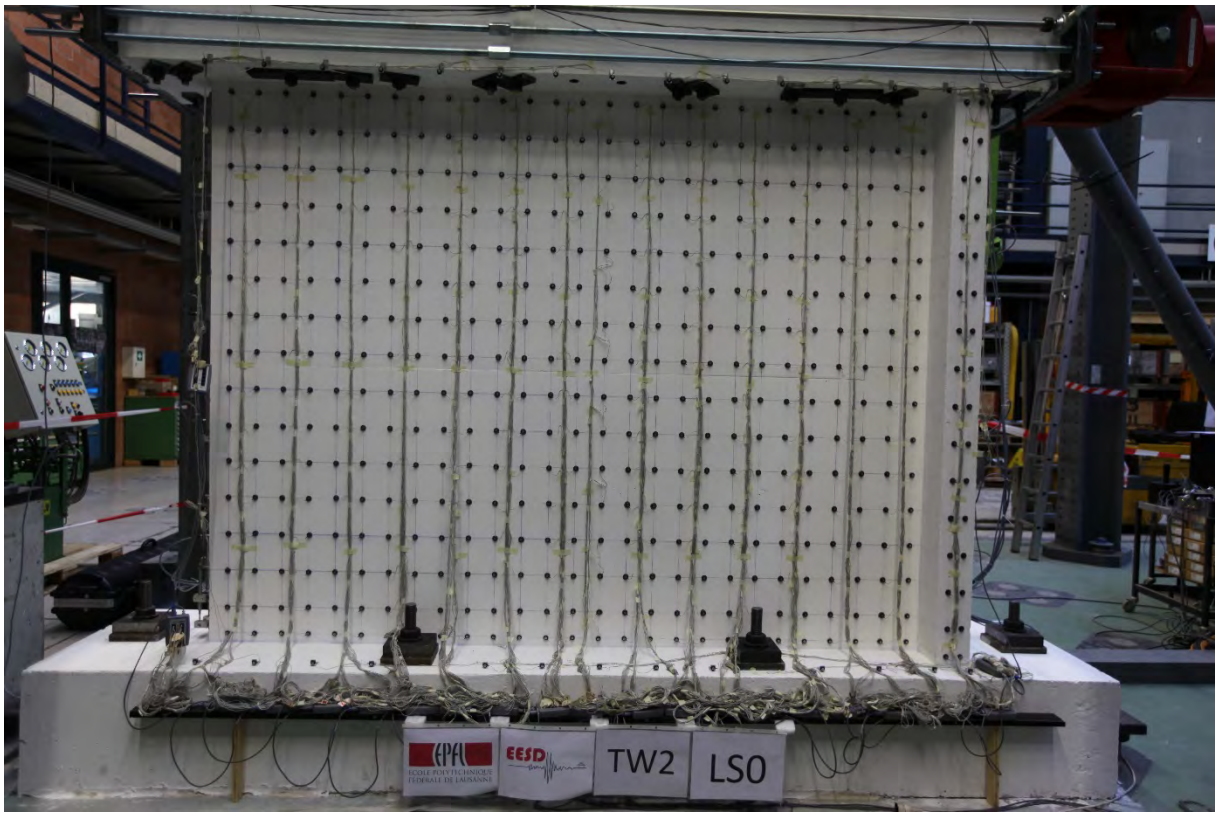

Figure 20. Grid of LEDs used for the optical measurement system (Eastern face of the wall).

On the Western face of the wall, a speckle pattern was applied to enable the use of digital image correlation techniques. While in TW2 only the lower corners of the wall were monitored, see Figure 21 (a), in TW3 the monitored area covered the entire wall face, see Figure 21 (b).

The evolution of the crack patterns during the test was sketched at each load stage and the crack width was determined manually using a crack-width comparator at a few points along the cracks, also at each loading stage. The combination of the crack maps and widths represent the progress of damage distribution in the test unit with loading, which is what the mathematical models of chapter 3 try to simulate from computed engineering demand parameters.

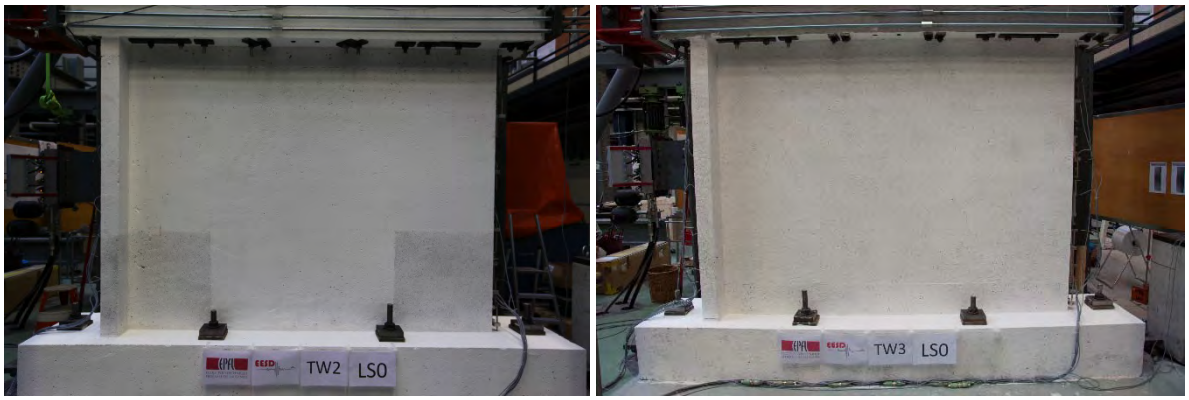

(a) (b)

Figure 21. Digital image correlation speckle pattern for walls: (a) TW2, (b) TW3 (the pattern is barely visible in the photo due to the very small diameter of the ink drops).

Photos of all faces of each test unit were taken at every load stage, as well as of all relevant signs of local damage (cracks, spalling or crushing of concrete, rebar buckling and fracture, etc). Moreover, videos of the wall deformation occurring in-between successive load stages were made. This resource proved very useful in the *a posteriori* analysis of the wall behaviour, contributing to a better understanding of the progression of damage and the transfer of forces between distinct deformation modes of the member.

2.3. Test Results

2.3.1. TW2

Figure 22 shows the force-drift response of wall TW2. It shows stable hysteretic loops up to 0.75% drift when loading towards the web side (LS17). During the following cycle in the same direction (LS19), at 1% drift, the wall lost almost half of its force capacity. In other words, it can be considered that it attained failure. As expected, when loading towards the flange side (even values of load stages), the member depicted a much more ductile response and only showed signs of degrading force capacity above drifts of 1.75%. Failure in this direction can be considered to have occurred at around 2.2% drift, corresponding to an approximate drop of 20% of the member capacity. It should be noted that, in Figure 22, there is an abrupt drop in the force-displacement response of the test unit at around 1.2% drift. Such drop does not correspond to any physical phenomenon but rather to the pressing of the 'emergency stop' button of the oil pressure system feeding the actuators. This was judged required by the supervisors of the test, as it was considered that the advancing damage of the test unit could induce a possible collapse putting at risk the integrity of diverse laboratory equipment (e.g. LVDTs, which were therefore removed).

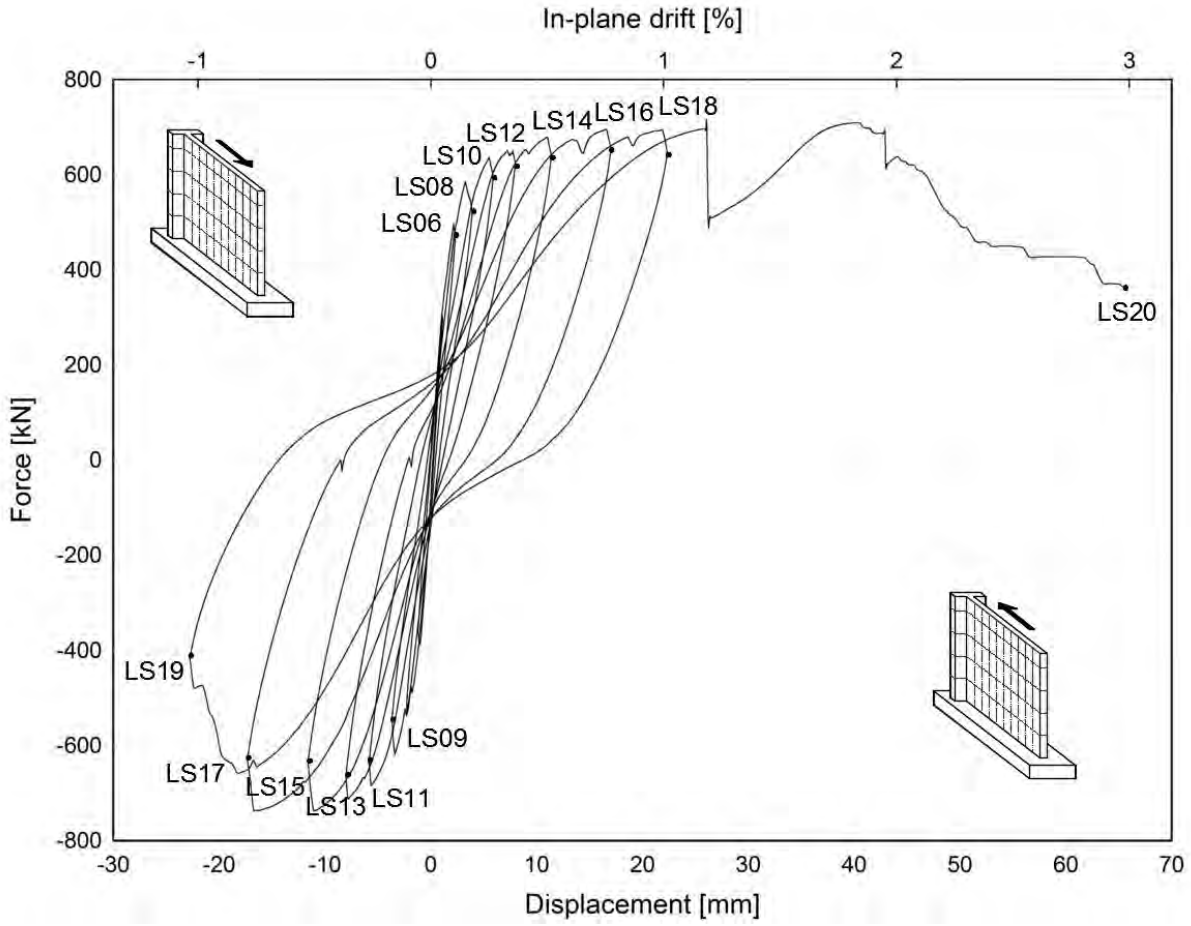

Figure 22. Force-drift response of wall TW2.

The first visible crack was detected at LS06, corresponding to a very small drift of 0.1%, see Figure 23 (a). Crushing of the concrete cover was signalled by the appearance of the first vertical cracks, as depicted in Figure 23 (b). The horizontality of the wall cracks indicates a predominantly flexural type of member behaviour, as depicted in Figure 24 (a) for LS18. At this loading stage, the concrete spalled off along a height of approximately 10 cm at the web end – see Figure 24 (b). As referred above, this load stage corresponds to the last one wherein the wall depicted a stable behaviour in both directions.

Upon further loading to LS19, extensive crushing of the concrete at the web edge took place, in a region occupying approximately 70 cm length and 15-20 cm height (Figure 25). This phenomenon affected the load carrying capacity of the wall and induced the failure of the member in this direction. Therefore, it was decided to not load again the wall in the same direction.

Following load reversal to LS20, the wall showed a stable ductile behaviour up to around 2% drift. Concrete cover attained crushing and minor spalling off occurred, as shown in Figure 26 (d). However, the progressive loss of the wall capacity beyond 2% drift can be attribtued to the consecutive fracture of longitudinal rebars at the (opposite) web end, which was distinctly heard during the test. Figure 26 (b) and (c) provide visual evidence of the foregoing phenomenon. Figure 26 (a) shows the condition of the test unit at the end of the experiment.

It should be noted that very small out-of-plane displacements were observed both for TW2 and TW3 (less than 1 cm). However, as discussed in the conclusions, it is not possible to straightforwardly disregard the pernicious effects of this failure mode in the behaviour of wall buildings characteristic of the Swiss building stock of the 50s-70s.

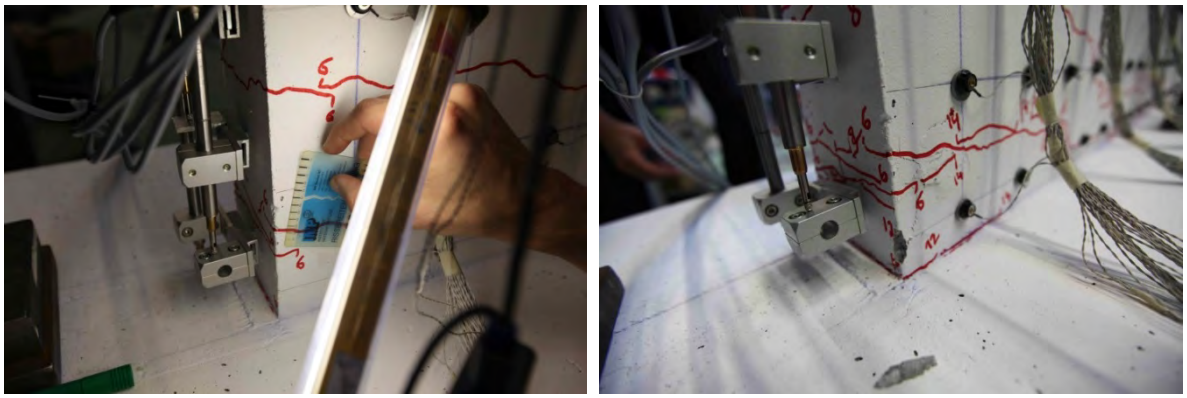

(a) (b)

Figure 23. (a) Appearance of the first crack at LS06; (b) First vertical cracks at the web end (South) at LS15.

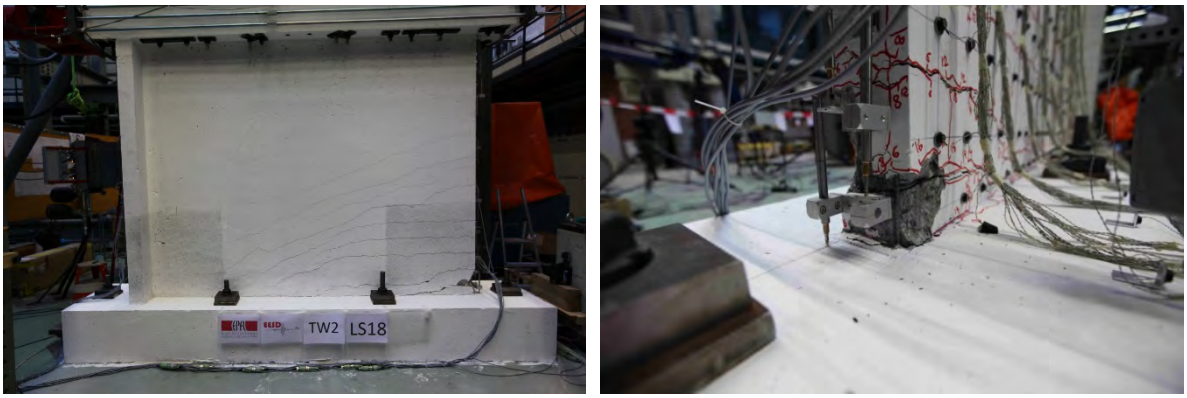

(a) (b)

Figure 24. At LS18: (a) Crack pattern; (b) Damage at the web end.

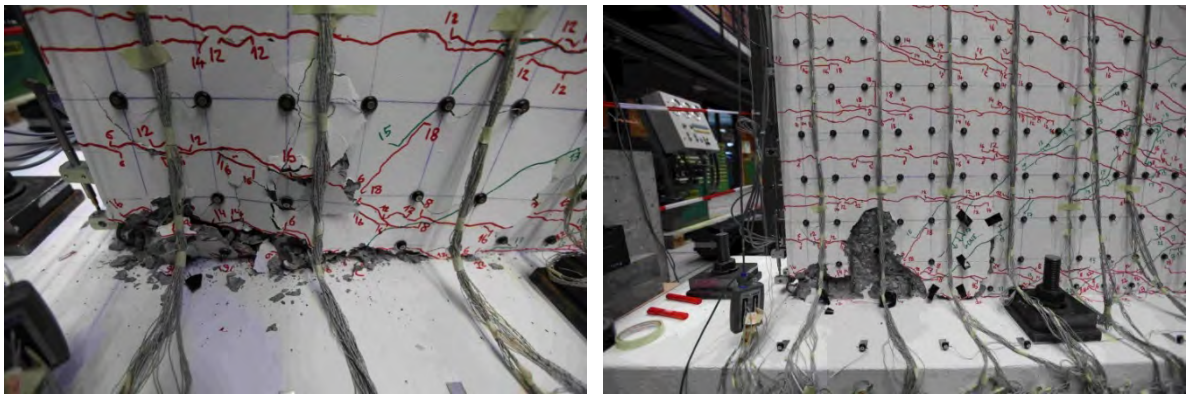

Figure 25. Damage at the web end at LS19.

(a) (b)

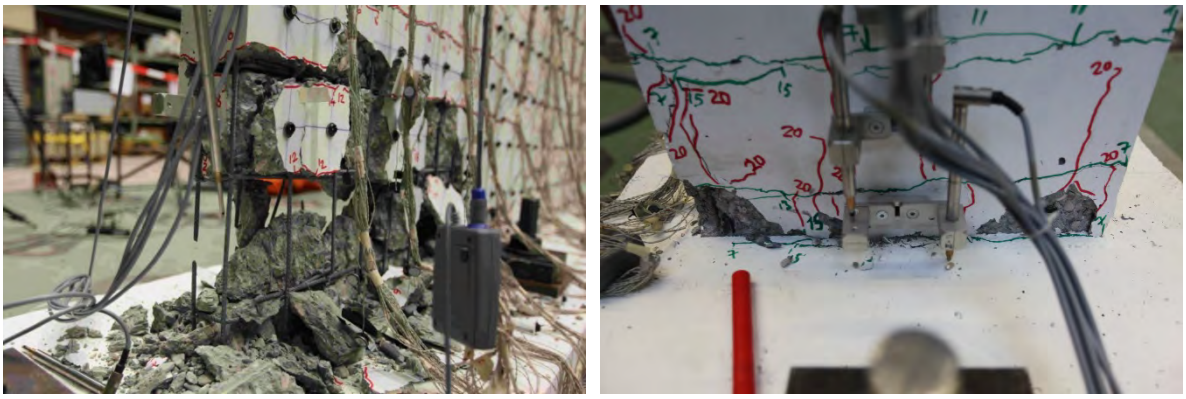

(c) (d)

Figure 26. (a) Overview of wall condition at final load stage LS20; (b), (c) Close-ups at web edge, depicting rebar fracture; (d) Close-up at flange end, showing limited concrete spall-off.

2.3.2. TW3

The global response of wall TW3 can be observed in Figure 27. Comparing these results with those of Figure 22 show that the member response is quite similar when loading takes place towards the web side (negative values of drift). On the other hand, when loading occurs towards the flange side (positive values of drift), the test unit does not attain quite the same value of force capacity, and the degradation of strength starts at a lower drift level, after a drift of 0.75%. The drift level corresponding to an approximate drop of 20% of the member capacity is around 1%, which represents less than 50% of the corresponding drift for wall TW2. The local effect of the lap splice, which is detailed below, can explain this clear comparative decrease of the wall performance at the global level.

Figure 28 to Figure 36, which are self-explanatory to a great extent, show the evolution of damage in the member up to failure. The first clear differentiating effect of the presence of a lap-splice, with regards to wall TW2, is depicted in Figure 29 at LS14. It can be seen that a concentration of deformation takes place, when the web is in tension, in a single large crack at about the lap splice level (22 cm above the foundation). This is caused by the double longitudinal reinforcement content over the length of the lap splice. It is noted that at LS16, although not clearly visible from the pictures in Figure 31, the cracks above the lap splice started to reduce their width in comparison to previous load stages. This can again be ascribed to an internal redistribution of stresses within the member associated to the localization of the deformations in the crack at lap splice height. This effect is even more pronounced for LS18 (Figure 33), wherein the cracks above the lap splice reduce their width to less than 0.1 mm.

The accelerated progression of web crushing, which took place between LS15-LS17-LS19-LS21, was accompanied by a drop in the member capacity, and can be observed in the pictures of Figure 30, Figure 32, Figure 34, and Figure 36. The very extensive crushing that took place during odd loading stages can certainly be related to the large crack width formed during the preceding even loading stages. Namely, it can be the result of in-plane offsets in the crack faces, which yielded a reduced compressive strength. It is also possible that slight out-of-plane rotations of concrete blocks reduced the contact area leading to premature crushing. It was the crushing of the web region that prevented the wall from developing a larger capacity and ductility in the opposite loading direction. Although there were some rebar fractures in the large lap splice crack, as depicted in Figure 33 (a), they were not the primary cause for the decrease of wall bearing capacity at positive drifts, as it happened for TW2. Hence, the damage concentration associated to this failure mechanism controlled clearly the member behaviour in both loading directions.

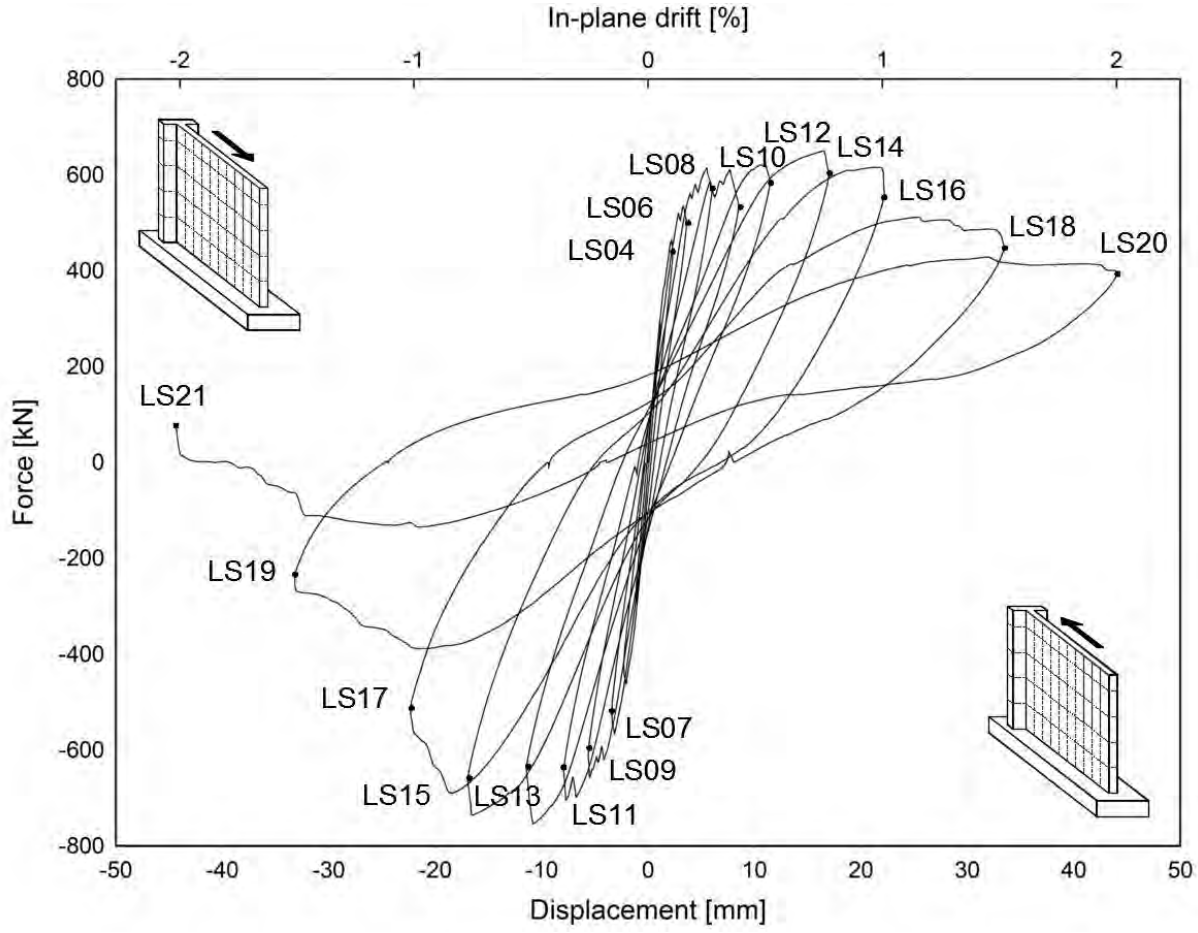

Figure 27. Force-drift response of wall TW3.

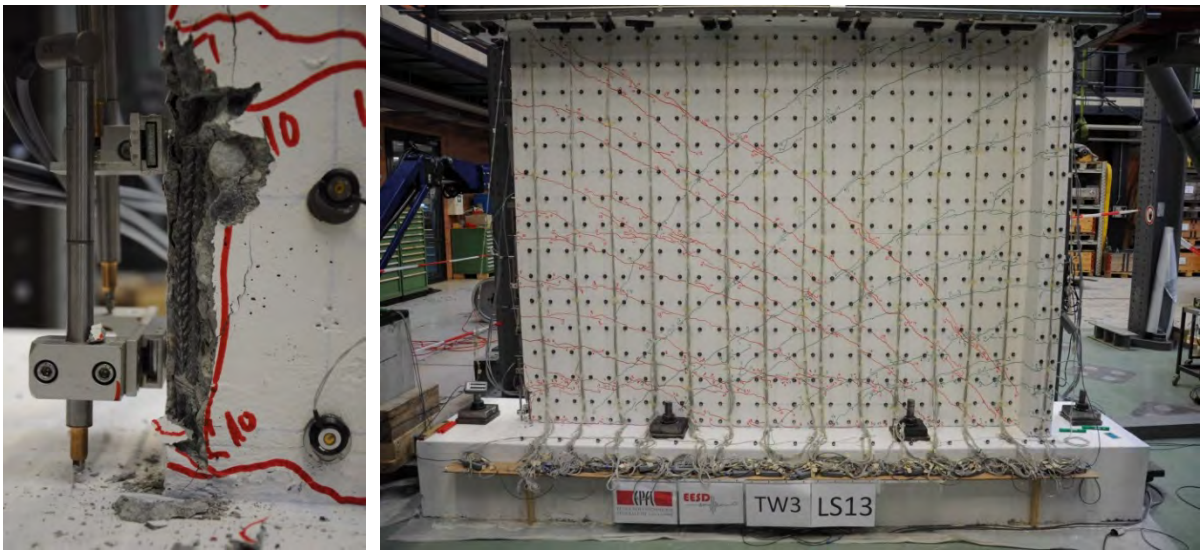

(a) (b)

Figure 28. Load stage LS13: (a) spall off of concrete cover along a height of 15 cm at the web end; (b) Overall crack pattern along the wall.

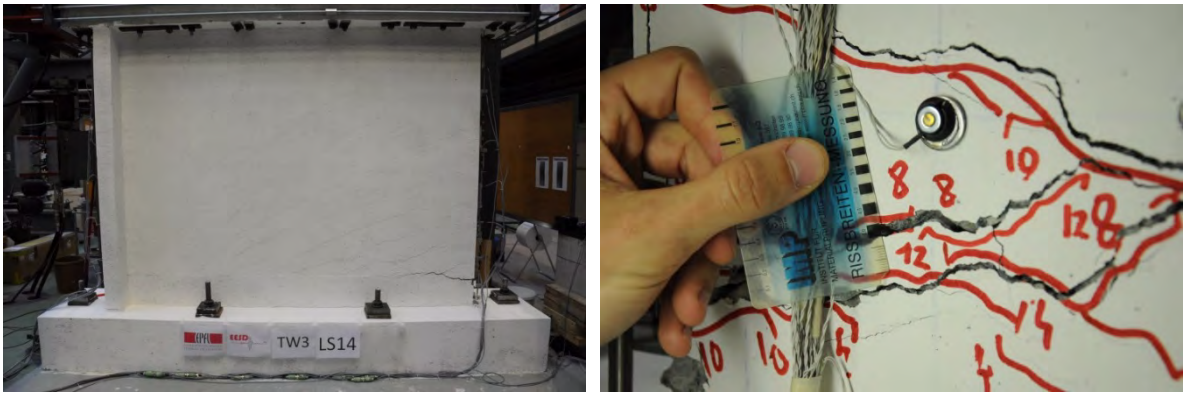

(a) (b)

Figure 29. Load stage LS14: Crack of 5 mm width at about lap splice level (22 cm above the foundation), along a length of around 50 cm.

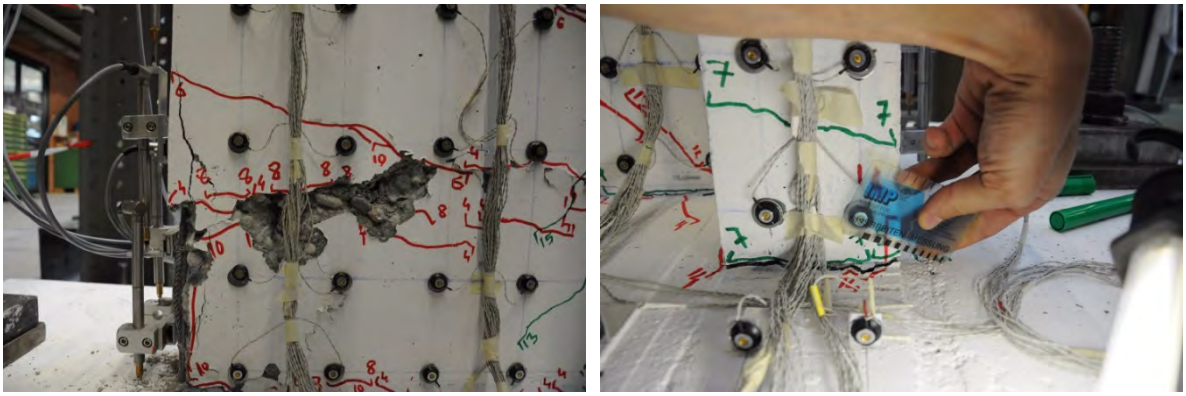

(a) (b)

Figure 30. Load stage LS15: (a) Crushing at the web end (length of around 25 cm at a height of 22 cm); (b) Crack beneath entire flange open.

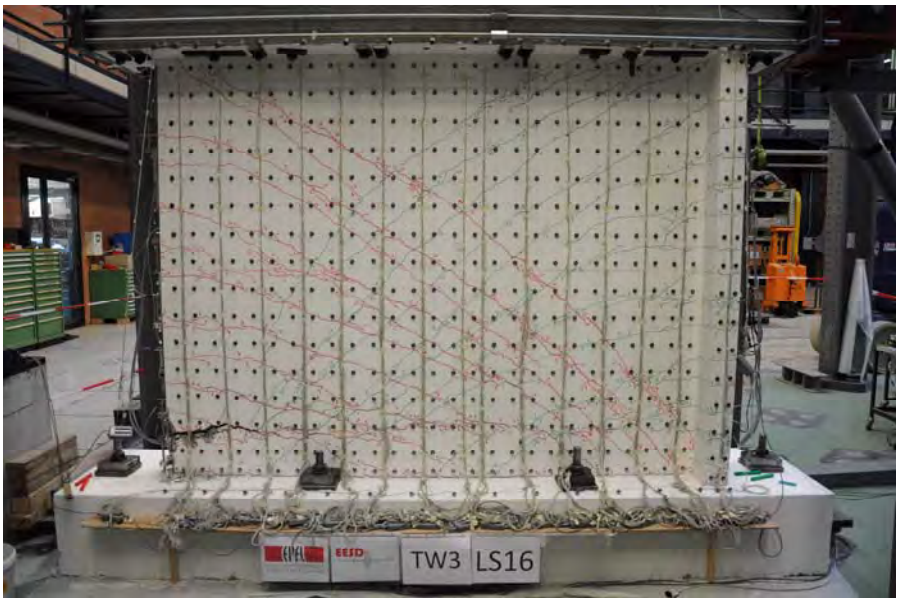

(a)

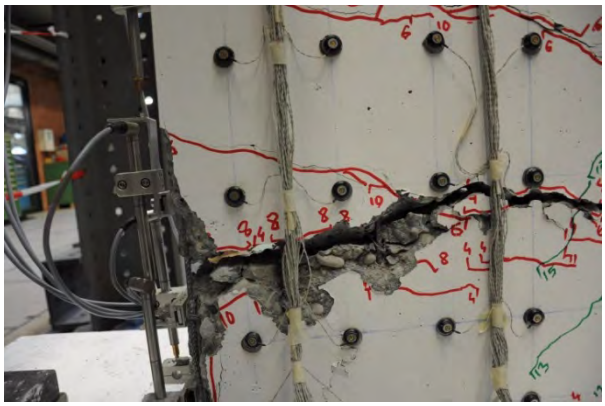

(b)

(c)

(d)

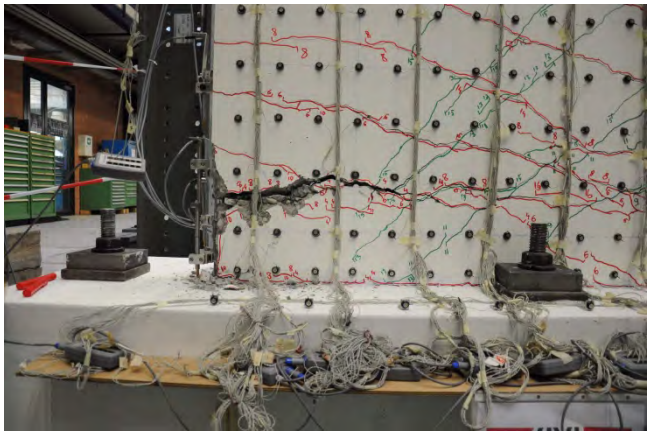

(e)

(f)

Figure 31. Load stage LS16: (a) Wall crack pattern; (b) – (e) Crack of 18 mm width at about lap splice level (22 cm above the foundation), along a length of around 60 cm; (f) Clear bond-slip failure in one of the rebars at the web extremity, of a few centimetres.

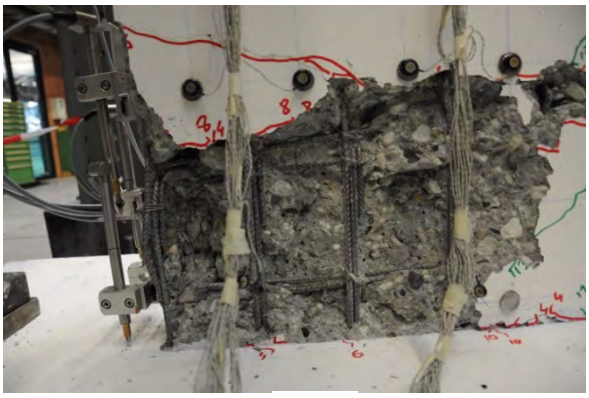

(a)

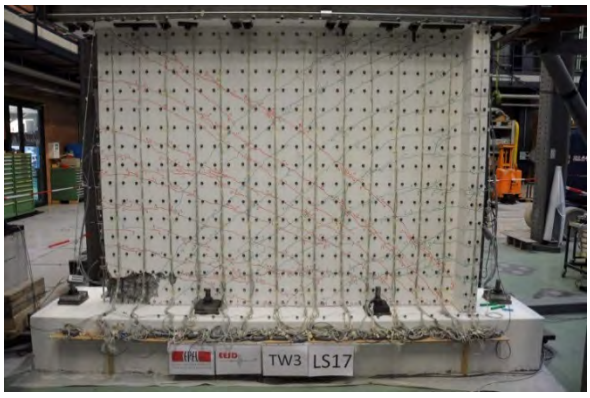

(b)

(c)

(d)

Figure 32. Load stage LS17: (a), (b) Crushing at the web end (length of around 40 cm at a height of 22 cm); (c), (d) Buckling of rebar that had previously slipped.

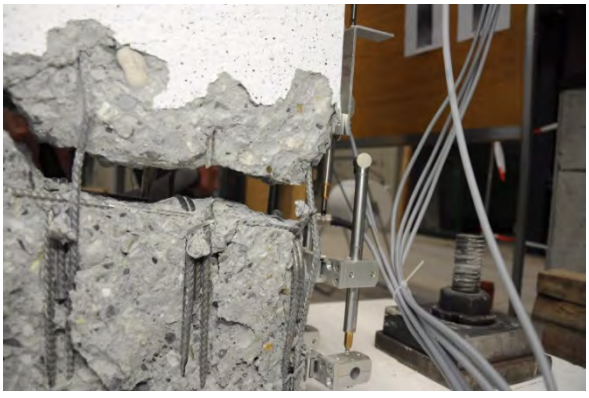

(a)

(b)

Figure 33. Load stage LS18: (a) Crack of 35 mm width at about lap splice level (22 cm above the foundation), along a length of around 100 cm; (b) Rebar fracture and extension of bond-slip failure to neighbouring rebars at web edge.

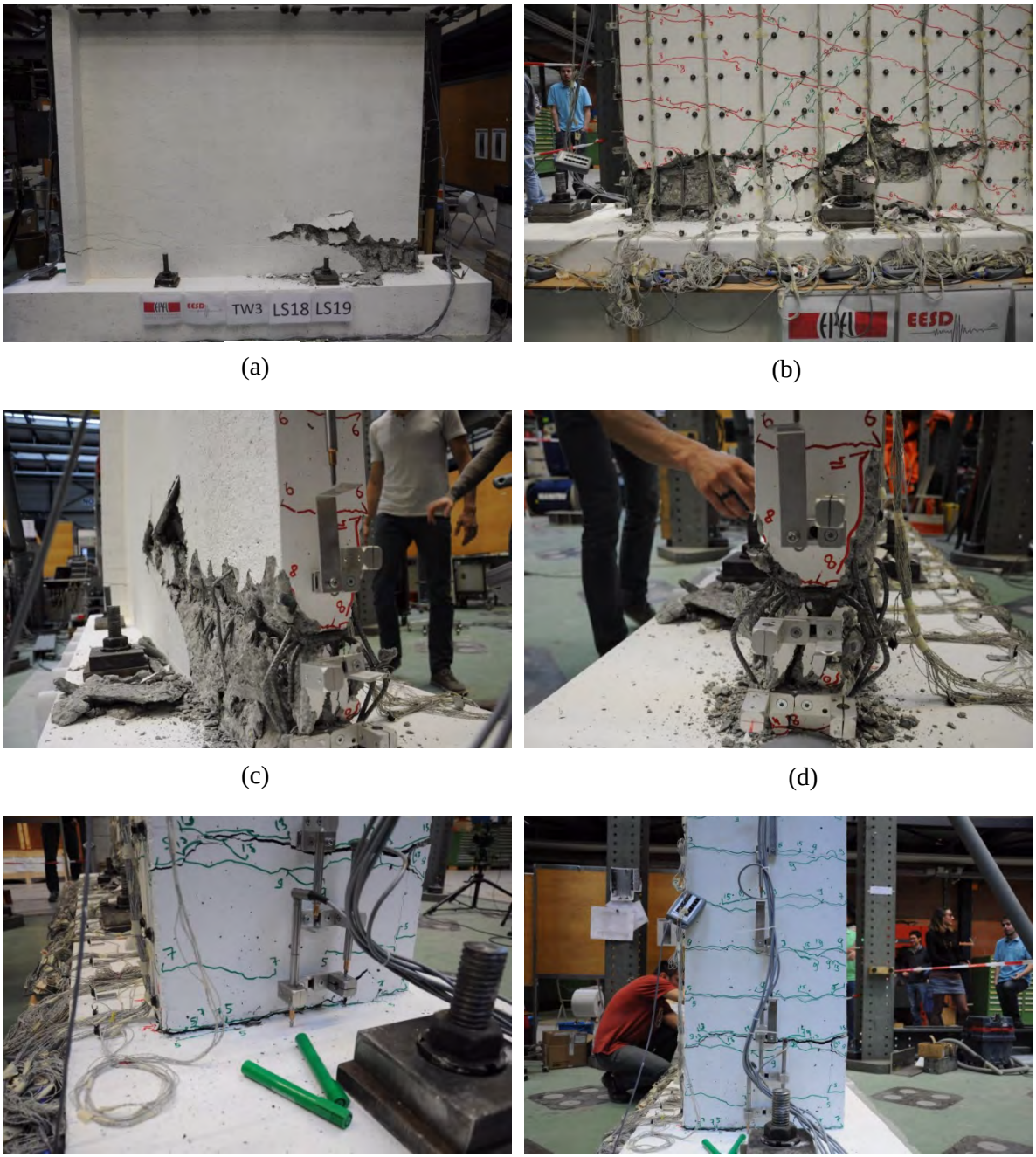

(a) (b)

(c) (d)

(e) (f)

Figure 34. Load stage LS19: (a) – (d) Crushing at the web end (length of around 150 cm at a height of 22 cm); (e), (f) Crack openings at the flange side.

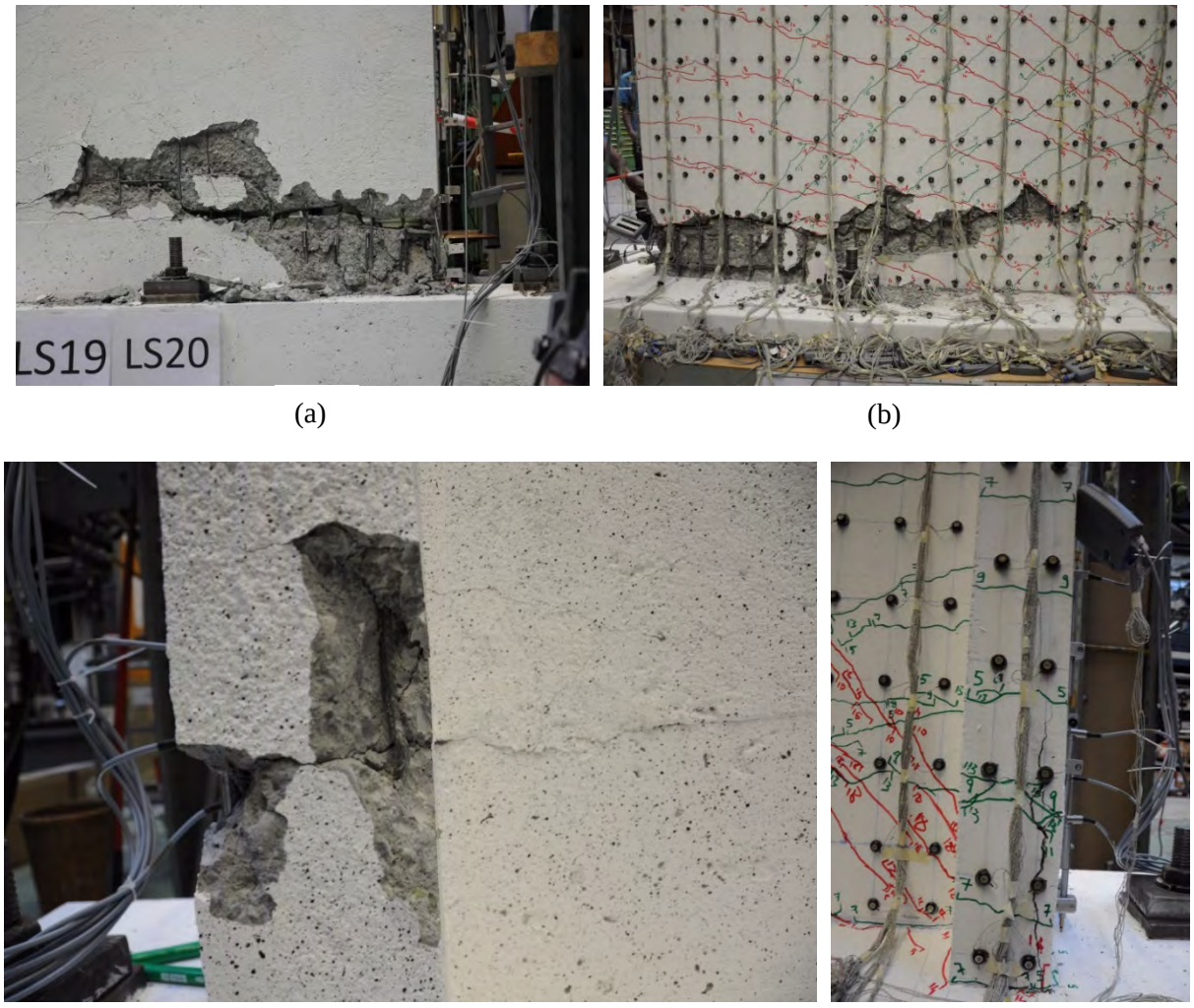

(a) (b)

(c) (d)

Figure 35. Load stage LS20: (a), (b) Crack at lap splice level stretches for a length of around 160 cm; (c) Spalling off of concrete cover at Western side of the flange; (d) Vertical cracks at Eastern side of the flange, indicating cover concrete crushing.

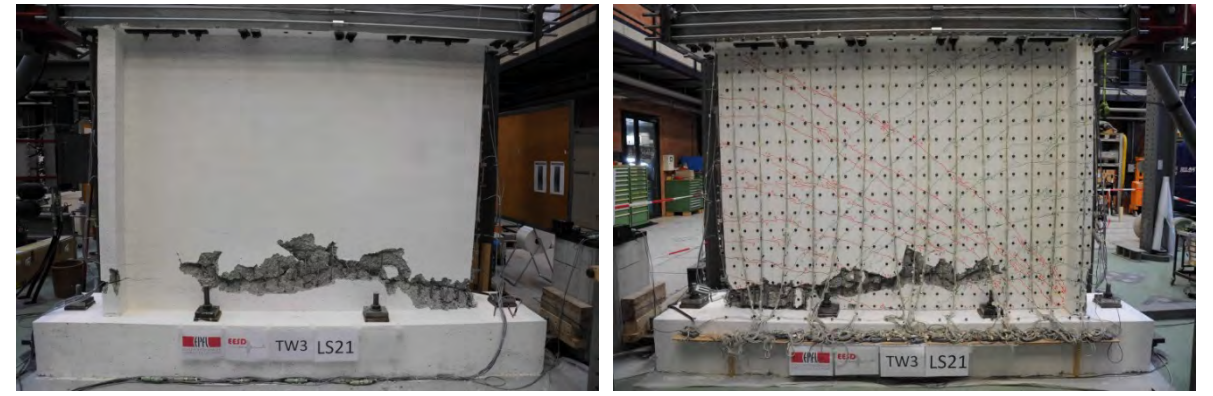

(a) (b)

Figure 36. Load stage LS21: Final condition of wall TW3. Crushing from the web extremity extends throughout a length of 220 cm.

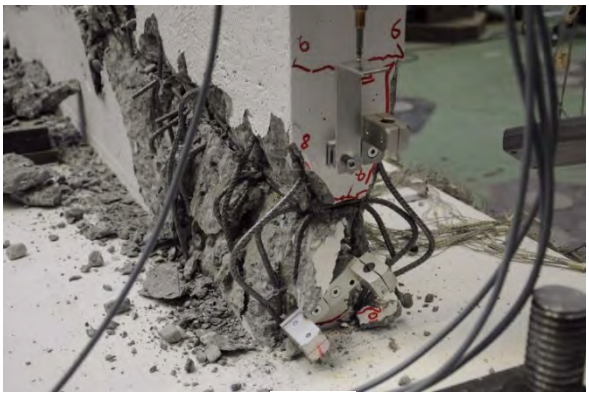

(c)

(d)

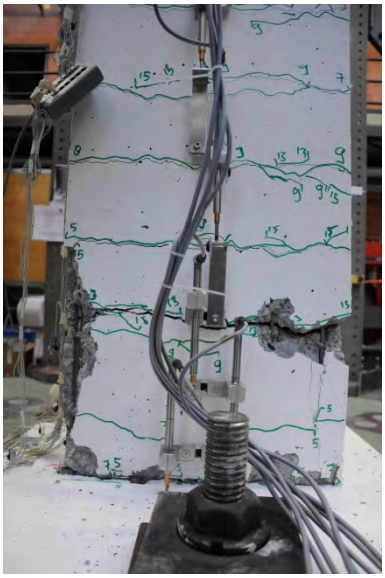

(e)

(f)

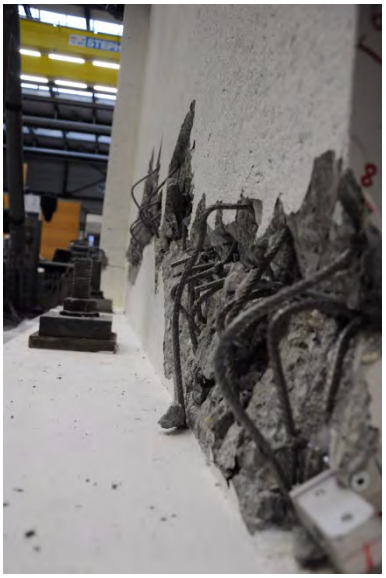

(g)

Figure 36 (cont). Load stage LS21: Final condition of wall TW3. Close-ups of the web and flange regions.

2.4. Conclusions from the Experimental Programme

The test programme comprised two quasi-static cyclic tests on RC walls that are representative of the wall structures constructed in Switzerland between 1950 and 1970. The two walls differed with regard to the splicing of the longitudinal reinforcement. The first test unit (TW2) is a reference test unit with continuous longitudinal reinforcement. The second test unit (TW3) represents the construction practice of the period of interest when longitudinal reinforcement was always spliced above the foundation, i.e., in the zone where large plastic deformations are expected. The lap splice length corresponded to approximately 35 bar diameters, which was considered to be a realistic (average) value for national construction practices of the time. Nevertheless, the review of several construction plans showed that there is some degree of variability regarding the length of the lap splices adopted in different structures. In that sense, it is obviously expected that walls with longer lap splices will depict a behaviour that progressively bridges to that of wall TW2. The results of the latter can also be looked at as being more representative of more modern construction practices in Switzerland.

When loading towards the wall end without flange (negative values of the drifts in the plots), the two test units failed due to crushing of the wall base. A first interesting observation, evidenced in Figure 37, is that the behaviour of the wall in this direction was absolutely identical for both walls. The fact that the presence of lap-splices did not influence the response of the member (at the global level) in

this direction is not surprising. However, it is relevant to note that damage (at the local level) does not concentrate equally in the two test units, which clearly influenced the response of the specimens for loading in the opposite direction. In fact, when loading towards the flange (positive values of the drifts), the experimental test of TW3 showed a softened response with respect to TW2. The lap splice led to a reduction of the deformation capacity by about 50%, from approximately 2% (in wall TW2) to 1% (in TW3). While the drop in resistance of wall TW2 was mainly related to consecutive rebar fractures in tension (i.e., at the web edge). Due to the double longitudinal reinforcement over the length of the lap splice in TW3, deformations concentrate initially in a crack above and below the lap splice. The widths of these cracks can be rather large and led to lap splice failure and bar fracturing.

In order to appraise the behaviour of wall structures within the Swiss building stock, it seems important toappreciate the drift capacities that could be reached without significant loss of strength. Shortly, the tests have shown that–with regard to modern international standards—only low values of drift can be reached with safety, of the order of 0.75% to 1% (either due to crushing at the free edge of the wall, or due to failure associated to a lap-splice mechanism). Whilst such wall performance would be inadmissible for high seismicity regions, it may be acceptable for regions of low to moderate seismicity (as Switzerland), especially if the density of walls prevents large inelastic demands in the building members.

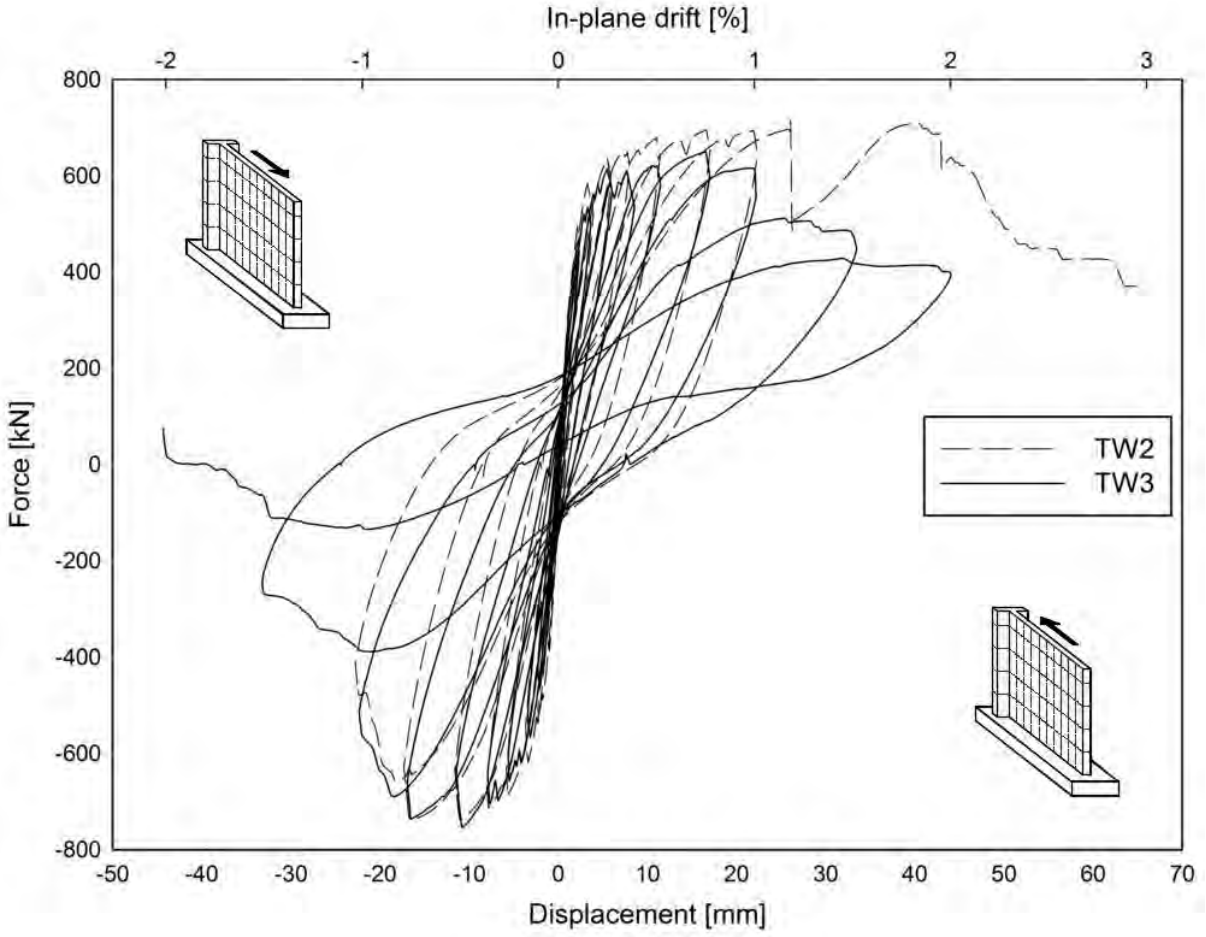

Figure 37. Comparison of the force-drift response of walls TW2 and TW3.

3. ENGINEERING MODELS FOR THE ASSESSMENT OF THIN RC WALLS

3.1. Introduction

Unlike frame structures, shear deformations in RC walls contribute typically in a significant manner to the total deformations even if the walls are designed to develop a flexural mechanism. Since the shear deformations influence the axial strain distribution in the wall section, the RC walls should be ideally modelled using solid, shell or membrane elements. However, due to the large computational costs associated to these models and the expertise required for their setup, RC walls are often analysed using beam element models (Euler-Bernoulli or Timoshenko) or even simple plastic hinge models. For the purpose of the present report, the existing modelling approaches were herein divided into three main categories: plastic hinge analyses (PHAs), distributed plasticity models (DPMs), and shell element models (SEMs). This selection was based on the following criteria: On the one hand, it was intended to use simulation methods of distinct levels of complexity, roughly spanning the existing modelling spectrum. On the other hand, only the approaches and software that are commonly used and available to researchers and specialized engineers were considered.

Theoretical and numerical features of plastic hinge analysis and distributed plasticity models will be analysed in more detail in the following sections. For what concerns nonlinear shell element models, they are powerful simulation techniques that take into account directly the interaction between axial force, flexure and shear (Ile & Reynouard, 2005). Modelling the behaviour of RC members subjected to torsion with beam elements is a very challenging issue (Mazars et al., 2006), and in such case the use of shell elements is again shown to be a suitable option. Although initially limited to research purposes (Sittipunt & Wood, 1993), the increase of computational power is progressively bringing this modelling approach closer to being a practical tool for design engineers, delivering reliable and robust results (Palermo & Vecchio, 2007). Since shell elements, associated to multiaxial constitutive laws, are amongst the available tools of analysis that provide more detailed results, they have been used to improve or calibrate modelling techniques demanding less computational power (Beyer et al., 2014). It should be noted that there are other wall modelling strategies that do not fit clearly into any of the three previously mentioned categories. These hybrid methods traditionally borrow some features from the each approach and in general offer significant additional flexibility in terms of definition of input parameters. Among these hybrid methods the so-called multiple-vertical-line element and ensuing developments (Orakcal et al., 2006), as well as the ‘wide-column models’, composed of an assembly of vertical beam-column elements and horizontal links to represent the wall segments (Beyer et al., 2007, 2008) are particularly often applied when modelling RC wall buildings. Three-dimensional lattice models have also been used for the simulation of the experimental torsional and biaxial cyclic response of RC structural members (Miki & Niwa, 2004). This strategy has been further developed by Yu and Panagiotou (Lu & Panagiotou, 2012, 2014), who apply a 3D beam-truss model for nonplanar RC walls which also accounts for mesh-size effects. They use nonlinear beam and truss elements in the vertical and horizontal directions, nonlinear truss elements in the diagonals to represent the diagonal field of concrete, and linear elastic beams to simulate the out-of-plane stiffness.

Exploring the complex range of available modelling approaches naturally raises interest within the scientific community (Belletti et al., 2013; Beyer et al., 2014; Yazgan & Dazio, 2011). However, most of the comparisons typically focus on the global level of analysis and do not address comprehensively the relation between the latter and the local levels of the mathematical model in consideration. One of the goals of the present study is to compare some of the most common modelling approaches for the simulation of the inelastic behaviour of RC walls. The consideration of shear modelling in the different approaches, confinement effects, and lap-splice modelling, are shortly addressed in sections 3.2.1, 3.2.2 and 3.2.3, respectively.

3.2. Overview

The present section recalls the underlying assumptions and the distinct levels of analysis that are associated to each of the mathematical models used in this study, pointing out how they relate and compare. An effort was made to summarise the most classical features of traditional PHAs, DPMs, and SEMs in Table 3. The distributed plasticity models are further subdivided into displacement-based (DB) and force-based (FB) approaches, since these two beam-column element formulations correspond to fundamentally distinct finite element formulations that yield different results and hence require specific interpretations (Table 4). A solid understanding of the information in the tables below, which should be self-explicative, enables more insightful interpretations of the numerical results and critical comparisons between the approaches. A few pertinent notes follow.

The first short remark relates to the classical plastic hinge analysis (PHA). It was developed for hand calculations in the mid-20th Century. A computational counterpart appeared later on: it is the category of beam-column finite elements that are commonly referred to as lumped (or concentrated) plasticity models (LPMs), wherein a flexural hinge representing the inelastic behaviour is assigned to each extremity of the element. To underline their common root, the ‘plastic hinge analysis’ and ‘lumped plasticity models’ are described together in the first row of Table 3 but the points in which they differ are explicitly indicated by referring to the acronyms ‘PHA’ and ‘LPMs’.

Secondly, it is highlighted that there is a multitude of modelling approaches spanning between the categories pointed out in the tables below. Although it is not possible to address herein all such hybrid proposals, they inevitably share some of the advantages and limitations of the enveloping approaches. Furthermore, the whole spectrum of mathematical models should be looked upon as being composed of complementary—rather than alternative—tools, as there is not an optimal approach as such. For example, in the absence of detailed knowledge about a member or a structure, the most judicious decision is arguably to carry out simple PHA to obtain estimates of possible bounds of the inelastic response; setting up a refined finite element model will most likely ask for unknown (and therefore questionable) assumptions on geometry, detailing, or mechanical characteristics, and the resulting ‘detailed’ outcome will be as trustworthy as the ‘unrefined’ plastic hinge output. A similar type of rationale can also be found in current assessment codes (EN1998-3, 2005).

The third group of observations addresses important issues regarding the different levels of analysis. The inner one, for any modelling approach for the inelastic behaviour of structures, corresponds to the material constitutive relations. The next level in the hierarchy of analysis is the sectional level (herein considered as a local level as well), which is shared by both the PHAs and the DPMs. However, PHA requires a simplified approximation for the moment-curvature relation, traditionally in a bilinear form, whilst DPMs take into account the complete sectional response, considering additionally the explicit and load-dependent interaction between the axial force and the bending moment(s). Another fundamental difference between the two modelling approaches—which again emphasizes the approximate character of the plastic hinge models—lays in the link between the local and the global levels of analysis:

- Plastic Hinge Analysis. After over half a century of proposals on mathematical models for this modelling technique, a universally accepted methodology for PHA has not yet been agreed upon. For a review on the history of PHA models the reader is referred to Hines (Hines, 2002). It is acknowledged that the top lateral displacement of a RC cantilever wall is comprised of flexural, shear and slip displacements. In classical plastic hinge analysis—mainly directed to the analysis of members with large shear span ratios—shear and slip displacements are often

neglected[4]. The remaining total flexural displacement is composed of yield and plastic components, which are computed based on *assumed* curvature profiles along the member height. They have been the subject of different proposals [37], which produce distinct estimates of both yield and plastic displacements. Such differences are mainly related to: (i) the fact that the assumed curvature profiles account differently for the influence of tensile strain penetration and the spread of plasticity caused by the presence of diagonal cracks (tension shift), and (ii) the mathematical hypotheses to compute the plastic displacements: although PHAs are based on assuming constant inelastic curvatures over an *equivalent plastic hinge length* L_p, some approaches consider the centre of this plastic rotation at midheight of the plastic hinge (Paulay & Priestley, 1992), while others assume it at the member end (Priestley et al., 2007).

However, the most critical parameter in the link between the sectional level (i.e., yield and ultimate moments and curvatures) and the global level of analysis (i.e., yield and ultimate top lateral displacements of the member) in PHA is the formula for the equivalent plastic hinge length. It should be apparent, from the discussion above, that L_p: (i) is a fictitious pseudo-empirical length from which the plastic displacements can be computed, calibrated to match the results of a selected data pool of experimental tests, and (ii) depends on the hypotheses of the PHA model, in particular the assumed curvature profile, deformation mechanisms considered, type of material and members forming the data pool (beams, columns, walls), etc. (iii) plastic hinge length, strain limits and PHA formulations should only be used in combinations that were calibrated against experimental results. Unfortunately, applications on earthquake engineering often tend to employ indistinctly the many existing formulae for L_p, without regards for the corresponding assumptions of the mathematical model. This is currently one of the main problems associated with this modelling approach.

Terminological misuses have however seen other regrettable developments. In fact, the very large number of proposals for the equivalent plastic hinge length (Arbulu, 2006) has led many authors to simplify the term to ‘plastic hinge length’. The elimination of an explicit reference to the *equivalent* character of L_p—as established above, it is a fictitious (conventional) quantity—has opened the doors to additionally mixing it up with the concept of *real* plastic hinge length (or, reworded for clarity: ‘length of the plastic hinge’). The absence of a universally accepted definition for the latter, as discussed further down, has further aggravated this flawed fusion of meanings.

The previous *status quo* has constrained some researchers to consciously avoid altogether the term ‘plastic hinge length’ as a synonym of the *real*[5] (physical) length of the plastic hinge. Alternative nomenclatures have therefore emerged, often related to flexure-controlled members: some authors mention a ‘length of plastification’ that represents the actual length over which the ‘real distribution of plastic curvatures’ extend (Fardis, 2009); others use the expression ‘critical region length’, defined as ‘the extent of the member region that needs to be confined effectively by transverse reinforcement so that the member can behave according to the performance level (in terms of flexural ductility) set by the designer’ (Pam & Ho, 2009); others, still, use the expression ‘severely damaged region’ (Bae & Bayrak, 2008), or opt for the even more general and less compromising designation of ‘characteristic length’, taken as the ‘physical size of the region into which the strain can localize and the dissipative softening effects take place’ (Almeida et al., 2012).

It is noted that although an established definition for the *real* plastic hinge length is still missing, as mentioned above, it should reflect the damaged member region wherein spalling of concrete cover with penetration into the core region is observed, as well as local buckling or

[4] Proposals for plastic hinge analyses wherein shear displacements are accounted for will be analysed in the present document; they can be useful to estimate wall behaviour.

[5] As opposed to *equivalent.*

yielding of longitudinal rebars, and/or yielding of transversal steel. The deterioration of nomenclature has consequences to engineering practice in design and assessment.

- Distributed Plasticity Models. In this category of models it is not necessary to specify a value for the *plastic hinge length* to connect the local level of analysis to the global (element) level of analysis. This comes out as a consequence of the employed formulations (see Table 4 for details on the two main approaches), which allow the spread of inelasticity throughout several control sections along the member. Phenomena such as strain penetration or tension shift, which are in general indirectly accounted for in the equivalent plastic hinge length for PHAs, would have to be considered separately for distributed plasticity models but standard approaches are yet to be established. Shear and slip deformations also require *ad hoc* modelling techniques.

  However, DPMs are not exempt from the consideration of a quantity related to the formation of a plastic hinge. This is due to the occurrence of a numerical feature named localization, which occurs after the peak of the moment-curvature curve (in the controlling section wherein it is first attained), i.e. during the softening part of the response. In order to counteract this phenomena, a regularization method should be applied but is often not available in standard finite element codes. Regularization requires the specification of a regularization length (Almeida et al., 2012; Coleman & Spacone, 2001; Scott & Fenves, 2006), which should be the *real* plastic hinge length (or, as discussed above, the 'length of plastification', 'critical region length', 'severely damaged region', or 'characteristic length') and not the equivalent plastic hinge length.

Finally, it is noted that the present work does not focus on nonlinear geometrical effects. Although they play a negligible role for the numerical examples addressed later, they have been explicitly considered in the analysis with distributed plasticity models and refined membrane models (Crisfield, 1990; Wong et al., 2013).

Table 3. Overview of the main features of the modelling approaches under comparison.

MODELLING APPROACH	ACCURACY	COMPUTATIONAL COST	EASE OF USE (SETTING UP MODEL)	MODELLING OF PHYSICAL PHENOMENA				
				Flexural Deformation	Shear Deformation (and Flexure-Shear Interaction)	Tension Shift	Anchorage Slip (Strain Penetration)	P-Δ Effects
PLASTIC HINGE ANALYSIS (PHA) / LUMPED PLASTICITY MODELS (LPMs)	↓ From the considered modelling approaches, it is the crudest simulation technique. ↓ The accuracy of the results strongly depends on the formula for the equivalent plastic hinge length L_p. ↓ (PHA) Local EDPs (e.g., strains) should not be back-calculated from the results of the analyses. ↓ (PHA) It can only capture the response of a member.	↑ (PHA) The method can be implemented in a spreadsheet (associated to a sectional analsis procedure to compute the moment-curvature). ↑ (LPMs) Computational time is small, allowing to carry out simple sensitivity studies.	↑ (PHA) The method is easily set up with the aid of a spreadsheet. ↓ Experience is required to choose L_p (PHA) and the moment-rotation envelope (LPMs). ↓ (LPMs) The selection of a set of rules for the hysteretic moment-rotation behaviour is not straightforward.	• It is considered lumped at a pre-defined plastic hinge location.	↓ There are several proposals to account for shear deformations in PHA, but the limitations of the base assumptions of this method prove in general to be an obstacle to increased accuracy. ↓ Similar difficulties are found with LPMs.	• (PHA) These phenomena are indirectly accounted for in the expression for L_p. ↓ (LPMs) It is often unclear if they are considered in the moment-rotation relations.		↑ (LPMs) They can be accounted for in the FE formulation. ↓ (PHA) Usually, they are not considered.
DISTRIBUTED PLASTICITY MODELS (DPMs)	↑ It is possible to use local EDPs (e.g., strain demands in specific fibres) from the analyses. • In general, it provides satisfactory results for members behaving mainly in flexure.	• For structures composed of many elements and a large number of fibres per section, computing time can increase considerably for nonlinear dynamic time-histories. Pushover analyses are however generally fast.	↑ Hysteretic behaviour is implicitly defined at the uniaxial material stress-strain level. ↓ The definition of the integration scheme and number of integration sections requires expertise (type of formulation, localization issues, etc).	↑ DPMs capture flexural deformation and its spread along an assumed number of integration sections along the element (see Table 2-2).	• It is a topic of active research. It typically implies moving from the framework of Euler-Bernoulli to Timoshenko beam theory, which complicates the development of the model (and the requirements for material constitutive relations).	↓ It is not considered in the model. Some authors try to indirectly simulate it with DB elements (see Table 2-2) of calibrated length.	↓ Requires explicit (separate) modelling, e.g. with a 'zero-length' element.	↑ They can be accounted for in the FE formulation.
SHELL ELEMENT MODELS (SEMs)	- If full knowledge on the member geometry, detailing, and material mechanical properties is available, SEMs provide the most refined simulation output. - The details of the structural member along its height can be explicitly modelled, avoiding the need to 'lump' the behaviour of the member into integration sections (DPMs) or plastic hinges (PHA / LPMs).	↓ This modelling technique imposes by far the largest computational burden, hence it is suitable for research purposes (or very specialized engineering applications).	↓ Setting up the model can be time-consuming, especially if the geometry, detailing, or material properties are non-uniform. ↓ The computational cost of the analyses, alongside the model set-up, usually limit the simulation to a single member or a very small number of elements and load cases.	↑ Flexure, shear and flexure-shear interaction are directly accounted for at the level of material constitutive relations. Refining the mesh of finite elements in the 2 (or 3) dimensions improves the quality of the results, allowing for an explicit modelling of the effect of tension shift, which can be important in RC walls.			↓ Requires explicit (separate) modelling. There is little available guidance on how to simulate it reliably.	↑ They can be accounted for in the FE formulation.

MODELLING APPROACH (cont.)	LEVELS OF ANALYSIS			CONSIDERATION OF THE DEVELOPMENT OF A PLASTIC HINGE	NUMERICAL LOCALIZATION ISSUES
	CONSTITUTIVE RELATIONS (LOCAL LEVEL)	SECTIONAL RESPONSE (LOCAL LEVEL)	ELEMENT RESPONSE (GLOBAL LEVEL)		
PLASTIC HINGE ANALYSES (PHA) / LUMPED PLASTICITY MODELS (LPMs)	1D Material Laws ↑ The models are easier to understand, interpret, and validate than evolved 2D/3D constitutive laws. ↑ (DPMs) Hysteretic behaviour is implicitly defined at the uniaxial material strain-stress level. • (LPMs) Lumped plasticity models may include hysteretic rules for the hinge behaviour, which can account for many physical phenomena (e.g. cyclic degradation in stiffness and strength, pinching under reversal, etc). However, the choice *a priori* of the most suitable model is far from straightforward. ↓ 2D and 3D features of the concrete behaviour cannot be directly simulated, such as confinement, compression softening, lateral expansion, etc.	↓ (PHA) It uses an approximation (typically bilinear) of the original moment-curvature curve for a particular value of N (recommended to be obtained from an elastic analysis under gravity loading). ↓ It does not account for the bending moment -(varying) axial force interaction.	↓ Assumes that plasticity concentrates in the element ends. This hypothesis is typically valid for walls and columns, while it may be unsuitable for beams and girders: gravity loads may shift the plastic hinges away from member ends. ↓ (PHA) Results are highly dependent on the accuracy of the formula for the equivalent plastic hinge length L_p. ↓ If a bilinear approximation of the moment-curvature relation is used (assuming a positive post-yield slope), it is not possible to model the softening branch of the response. This is the case of classical PHA, and in general also the case of LPMs.	• (PHA) It is reflected by the equivalent plastic hinge length L_p: this parameter does not stand for itself, it is associated to the specific set of hypotheses of the particular PHA in use (assumed curvature profile, deformation mechanisms considered, etc). ↓ (PHA) Existing formulae for L_p were calibrated to produce matching predictions of experimentally measured ultimate displacements; therefore they are not, in theory, applicable to predict the full member response. ↓ (LPMs) The same dependance on the equivalent plastic hinge length can be found, either directly or indirectly via the definition of the moment-rotation relation.	• (PHA) Classical plastic hinge analyses do not show localization issues, but neither do they capture the post-peak member response. ↓ (LPMs) Localization occurs if a trilinear approximation of the moment-curvature relation with a softening branch is defined for the plastic hinge.
DISTRIBUTED PLASTICITY MODELS (DPMs)		↑ No approximation is required for the moment-curvature curve. ↑ Bending moment-(varying) axial force interaction is directly modelled. This is usually not fundamental for beams or girders, which have a small level of axial force. However, if the overturning moment in the structure is significant, the axial force in the columns can vary considerably and therefore the interaction may become very relevant.	• The response is highly dependent on the finite element formulation. Shortly, two main types of approaches exist: displacement-based and force-based (see Table 2-2). Expertise is required to select sensible discretization options.	↑ DPMs do not require non-local parameters to simulate the pre-peak branch of the member behaviour, since inelasticity can spread along the integration sections of the element. • The post-peak response is however dependent on the discretization options assumed for the member. In such phase it is fundamental to try to relate them to the physical characteristics of the development of a plastic hinge (see next column).	• During the post-peak (softening) response, a regularization technique is required to counteract localization issues. It should make use of an expression for the *real* plastic hinge length (not to be confused with the equivalent plastic hinge length L_p, see discussion in the text).
SHELL ELEMENT MODELS (SEMs)	2D / 3D Material Laws ↑ They are the most accurate ones, as they reflect the 'real' behaviour of the material. ↓ Due to the complexity of these constitutive laws, it is not always easy to interpret the results and debug inaccurate or unexpected output.	↑ Such level does not exist, which simplifies the connection to the level of element response. ↓ Quantities that are familiar to the engineer, such as bending moment and curvature, do not exist; the latter, which can be required for design computations, can only be (approximately) obtained through post-processing operations.	↑ Membrane or shell finite elements are relatively easy to understand by the engineer, especially if simple formulations are employed (which is typically the case, e.g. elements with a reduced number of nodes).	↑ Like DPMs, SEMs do not require non-local parameters to simulate the pre-peak branch of the member behaviour. • Again similarly to DPMs, the post-peak response depends on the assumed FE discretization. A connection with the real spread of damage along the member is therefore required (see next column).	• The occurrence of localization in SEMs is a numerical issue that can be tentatively regularized by one of the available methods. Unfortunately, such techniques are often not included in FE software and there are few validations of their application to the inelastic behaviour of RC members. It can therefore be difficult to control these effects.

Table 4. Simplified comparative overview on displacement-based vs force-based formulations.

DISTRIBUTED PLASTICITY MODELS	DISPLACEMENT-BASED FORMULATION (DB)	FORCE-BASED FORMULATION (FB)
HYPOTHESES	• Assumed displacement field along the element: cubic Hermitian polynomials for the transverse displacement field and linear Lagrangian interpolation functions for the axial displacement ⇒ Linear curvature and constant axial strain (at the reference axis) along the element.	• The force field is obtained through an exact solution of the differential equations of equilibrium. E.g., for nodal loading it corresponds to a linear Lagrangian shape function for the bending moment and a constant approximating polynomial for the axial force along the element.
FINITE ELEMENT IMPLEMENTATION	↑ Straightforward state determination algorithm, corresponding to classical finite element implementation (no iterative routines are involved).	↓ The inter-element continuity of displacements is more difficult to enforce, requiring an iterative solution algorithm based on the transference of residual deformations from the section level to the element level. Actually, both residual displacements (at the section and at the element level) can be accepted,which further skips the need for iterations during the element-section state determination.
ACCURACY	↓ DB elements only provide the exact solution for the problem of an element with linear elastic material subjected to nodal forces. Linear curvature and constant axial strain at the reference axis along the element are unsatisfactory for nonlinear analysis and/or members subjected to span loads. ↓ Equilibrium is only verified in average, which leads to a number of critical issues: unrealistic variations of axial force between different integration sections of the element, inaccurate sectional response, etc. ↓ 'Artificial' consideration of span loads.	↑ FB elements always provide the exact solution for frame problems since the corresponding interpolation functions satisfy the beam equilibrium equations exactly (i.e., in a strict sense), irrespective of the material constitutive behavior (even if highly nonlinear), which explains the formulation appropriateness for nonlinear analysis. ↑ Direct (exact) consideration of the effects of span loads.
APPLICATIONS	↑ DB elements are still widely used because: (i) many FE software are still based on this approach, (ii) curvature and strain demands in the sections are generally smaller than with exact FB elements, which is sometimes convenient, (iii) some authors use it to indirectly simulate other physical phenomena such as tension shift. • It provides a stiffer and stronger prediction of the objective ('exact') response. ↓ Meshing of the member into several elements is required to capture the nonlinear structural response or the behaviour of members subjected to span loads.	↑ No meshing is theoretically required, i.e. only a single FE is required to model each structural member. • It provides a more flexible prediction of the objective ('exact') response. • The analyst should evaluate whether, in order to build a proper mass matrix for dynamic loadings, more than one element should be used.
LOCALIZATION	• Localization can occur in all the integration sections of the element. In such a case, the length of the most strained member corresponds to the *real* plastic hinge length, which can be used as a regularization criterion.	• Localization takes place in only one integration section (the one where the demand is higher). There are a few regularization techniques available to obtain objective results, which require the specification of the *real* plastic hinge length.

3.2.1. Shear Deformation

As stated before, shear deformations in wall-type structures can be a significant portion of the total deformation and thus should in general be modelled. A review of results from quasi-static cyclic tests on RC walls showed that the ratio of shear to flexural deformation remains approximately constant if the wall is deforming in flexure and increases if the wall is deforming in shear (Beyer et al., 2011). For walls subjected to in-plane loading that failed in flexure and had shear span ratios larger than 2.0, the ratio of shear to flexural deformations determined from experimental results varied between 5 and 40% and depended mainly on the ratio of compression zone depth to wall length and the shear span ratio (Beyer et al., 2011). The rule-of-thumb $L_s/h>3$ is useful to select members wherein the impact of shear deformations on local and global EDPs will be small and can therefore be neglected (Priestley et al., 2007). If the ratio of shear to flexural displacements is less than approximately 10%, its effect on EDPs in statically determined systems is typically small. Note, however, that the shear flexibility can influence the force distribution in statically indetermined systems even if the shear flexibility is low (Beyer et al., 2008, 2014). Shear deformations, as well as shear-flexure interaction, can be accounted for in different ways depending on the chosen modelling approach (Lodhi & Sezen, 2012). Hereinafter they are briefly discussed for PHA, DPMs, and SEMs.

Three well-known methods of PHA accounting for shear deformations available in the literature are now addressed. They are based on the observation that the shear to flexural deformation ratio (Δ_s/Δ_f) of flexure-dominated walls is roughly constant in the inelastic phase of the response (Dazio et al., 2009). A first proposal for the evaluation of the abovementioned ratio was made by Hines et al. (Hines et al., 2004), as a function of the shear span ratio, the crack angle, and a correction factor accounting for the increase in shear deformations due to poor transversal reinforcement or thin webs. More recently, Priestley et al. (Priestley et al., 2007), based on the work of Miranda et al. (Miranda et al., 2005), suggested a method that takes into account three different stages of the response: (i) prior to

shear cracking, elastic shear stiffness is proportional to the reduction in flexural stiffness; (ii) in-between shear cracking and the attainment of the nominal flexural strength, shear stiffness is computed according to the strut and tie model proposed by Park and Paulay (Park & Paulay, 1975); (iii) in the inelastic range, the ratio Δ_s/Δ_f is assumed to be constant. Finally, the equation proposed by Beyer et al. (Beyer et al., 2011) indicated in section 3.3.1, to compute the ratio Δ_s/Δ_f, accounts for the curvature demand, crack angle, shear span, and the novel additional influence of the mean axial strain in the shear deformations. The latter is the method adopted in the present study. Several LPMs, as finite element counterparts of PHA, can obviously also account for shear deformation and flexure-shear interaction through similar or alternative assumptions (Lodhi & Sezen, 2012; Xu & Zhang, 2011; Zhang, Xu, & Tang, 2011).

For DPMs, the consideration of shear deformation requires an extension of the classical Euler-Bernoulli beam theory hypothesis, i.e. plane sections can no longer be assumed perpendicular to the deformed beam axis. Hence, a Timoshenko framework is generally considered, either associated to a displacement-based formulation (Ceresa et al., 2009; Guedes & Pinto, 1997; Mazars et al., 2006; Navarro Gregori, Miguel Sosa, Fernández Prada, & Filippou, 2007) or a force-based approach (Marini & Spacone, 2007; Petrangeli, 1996; Remino, 2004). Timoshenko hypothesis implies a constant shear strain profile throughout the section. However, other more advanced shear strain profiles have also been considered in the literature, for instance parabolic patterns which satisfy equilibrium during elastic behaviour (Petrangeli et al., 1999). Additionally, coupling between shear and flexural deformation mechanisms was also modelled in a simplified way with displacement-based (Martinelli, 2002) and force-based element approaches (Mergos & Beyer, 2013; Ranzo & Petrangeli, 1998). Unfortunately, the previous proposals for coupling shear and flexural deformations are not readily available in existing structural analysis software and thence they were not considered in the present study.

In SEMs, the shear deformation is directly accounted for by the membrane element formulation, which requires a bidimensional or tridimensional constitutive model. In the application example, simulated with VecTor2 (Wong et al., 2014), a plane stress rectangle is used in association with the Modified Compression Field Theory (Vecchio & Collins, 1986) and the Disturbed Stress Field Theory (Vecchio, 2000).

3.2.2.Accounting for Confinement in Different Approaches

The effect of active and passive confinement of concrete has raised the interest of researchers since the 1920s (Richart, Brandtzaeg, & Brown, 1928). Confinement increases the strength and the deformation capacity of concrete. However, it also plays a role in other phenomena such as the brittle-to-ductile transition under confinement (Imran & Pantazopoulou, 1997). The way to account for confinement effects depends on the framework wherein the concrete constitutive model is developed: nonlinear elasticity, plasticity theory, damage theory, fracture mechanics, etc. Therefore, the three modelling approaches employed in this study (PHA, DPMs, SEMs) ask for distinct considerations.

The computation of the sectional response in PHAs and DPMs requires the cross-sectional integration of uniaxial stress-strain curves defined for each concrete fibre. Those relations are adjusted through confinement models, which typically use a coefficient to compute the compressive strength of confined concrete f'_{cc} from the specified cylinder strength f'_{c}. That coefficient depends on the passive confinement produced by the reaction of the transverse reinforcement to the lateral expansion of the concrete. A distinct coefficient, also function of the confining stresses, allows obtaining the confined concrete strain at maximum strength ε_{cc} from its unconfined counterpart ε_{c}.

Many uniaxial concrete models assume that such confining stresses (and strains) are similar in the two lateral directions (Samani & Attard, 2012). However, indications are often missing on how to derive this uniform lateral pressure for the case of RC members such as walls. Other proposals, where confining stresses are also assumed to be identical in both directions, do however provide explicit recommendations in that regard, e.g., the one proposed by Cusson and Paultre (Cusson & Paultre, 1995). The renowned model by Mander et al. (Mander et al., 1988) considers the possibility of having different confining stresses in the two lateral directions, and indicates how to compute them for RC members. The failure surface described by Willam and Warnke (Willam & Warnke, 1974) is then used to obtain f'_{cc}. The corresponding strain is obtained following the indications of Richart et al. (Richart et al., 1928). This model is of more straightforward application than the model by Cusson and Paultre (Cusson & Paultre, 1995), and will thus be adopted for the case study.

It is noted that the simpler form of the model by Mander et al. (Mander et al., 1988) is mainly related to the assumption that the lateral confining pressure is developed from equilibrium with transverse reinforcement at yield. Such hypothesis is not considered in the work by Cusson and Paultre (Cusson & Paultre, 1995), who use an iterative approach to compute the stress in the transverse reinforcement at the peak concrete strength. The introduction of the previous adjustments were based on the findings by Cusson and Paultre (Cusson & Paultre, 1994), who showed that the yield strength may not be reached with low confinement or when transverse reinforcement is made of high-strength steel. A more recent improvement of the model, made by Légeron and Paultre (Légeron & Paultre, 2003), proposes a direct procedure to compute the transverse reinforcement stress and consequently the equivalent confinement pressure.

The concrete models that provide direct applications to RC behaviour make use, in general, of a geometrical effectiveness coefficient of confinement. Originally developed by Sheikh and Uzumeri (Sheikh & Uzumeri, 1982), it reflects the effectiveness of the transverse reinforcement in confining the concrete and accounts for the fact that the maximum lateral pressure due to transverse reinforcement is not uniformly applied throughout the volume of the concrete core. Midway between the layers of transverse reinforcement, the area of effectively confined concrete is minimal due to arching action and can be computed from the spacing and tie configuration.

3.2.3.Lap-Splices

In order to facilitate building construction, lap splices in RC walls were based just above the foundation, i.e., in the region that undergoes the largest plastic deformations. The underlying rationale for the use of this technique is that the force can be transferred from one bar to another via the concrete surrounding the bars. However, if the length of such lap-splice is small, failure may take place when the member is subjected to horizontal loads. Under monotonic loading, the lap splice might fail due to cracking of the concrete under tension. Under cyclic loading, the concrete surrounding the bars is subjected to alternating compression and tension. Under such loading conditions the lap splice failure might also be initiated due to vertical splitting cracks that develop when the wall end is in compression. Upon load reversal the concrete may no longer be able to resist the horizontal tensile stresses that would be required to transfer the tensile loads from one bar to another. This compression failure of the lap splice often occurs after the onset of yielding of the wall. Hence, the wall is often capable of developing its full moment resistance but the deformation capacity of the wall can be significantly reduced when compared to walls without lap splices at the wall base.

Modelling the lap splice behaviour directly is very challenging as it requires the explicit modelling of the bars and non-perfect bond laws. Literature review shows that it has only been successfully achieved in very few cases, wherein the authors make use of very specific models that are not available in advanced structural analysis software for engineering practice. Besides, the lack of general recommendations for modelling purposes is worrisome. For this reason, lap splices are typically not

included in wall models but the effect of their presence is accounted for by reducing the failure strain limits. Such an approach is outlined in section 3.3.3.

3.3. Comparison of Numerical Simulations to Experimental Results

3.3.1. Modelling Approaches

Within the scope of the present work, it is noted that only the SEMs accurately account for shear deformations. These models will be used as benchmark to assess the extent to which pure flexural models, such as beam elements based on the Euler-Bernoulli hypothesis, can capture responses that have non-negligible shear deformations. It should be underlined that the authors not only wish to validate the results of different modelling approaches against experimental results, but also to evaluate and interpret the scatter of the response provided by distinct state-of-the-practice simulation methods that build on the same (or as-close-as-possible) input parameters, constitutive relations, confinement models, etc. Still, for each simulation technique there is a large number of non-obvious modelling choices (mesh discretization, certain parameters in the material models, confinement definition, etc.) that affect the outcome of the inelastic analyses. Furthermore, there is also typically a significant level of uncertainty associated to several geometrical characteristics, material properties, or reinforcement details of the RC specimen. The two facts above combined make it generally possible to justify combinations of these modelling degrees of freedom that show a versatile, at times surprising, ability to match selected experimental results.

Three different modelling techniques are used to simulate the response of the wall described in the previous section. As indicated in Table 3, they rank in ascending order of complexity as follows: plastic hinge analyses (PHAs), distributed plasticity models (DPMs) and shell element models (SEMs). The specificities of each model employed in the analyses are thoroughly described in the following paragraphs.

Two plastic hinge models were considered. The first, which does not account for shear deformations, is based on the flexural PHA formulation proposed by Priestley et al. (Priestley et al., 2007), with the adaptations therein suggested for wall-type structures. The equivalent plastic hinge length is expressed as:

$$L_p = kL_s + 0.2h + L_{sp} \geq 2L_{sp} \tag{1}$$

where k is a factor accounting for the spread of plasticity due to strain hardening of the reinforcement, L_s is the shear span (distance from the point of contraflexure to the critical section of the member), $0.2h$ is an additional term accounting for the effect that tension shift plays on walls, and L_{sp} is the strain penetration length which is given by:

$$L_{sp} = 0.22 f_{yl} d_{bl} \tag{2}$$

with f_{yl} and d_{bl} being the yield strength and diameter of the longitudinal reinforcement. The ultimate flexural displacement is the sum of the yield and plastic flexural displacements:

$$\Delta_u = \Delta_{yf} + \Delta_{pf} = \frac{\emptyset_y}{3}\left(L_s + L_{sp}\right)^2 + \left(\emptyset_u - \emptyset_y\right) L_p \left(L_s - \left(0.5L_p - L_{sp}\right)\right) \tag{3}$$

The yield and ultimate curvatures were obtained from the bilinear idealization of the moment-curvature curve. The sectional analysis was performed with the open source software OpenSees (OpenSees, 2013)—herein labelled as 'OS'—discretising the section into 200 fibers. Cover and core concrete were modelled using the library uniaxial material 'Concrete 04', which is based on the model proposed by Popovics (Popovics, 1973). The mechanical properties of the core concrete were

determined according to Mander et al. (Mander et al., 1988) with a geometrical effectiveness coefficient of confinement C_e=0.5, as recommended by Priestley et al. (Priestley et al., 2007) for wall-type elements. The concrete parameters used in the models can be found in Table 5. The Dodd Restrepo model was used for the reinforcement bars because, as shown in Figure 39(c), it represented the solution that best fitted the experimental data (Table 6). Rebar buckling was not considered in the model.

The second PHA model, which accounts for shear deformation, was the one developed by Beyer et al. (Beyer et al., 2011). In this model, the total deformation is computed as the flexural deformation times the ratio of shear to flexural deformations:

$$\Delta_u = \left(\Delta_{yf} + \Delta_{pf}\right)\left(1 + \frac{\Delta_s}{\Delta_f}\right) \tag{4}$$

The ratio of shear-to-flexural deformation can be estimated as:

$$\frac{\Delta_s}{\Delta_f} = 1.5\,\frac{\varepsilon_l}{\phi tan\theta}\frac{1}{L_s} \tag{5}$$

where ε_l is the longitudinal strain along the centroidal axis of the wall, L_s is the shear span, ϕ is the curvature demand. ε_l and ϕ are derived from moment-curvature analysis for a maximum steel strain of 1.5%. θ is the crack angle at the top of the fan-like mechanism which, according to Hagsten et al. (Hagsten, Hestbech, & Fisker, 2011) and used by Hannewald (Hannewald, 2013), can be expressed in function of the reinforcement ratios:

$$\theta = arctan\left(\sqrt[4]{\frac{\rho_v + k_E\rho_h\rho_v}{\rho_h + k_E\rho_h\rho_v}}\right) \tag{6}$$

in which k_E is the ratio between the steel and the concrete elasticity moduli, while ρ_v and ρ_h are the geometrical reinforcement contents in the vertical and horizontal direction.

For the distributed plasticity models (DPMs), three distinct modelling options were considered to simulate the behaviour of the cantilever wall. They differed with regard to the beam element formulation (displacement-based vs. force-based, see Table 4), mesh discretization, and numerical integration scheme; their features are summarized in Table 7 and shown in Figure 38.

As indicated in Table 4, force-based formulations verify exactly beam equilibrium. Therefore, only one element was assigned to model the structural member. Additionally, in order to simulate the concentration of inelasticity at the wall base, a Gauss-Lobatto quadrature is preferred to a Gauss-Legendre quadrature since the former features an integration point at the element end and therefore at the wall base while the latter does not. During the pre-peak branch of the moment-curvature, the element response is a function of the numerical accuracy of the integration rule, and it has been shown that typically five integration points (IPs) are sufficient (Neuenhofer & Filippou, 1997). However, since the post-peak element response is highly dependent on the number of IPs, an additional scheme with nine IPs was also considered.

Table 5. Concrete properties used for modelling walls TW2 and TW3.

TW2, UNCONFINED CONCRETE				
Model	**Mechanical Properties**			
Popovics-Mander	f'_c	ε_c	E_c	f'_t
	[MPa]	[‰]	[MPa]	[MPa]
	50.7	2	31750	2

TW3, UNCONFINED CONCRETE				
Model	**Mechanical Properties**			
Popovics-Mander	f'_c	ε_c	E_c	f'_t
	[MPa]	[‰]	[MPa]	[MPa]
	43.3	2	30200	2

TW2, CONFINED CONCRETE				
Model	**Mechanical Properties**			
Popovics-Mander	f'_{cc}	ε_{cc}	E_{cc}	f'_{ct}
	[MPa]	[‰]	[MPa]	[MPa]
	55	2.86	31750	2

TW3, CONFINED CONCRETE				
Model	**Mechanical Properties**			
Popovics-Mander	f'_{cc}	ε_{cc}	E_{cc}	f'_{ct}
	[MPa]	[‰]	[MPa]	[MPa]
	47.4	3	30200	2

Table 6. Steel properties used for modelling walls TW2 and TW3.

Model	**Mechanical Properties**					
Dodd-Restrepo	f_y	f_u	E_s	ε_{sy}	ε_{sh}	ε_{su}
	[MPa]	[MPa]	[MPa]	[‰]	[‰]	[‰]
	465	620	200000	2.5	2.5	80

Table 7. Description of Distributed Plasticity Models (DPMs) used in the analyses.

Model	**Element type**	**N° elements**	**N° Integration Points**	**Integration Rule**
OS-FB-5IP	Force-Based	1	5	Gauss-Lobatto
OS-FB-9IP	Force-Based	1	9	Gauss-Lobatto
OS-DB-PH*	Displacement-Based	4	2	Gauss-Legendre

* The length of the element close to the base corresponds to the equivalent plastic hinge length.

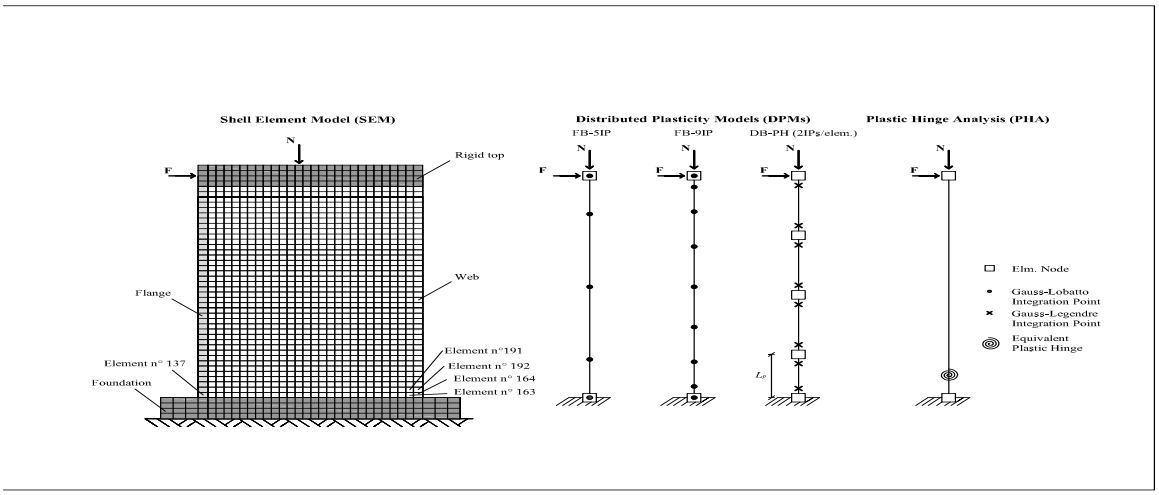

Figure 38. Employed modelling techniques for the simulation of the wall responses.

On the other hand, the displacement-based model discretized the member in four elements, each one with two Gauss-Legendre IPs. The reasons for the choice of this discretization is linked to the displacement interpolation functions of the DB finite element and is based on the findings by Calabrese et al. (Calabrese et al., 2010). It is noted that the length of the bottom element was defined as the equivalent plastic hinge length L_p given by eq. (1). Following the discussion in section 3.2, it should be underlined that the *real* plastic hinge length should have been used instead of the equivalent plastic hinge length. Unfortunately, there are still relatively few expressions in the literature for the *real* plastic hinge length that have been sufficiently validated.

The software used to carry out the analysis of the DPMs was OpenSees. The sectional discretization and the materials employed were the same described above regarding the moment-curvature analysis. Another goal of the study was to assess the differences between existing structural analysis packages that build on distinct uniaxial material models, as well as numerical implementations of finite element formulations and respective solutions. Therefore, the case of a FB element with 5 IPs was also analysed using the FE software SeismoStruct (SeismoSoft, 2013)—herein labelled as 'SS'—giving rise to the model 'SS-FB-5IP'. In both Seismostruct and OpenSees, the material model used to describe the concrete follows the constitutive relationship proposed by Popovics (Popovics, 1973). The model matching between the concrete models adopted in OpenSees and SeismoStruct is almost perfect, as shown in Figure 39 (a) and (b). On the other hand, it was not possible to find a steel constitutive law fitting properly the experimental results. Hence, the model by Menegotto and Pinto (Menegotto & Pinto, 1973) with the isotropic hardening rules proposed by Filippou et al. (Filippou, Popov, & Bertero, 1983) was employed, as depicted in Figure 39 (c).

The shell element simulation was carried out with 2D membrane software VecTor2 (Wong et al., 2014), designated as 'V2' in the figures, developed at the *University of Toronto* and based on the Modified Compression Field Theory (Vecchio & Collins, 1986). The structure is discretized by plane stress rectangles of RC material with smeared reinforcement (see Figure 38). The monotonic steel stress-strain curve is composed of three parts: an elastic branch, a yield plateau, and a nonlinear strain hardening phase until rupture. Besides the material properties, also the reinforcement ratios in the three directions of the reference system have to be given as input. They are reported in Table 1, both for the elements of the web and flange. The concrete constitutive law in the principal compressive direction follows the stress-strain relationship proposed by Popovics (Popovics, 1973) for normal strength concrete (as used in the OpenSees models). The cover concrete was not modelled because it

was shown not to be significant neither at the global nor at the local levels at the damage control limit state. Additionally, numerical accuracy concerns recommend aspect ratios below 3:2 for membrane mesh elements, which would require an extremely fine mesh for the concrete cover in the current wall.

The base model implemented in VecTor2 considered confinement effects by assigning explicitly the same peak strength and associated strain indicated above for the sectional analyses. Automatic strength enhancement due to confinement was disregarded, as well as all the other material effects available in the software (such as compression softening, tension softening, tension stiffening, dilation, etc.). This choice relates to the purpose of comparing the scatter of the response provided by different modelling techniques. Hence, the authors were primarily interested in minimizing the potential for discrepancies arising from effects at the material level that cannot be equally reproduced by all the modelling approaches. For example, if a confinement model had been ascribed to VecTor2 analyses, the concrete stress-strain relation in each element would change during loading, creating an inevitable inconsistency with respect to DPMs and PHAs (which have pre-defined and constant values for the confined concrete parameters in all the concrete layers).

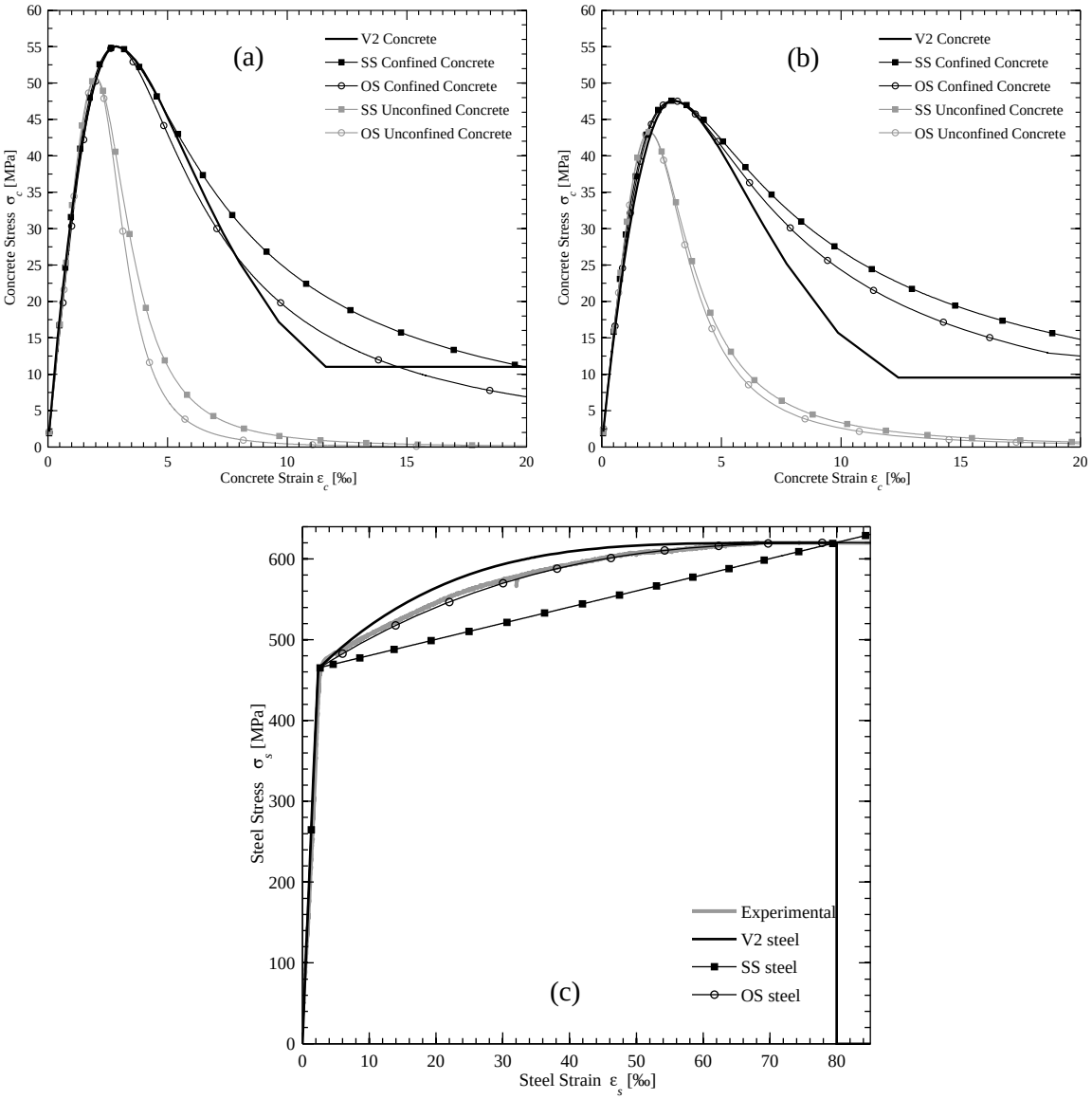

Figure 39. Adopted material constitutive laws: (a) concrete, TW2; (b) concrete, TW3; (c) steel (numerical vs experimental).

3.3.2. Simulation Results as Provided by Different Modelling Approaches

The shear force – drift curves of walls TW2 and TW2, as obtained for all models described in the previous section, are presented in Figure 40 and Figure 41. It is recalled that since the numerical models do not explicitly take into account bond-slip effects, they should only be applicable for comparison with the experimental results of wall TW2. As a matter of fact, it is clear that they capture in a much more satisfactory way the results of TW2, especially for positive values of drift. They seem to overestimate the member capacity (both in force and displacement) of wall TW3, which is partly related to the fact that its degradation is due to a physical phenomenon that is not taken into account by the models. This issue will be addressed in more detail in the following section. The comments of the next paragraphs are thus mainly directed towards Figure 40.

As a first overview, it can be stated that a general good agreement amongst all the proposed models and the experimental results is found up to peak response. The scatter in the predicted lateral force capacity of the wall is within acceptable limits, and the stiffness evolution up to the peak strength is well captured, and quite similar for all models. The obvious exception are the PHA models, which—due to the underlying bilinear moment-curvature assumption—exhibit a constant stiffness up to the yield point (see section 3.3.1). However, after the peak point, one can observe a relevant scatter of the predictions by the different modelling approaches, which is due to a numerical pathology named localization, wherein strains/curvatures concentrate at the bottom elements/cross-sections. It manifests even when similar models are considered, namely force-based elements; in particular, it is observed that the curves for OS with 5 and 9 IPs start diverging in the post-peak branch. This effect is in agreement with theoretical considerations (section 3.2).

The DPMs using force-based (FB) elements appear to give better results than the one employing displacement-based (DB) elements. For force-based DPMs with one FB element and five IPs, the differences between the models in OpenSees (OS) and SeismoStruct (SS) can be imparted to the distinct steel constitutive laws; the SS lower-bound stress-strain relation, see Figure 39 (c), reflects in a lower-bound prediction of the associated force-displacement curves.

For shear span ratios L_s/h <3, shear deformations are expected to play an increasing role in the member response (Priestley et al., 2007). In view of the ratio applied in the tests (L_s/h =1.17), shear deformations are therefore expected to be non-negligible and their effect on the global response of the walls becomes rather apparent: first off, the SEM capacity curve depicts an increased flexibility in relation to the results from DPMs. This is particularly evident for negative values of drift. Furthermore, the PHA accounting for shear displays a larger ultimate drift than the purely flexural PHA. It is observed that the latter—although arguably not applicable to the current walls due to their low shear span ratio—was included for comparative purposes against the PHA that accounts for shear. The figure also shows that the DB approach deviates from the remaining models, not only in terms of simulation of ductility but also in terms of lateral strength prediction. Such observation does not come as a surprise since DB formulations provide stiffer and stronger predictions of the actual member response due to the assumption of displacement interpolation functions (Table 4) (de Veubeke, 1965). An objective (‘exact’) response can only be obtained with a larger number of DB elements. In particular, it is advisable to adopt a small length for the elements wherein the member demand is higher. This condition is not met in the present case since the base element length corresponds to the equivalent plastic hinge length (as calculated for PHAs), which represents about 25% of the wall height. The remaining modelling techniques yield relatively similar predictions of the wall capacity and of the drift at peak strength.

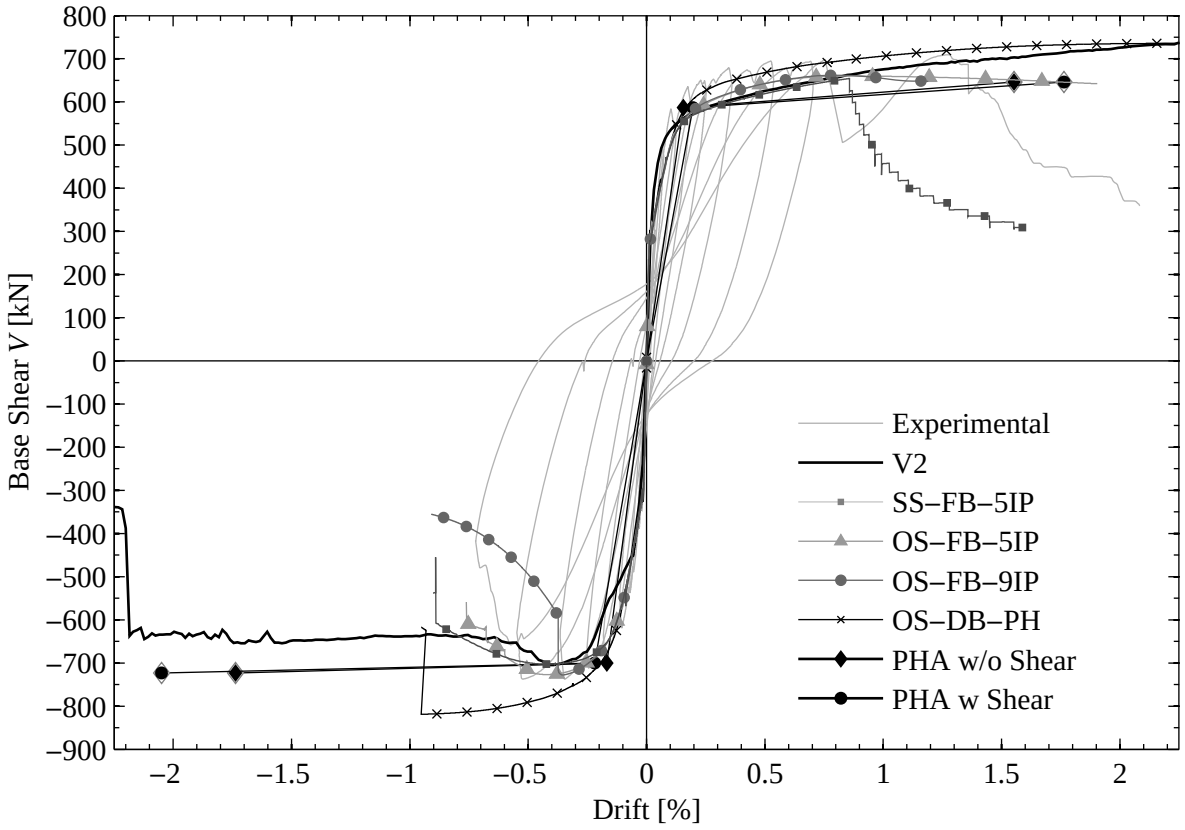

Figure 40. Force-drift response for wall TW2: comparison between the experimental and the numerical response obtained with different modelling approaches.

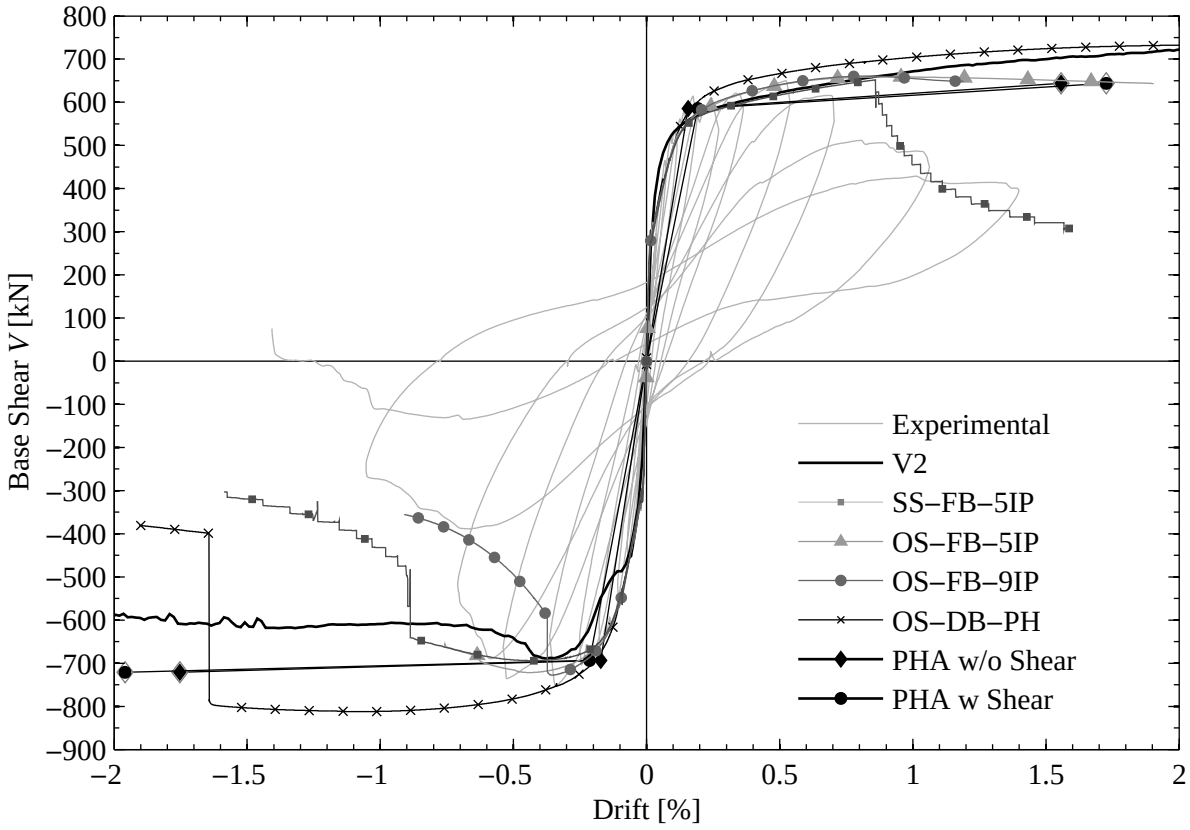

Figure 41. Force-drift response for wall TW3: comparison between the experimental and the numerical response obtained with different modelling approaches.

3.3.3.Modelling of Lap Splices for Wall TW3

The 'refined' plastic hinge model proposed by Priestley et al. 2007 is employed for comparison with the experimental results of the wall TW3. In this approach, the strain penetration is only considered after flexural cracking and the deformation Δ after first yield is calculated from the difference in current and first yield curvature. Between cracking Δ_{cr} and first yield displacement Δ_y', the deformation is then simply interpolated linearly. The equations on which the plastic hinge model builds on are reported hereafter:

$$\Delta_{cr} = \emptyset_{cr} L_s^2/3 \quad ; \quad F_{cr} = M_{cr}/H \tag{7}$$

$$\Delta'_y = \emptyset'_y \left(L_s + L_{sp}\right)^2/3 \quad ; \quad F_y = M_y/H \tag{8}$$

$$\Delta = \Delta'_y \frac{M}{M_y} + \left(\emptyset - \emptyset'_y \frac{M}{M_y}\right) L_p L_s \quad ; \quad F = M/H \quad \text{with} \quad \emptyset < \emptyset_u \tag{9}$$

The three important values of curvatures determining the changes in the curve behaviour are established as follows:

- Curvature at flexural cracking ϕ_{cr}: curvature corresponding to the first attainment of the concrete tensile strength in the extreme concrete fibres in tension;
- Curvature at first yielding ϕ_y: curvature corresponding to the attainment of first yielding by the longitudinal reinforcement ($\varepsilon_s = \varepsilon_{sy}$) or to the attainment of a concrete compressive strain (ε_c= *2‰*), whichever occurs first,
- Ultimate curvature ϕ_u: curvature corresponding to the ultimate condition. The tension and compression strain limits defining this situation are the steel strain corresponding to the onset of buckling (ε_s=0.6 ε_{su}) and the concrete strain at crushing (ε_c=ε_{cu} according to Mander et al.1988). Whichever of the two leads to the smaller ultimate curvature is determing the curvature capacity ϕ_u.

The moment curvature analysis was performed with the FE software Opensees and it is represented in Figure 42. The F-Δ curves obtained with this approach for both directions of loading are represented in Figure 43 with black dashed lines.

In order to account for the presence of lap splicing at the base of the specimen TW3, which can result in a substantial reduction of both the strength and the displacement capacity of the structural member, the procedure proposed by Hannewald (2013) is employed. It consists in three distinct steps: first, the load bearing capacity of the splice is checked based on the tensile strength of the concrete or the confining reinforcement of the splice. Second, if the flexural strength of the section is not reduced due to a weak splice, it is assumed to degrade under cyclic loading once the compression strain causing microcracking of the concrete has been reached. It is argued that, when these cracks develop, the tension strength of the concrete and thus the capacity of the splice is reduced till a residual value. In a third step, this residual strength is computed from the residual sectional moment capacity M_r which is calculated from the maximum eccentricity of the normal force within the core concrete. The normal force is assumed to result in a stress block with width b_c and length $a=P/(0.85f'_c b_c)$. With this assumption, the residual moment and hence the residual force follows to be:

$$F_r = \frac{M_r}{L_s} = P \, \frac{h_c - a}{2} \cdot \frac{1}{L_s} \tag{10}$$

It is important to note that the strain limits included in Step (2) were not calibrated to capture the crushing of the concrete at the height of the crack above the lap splice as it was observed for TW3 (see sections 2.3.2 and **Error! Reference source not found.**). These compression strain limits aim to capture the onset of the formation of vertical splitting cracks, which typically lead to a loss of the force capacity of the lap splice. For the crushing of the concrete at the height of the crack above the lap splice are not yet available. However, it will be shown that the compressive strain limits for lap splice failure lead to a good approximation of the displacement capacity for this type of failure mode.

Step (1): Evaluation of the strength of lap splices

The transfer of forces in a lap-splice is often described with two mechanisms: the bond mechanism transferring the force from one bar to the surrounding concrete and a truss mechanism transferring the load from one reinforcement bar to another through concrete and confining reinforcement. The concrete may in this case act as both strut (compression strength) and tie (tensile strength) while the transverse reinforcement provides a tie. The bond and truss mechanisms interact in a real structure, but models assume that one or the other controls the strength of the lap-splice. The strength of the lap-splice is therefore either expressed in terms of the bond strength between reinforcement and concrete or in terms of the tensile strength of concrete. In the first case, the force capacity of a lap-splice is assumed equal to that of an embedded bar with the same length. In the second case, the maximum tensile force of a splice is assumed to be the force which is necessary to form a splitting crack around the splice.

In the following paragraphs 3 different methods available in literature to evaluate the splice strength are illustrated. The obtained strength will be then compared with the maximum strength of the longitudinal reinforcement. In case the latter results bigger than the first, splice failure will be attained before the steel rupture and the steel stress strain law used for the moment curvature analysis will be accordingly reduced.

In Priestley et al. (1996) the resistance of the splice is related to the tensile strength of concrete through the following equation:

$$T_b = A_b f_s = f_{ct} p l_s \tag{11}$$

$$p = 0.5 s_l + 2(d_{bl} + c) \leq 2\sqrt{2}(c + d_{bl}) \tag{12}$$

where T_b is the maximum possible force of a reinforcement bar, f_{ct} is concrete tensile strength, l_s is the length of the lap-splice, s_l the spacing of the longitudinal bars measured between the center lines, d_{bl} the diameter of the longitudinal reinforcement bars and c the clear concrete cover of the longitudinal bars.

A similar approach to determine the strength of a splice has been suggested by Canbay and Frosch (2006). However, this model was not derived purely theoretically but validated against a wide experimental database containing 203 beams with unconfined splices and 278 beams with confined ones. The main equation providing the maximum allowable bar stress before bond failure is reported hereafter:

$$f_s = \frac{F_{sp} + F_{st}}{n_{bl} A_{sb} tan\beta} \tag{13}$$

where F_{sp} is the force corresponding to the formation of concrete splitting cracks, F_{st} takes into account the additional resistance provided by the presence of transverse reinforcement, n_{bl} and A_{bl} are respectively the number and the area of the splices and β is the angle between the radial splitting force and the axial force acting along the bar. For further information regarding the terms appearing in the above equation the reader should refer to the reference specified at the beginning of the paragraph.

A formulation based on the bond strength is proposed by Biskinis and Fardis (2010) to estimate the yield moment of a section with spliced reinforcement. Instead of using the yield strength of the reinforcement as limit, it is suggested to use the minimum value of yield and bond strength. To estimate the bond strength a formulation now included in the FIB model code (2012) is recommended:

$$f_s = 54\left(\frac{f_c}{25}\right)^{0.25}\left(\frac{25}{d_{bl}}\right)^{0.2}\left(\frac{l_s}{d_{bl}}\right)^{0.55}\left[\left(\frac{c_{min}}{d_{bl}}\right)^{0.33}\left(\frac{c_{max}}{c_{min}}\right)^{0.1} + k_m K_{tr}\right]\begin{cases}\leq \dfrac{k_b\sqrt{f_c}\,4 l_s}{d_{bl}} \\ \leq f_y\end{cases} \tag{14}$$

where c_{min} = min (c_b, c_{so}, c_{si}) and c_{max} = max (c_{so}, c_{si}) are the minimum and maximum value of the concrete covers and distance between longitudinal bars, respectively; confinement conditions are considered with factors k_m and K_{tr} while the factor k_b takes into account the conditions of bonding.

The calculated bond strength computed with all the aforementioned methods, as well as the maximum strength of the longitudinal reinforcement, are listed in Table 8.

As it can be seen, despite the scatter in the prediction of the maximum bond strength, in all cases the latter is largely higher than the ultimate steel strength. Therefore it was assumed that the presence of splices would not affect the maximum force capacity of the structural member.

Step (2): Definition of strain limits for the onset of splice degradation

As mentioned previously, the strength of a section with spliced bars might degrade once certain strains are exceeded in either tension or compression. Hence, the strain limit which defines the ultimate curvature of a section with a lap-splice should correspond to the strain at which splice failure initiates.

Priestley et al. (1996) assumed this strain to be the concrete compression strain corresponding to peak stress, ε_c = 0.002, because at this strain microcracking of the concrete initiates. They suggested this strain limit regardless of any confinement.

Hannewald (2013) observed that, in presence of confined concrete, the peak stress and the corresponding peak strain at which microcracking begins are inevitably larger than those for the unconfined case. Therefore it was proposed to assume the core concrete strain at peak stress ε_{cc} as strain limit for the onset of splice degradation. It is defined as:

$$\varepsilon_{cc} = \left(1 + 5\left(\frac{f_{cc}}{f_c} - 1\right)\right)\varepsilon_c \tag{15}$$

where f_{cc} and f_c are respectively the confined and unconfined concrete peak stress. The relation linking these two quantities can be found in Mander et al. (1988) as function of the effectiveness of the confinement which is taken into account by the following factor:

$$k_{con} = \left(1 - \frac{s}{2b_{con}}\right)\left(1 - \frac{s}{2h_{con}}\right)\left(1 - \frac{\sum s_{l,c}^2/6}{b_{con}h_{con}}\right) \tag{16}$$

In the above equation s is the stirrup spacing, h_{con} and b_{con} are the dimensions of the confined core, all measured to the centerline of the stirrups, and $s_{l,c}$ is the distance between those longitudinal bars that are confined by stirrup corners or cross ties. Considering that the section right above the foundation is subjected to the highest bending moment and hence concrete crushing with subsequent splice failure may initiate right above the foundation, the confined concrete strength needs to be estimated for this section. To do so, the foundation was treated like a stirrup in the sense that the distance between the foundation and the first stirrup above was assumed as stirrup spacing s and used for the calculation of the reinforcement ratio. It was also assumed that all longitudinal bars are restrained against lateral movement by the foundation and can hence be used to evaluate the third term in the above equation for k_{con}.

Table 8. Bond strength *vs* ultimate steel strength.

Approach	**f_s [MPa]**	**f_y [MPa]**
Priestley et al. (1996)	≅900	620
Canbay and Frosch (2006)	≅730	620
Biskinis and Fardis (2010)	≅930	620

Based on their database of experiments with spliced reinforcement, a relation expressing the ultimate deformation was also proposed by Biskinis and Fardis (2010) in terms of concrete compressive and steel tensile strains (obviously the first occurring amongst the 2 determinates the ultimate state). The latter was defined as a fraction of the limit strain for continuous bars under cyclic loading $\varepsilon_{su,cyc}$ ($\varepsilon_{su,cyc}$=0.6 ε_{su}):

$$\varepsilon_{su,s} = \left(1.2\frac{l_s}{l_{su,min}} - 0.2\right)\varepsilon_{su,cyc} \geq \frac{l_s}{l_{su,min}}\varepsilon_y \tag{17}$$

$$l_{su,min} = \frac{d_{bl}f_y}{\left(1.05 + 14.5\left(1 - 0.5\frac{s}{h_{con}}\right)\left(1 - 0.5\frac{s}{b_{con}}\right)\frac{n_{res}}{n_{bl}}\frac{\rho_v f_{yv}}{f_c}\right)\sqrt{f_c}} \tag{18}$$

where n_{res}/n_{bl} is the ratio of the number of restrained splices n_{res}, which are placed in a stirrup corner or held by a cross tie, to the total number of splices n_{bl}, s is the centerline spacing of the stirrups and h_{con}, b_{con} are the dimensions of the confined core defined by the center of the stirrups. The minimum splice length increases with increasing transverse reinforcement spacing, decreasing transverse reinforcement content and decreasing bond strength, expressed in terms of $\sqrt{f_c}$. For the ultimate concrete compression strain $\varepsilon_{cu,cyc}$, the authors propose a formulation that accounts for the size of the area of the confined concrete under compression and the effectiveness of the confining reinforcement:

$$\varepsilon_{cu,cyc} = 0.0035 + \left(\frac{1}{x_{c,con}}\right)^{\frac{3}{2}} + 0.4\frac{k_{con}\rho_v f_{yv}}{f_{cc}} \tag{19}$$

where $x_{c,con}$ is the depth of the neutral axis in the confined core in mm, ρ_v and f_{yv} are respectively the reinforcement ratio and the yield strength of the confining bars.

Similarly to what had been done for the strength limits, Table 9 lists the strain limits computed with the four equations illustrated above. The table also reports the curvatures corresponding to those strain limits ϕ_ε for both direction of loading as well as the ultimate curvature ϕ_u evaluated through the plastic hinge method. The obtained curvatures representing the onset of splice degradation as well as the ultimate curvature from plastic hinge analysis are plotted in Figure 42.

Table 9. Strain limits and corresponding curvature limits.

Approach	**ε [-]**	**$\phi_{\varepsilon\text{-DirA}}$[m×10^{-3}]**	**$\phi_{\varepsilon\text{-DirB}}$[m×10^{-3}]**
Priestley et al. (1996)	ε_c=0.002	-4.70	17.65
Hannewald (2013)	ε_c=0.0035	-10.09	37.96
Biskinis and Fardis (2010), concrete	ε_c=0.007	-20.62	61.98
Biskinis and Fardis (2010), steel	ε_s=0.021	-9.04	8.34
		$\phi_{u\text{-DirA}}$= -20.56	**$\phi_{u\text{-DirB}}$= 18.7**

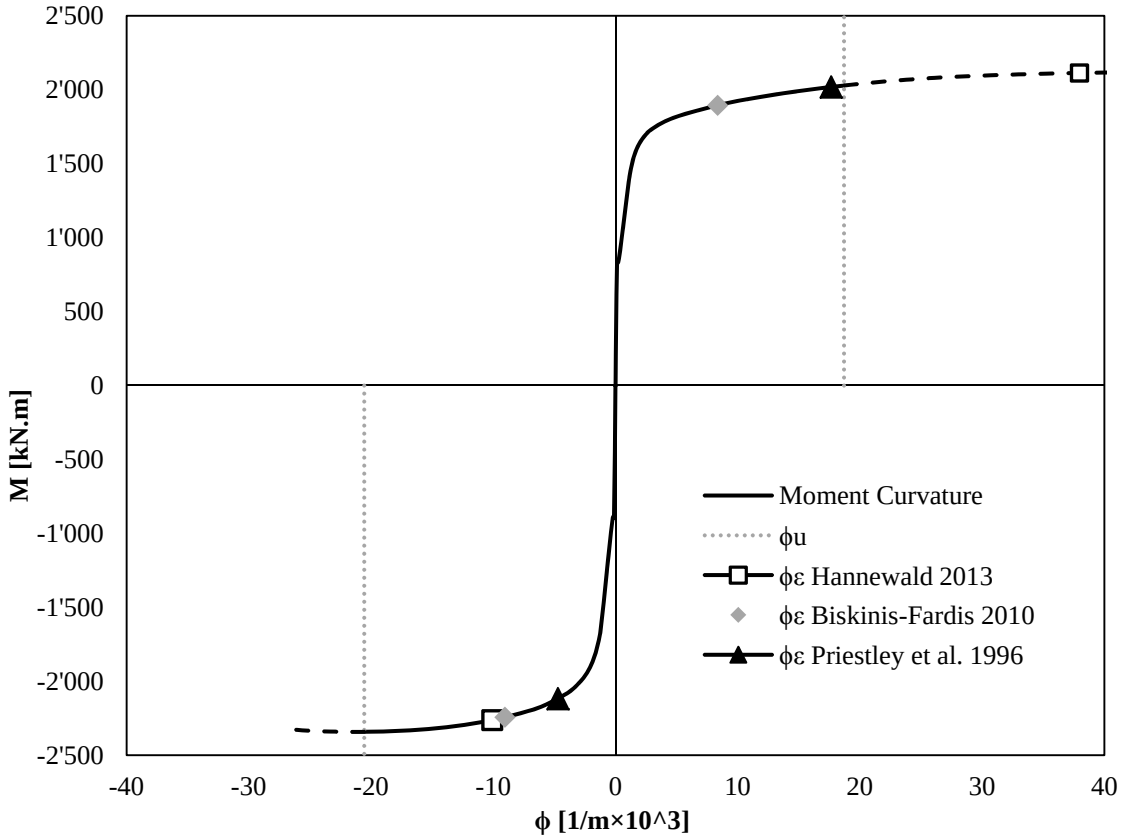

Figure 42. Moment-curvature analysis.

Hannewald (2013) considers only compression failure. The results show that such a failure mode does not become critical for the positive loading direction, when the flange is in compression since the curvature ϕ_ε exceeds the ultimate value ϕ_u, which is obtained when the effect of the lap splice is neglected. Biskinis and Fardis (2013) predict for this direction a lap splice failure due to tensile cracking.

For the negative loading direction, when the wall end without flange is in compression, Hannewald (2013) and Biskinis and Fardis (2010) lead to similar predictions of the curvature capacity while Priestley et al. (1996) lead to somewhat lower values. Biskinis and Fardis (2010) predict for this loading direction again a tensile failure.

Figure 43 shows the comparison between the experimental force-displacement results and the predictions obtained through the plastic hinge model—3 points method—illustrated at the beginning of this section. As expected from step 1, no strength degradation occurs and the wall in both directions is able to attain its maximum force capacity. For what regards the strain limits, those proposed by Biskinis and Fardis (2010) seem to provide a better estimate of the loss in member bearing capacity due to lap splice failure, as depicted by the experimental results. However, for both loading directions tensile failure is predicted. This leads to the conclusion that the compressive strain limit proposed by Biskinis and Fardis is overestimating the curvature capacity of lap splices of this type of walls. It is therefore recommended to replace the compressive strain limit by with ε_c=0.002, which is the limit by Priestley et al. (1996). This limit is also included in SIA 269/8 (2014). The results underline that a compressive strain limit alone is not sufficient to capture the deformation capacity of walls with lap splice but that this limit must be complemented by a limit on the tensile strains.

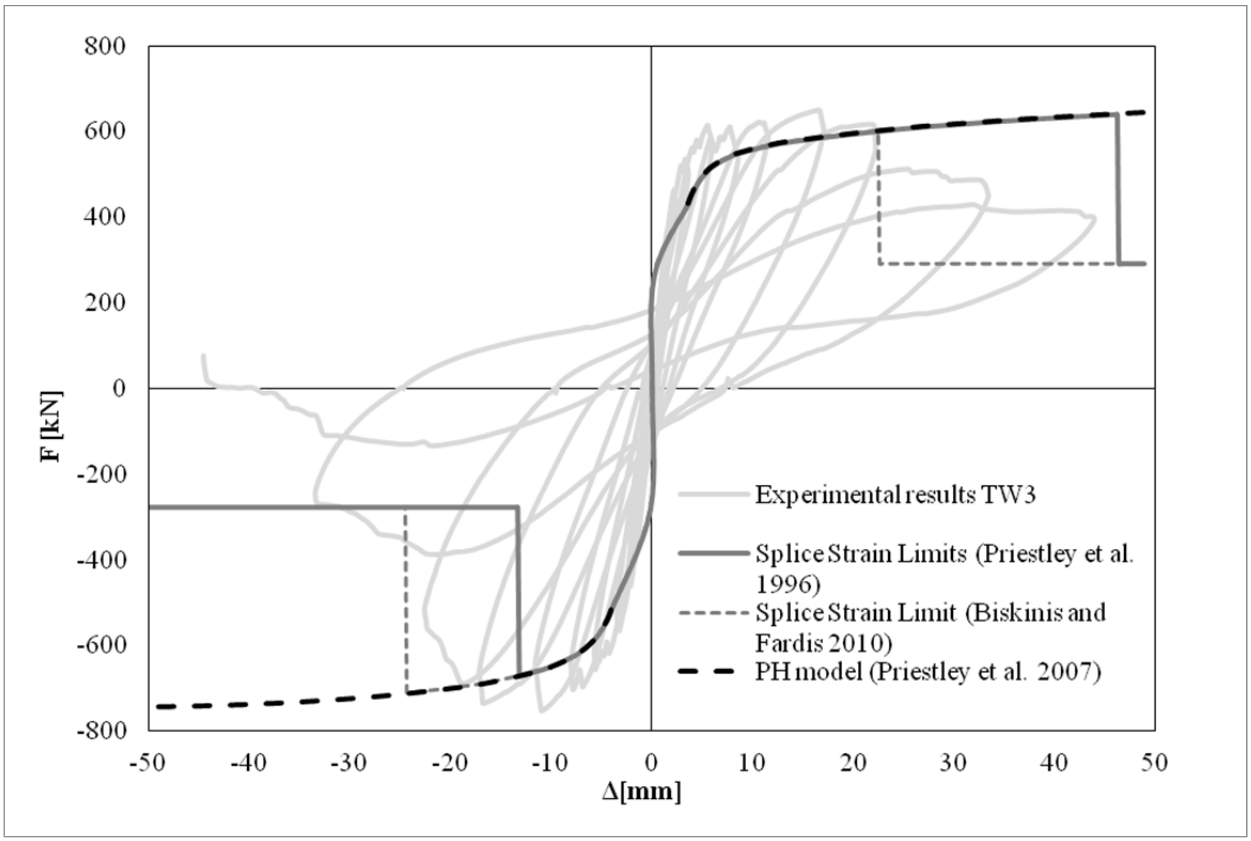

Figure 43. Comparison of experimental-numerical force-displacement curves for wall TW3, taking into account limits associated to lap splice failure.

4. RECOMMENDATIONS FOR THE SEISMIC ASSESSMENT OF RC WALL BUILDINGS WITH THIN RC WALLS

The objective of this section is to summarise the main characteristics of RC walls as constructed in the period of 1950-1970 in Switzerland and their seismic behaviour. Further, modelling recommendations for buildings with such walls are formulated and possible intervention methods described, which can be applied if the seismic safety of such buildings proves insufficient.

4.1. General Characteristics of RC Walls Constructed in 1950-1970

Section 1.3 outlined the general characteristics of RC wall buildings constructed in the period of 1950-1970 in Switzerland. For convenience they are summarised here:

- Large number of walls (walls are often the common element for carrying horizontal and vertical loads).
- Wall thickness of 15-20 cm; wall length often between 4-9 m.
- Longitudinal and transverse reinforcement ratios between roughly 0.3-0.8%; reinforcement ratios in longitudinal and transverse direction are often similar.
- Typical reinforcement detailing comprises uniformly distributed longitudinal reinforcement and transverse reinforcement placed on the inside of longitudinal bars.
- Concrete covers often as low as 1 cm.
- Lap splices at the wall base with a splice length of around 30-35 bar diameters.

When compared with today's construction practice in Switzerland (SIA, 2005), the buildings constructed in the period of 1950-1970 differ mostly with regards to:

- Placement of transverse reinforcement on the inside of the longitudinal reinforcement rather than on the outside.
- Lap splices with splice lengths of only about half the splice lengths required in current code if walls are designed according to non-ductile principles.
- Lap splices unconfined and covered by only a thin concrete cover.
- Wall thickness in some cases smaller than the required minimum wall thickness of 20 cm or a fifteenth of the storey height.

The influence of these differences on the wall behaviour was investigated by the quasi-static cyclic tests documented in chapter 2. The tests showed that these characteristics influence the seismic behaviour as follows:

- Placing the transverse reinforcement on the inside of the longitudinal reinforcement did not affect the behaviour noticeably with regard to the shear response. However, it might influence the behaviour of the lap splice indirectly in two ways. First, since the longitudinal reinforcement lies in the outmost layer, the cover up to the longitudinal bar is very low. This cover is essential for transferring the stresses between spliced bars. Second, the transverse reinforcement does not contribute to a confinement of the concrete in compression. Based on the test observations, it is possible that the second effect might have played a role and led to the premature crushing failure.
- Some of the lap splices failed due to the alternating compressive and tensile strains
- Some bars fractured in the crack just above the lap splice. Due to the double-reinforcement over the length of the lap splice, the deformations concentrate in two cracks. The first crack forms at the interface between foundation and wall and the second just above the lap splice. In

TW3, the crack width of the crack above the lap splice was significantly larger than the width of the crack below the lap splice.

- Unconfined concrete at wall ends is prone to crushing. Just above the foundation the concrete is confined by the foundation. The wall is therefore most vulnerable to crushing about a wall thickness above the foundation. In walls with lap splices, the crushing tends to concentrate in the crack above the lap splice. Due to the opening and closing of the crack, this can be the result of in-plane offsets along the crack faces, which yielded a reduced compressive strength. It is also possible that slight out-of-plane rotations of concrete blocks reduced the contact area leading to premature crushing.

4.2. Suitable Assessment Methods for RC Wall Buildings Constructed in 1950-1970

For the analysis of RC wall buildings constructed between 1950-1970 in Switzerland, a two stage analysis approach is recommended: In a first stage, a linear elastic dynamic analysis is recommended using the response spectrum method (RSM, SIA 261, 2003). If the building does not pass the seismic assessment check, it should be assessed by means of the capacity spectrum method (CSM). The CSM is outlined in the new seismic assessment code for existing structures SIA 269/8 (2014), which is currently in the consultation phase and will be published presumably by the end of 2014. The SIA 269/8 also provides the entire risk framework for the assessment of existing structures, which includes, for example, considerations with regard to the required compliance factor. These are not repeated here but the following discussion focuses on aspects that are specific to RC wall buildings constructed between 1950-1970.

4.2.1. Force-Based Method

It is generally recommended to use the RSM rather than the equivalent lateral force method for the analysis of RC wall buildings. The RSM accounts explicitly and in an analytically sound manner for higher mode effects and the effect of structural irregularities, which are often relevant for the building type discussed here. For buildings that are irregular in plan or elevation or have a first period longer than 2s, the equivalent lateral force method is not applicable.

The RC walls in these buildings are not capacity designed. For this reason the analysis should be based on a force-reduction factor of q=2 (SIA 262, 2004). Note that the SIA 261 (2003) applies the force-reduction factor to all modes while numerical analyses of inelastic systems have shown that it should be only applied to the first mode (Priestley et al., 2007). If higher modes are important and a shear critical behaviour feared, it is recommended to consider analysing the building for q=2.0 for the first mode and q_e=1.5 for all other modes. This modified multi-modal superposition rule has been shown to yield better approximations of the nonlinear response than the current code provisions (Priestley et al., 2007).

4.2.2. Displacement-Based Method

The displacement-based assessment can be carried out by means of the capacity spectrum method (CSM), which is described in SIA 269/8, or nonlinear time-history analysis (NTHA). The CSM appeals through its simplicity but in its original formulation it may not account for higher mode effects.

SIA 269/8 requests that the shear force demand is computed by amplifying the shear force obtained from the pushover analysis by an amplification factor κ:

$$V_{d,j}^{+} = \kappa \cdot V_{d,j} \tag{20}$$

where κ is the amplification factor. V_d should be taken as the maximum shear force obtained from the pushover analysis up to failure of the wall j. SIA 269/8 recommends estimating the amplification factor according to SIA 262 (2004):

$$\kappa = 0.9 + \frac{n}{10} \leq 1.5 \tag{21}$$

(1)

where n is the number of stories. This factor can only be a rather rough estimate of the actual shear amplification and might underestimate the influence of higher modes on the shear force demand. In case of particular irregular or high-rise buildings it is recommended to use either NTHA or account in a more advanced way for higher mode effects when using the CSM. Different research groups have proposed such modifications to the CSM. For the type of structures considered here, the approach proposed by Kreslin and Fajfar (2012) is recommended.

4.3. Modelling of RC Wall Buildings Constructed 1950-1970

4.3.1. Walls

All RC walls should be included in the model. If unreinforced concrete walls are present, these should also be included since they can contribute significantly to the initial stiffness and strength of the building. Concerning the stiffness values assigned to the walls, the following recommendations are made. These recommendations are based on those in SIA 269/8 but are detailed here for RC wall buildings:

a) Flexural stiffness of RC walls

In general, during a seismic event, the walls of the first storey are subjected to extensive cracking of the concrete and possibly yielding of the reinforcement. For these wall elements, and when employing plastic hinge analysis, the flexural stiffness should correspond to the effective stiffness at the onset of yielding:

$$EI_{eff,2} = \frac{M_y}{\phi_y} \tag{22}$$

where M_y is the nominal yield moment. The yield curvature ϕ_y of a wall can be estimated as from the bilinear approximation of the moment-curvature relationship of the wall section. Alternatively, if the moment-curvature is not computed by means of a section analysis program, it can be estimated from the yield strain ε_{sy} of the reinforcement and the wall length l_w (Priestley et al., 2007):

$$\phi_y \approx \frac{\kappa \varepsilon_{sy}}{l_w} \tag{23}$$

For κ the following values can be assumed (Priestley et al., 2007): rectangular wall section κ =2.0; flanged walls κ =1.5. If the structure remains largely elastic (i.e., it satisfies the flexural capacities for q=1.5), the first storey walls should be assigned flexural stiffnesses corresponding to the stiffness value proposed in SIA 269/8 for elements that remain elastic:

$$EI_{eff,1} = \frac{EI_{gross} + EI_{eff,2}}{2} \tag{24}$$

For the storeys above the first storey, the model should be based on $EI_{eff,1}$.

b) Shear stiffness of RC walls

The shear flexibility of the walls should in general be included in the model. The shear flexibility should be reduced to account for cracking of the concrete and yielding of the reinforcement. Modelling the shear flexibility of RC walls in beam element models poses several challenges. This section summarises the challenges related to modelling shear flexibility, which were discussed in detail in section 3.2.1.

In routine analysis it is often assumed that shear stiffness is proportional to GA_s where G = shear modulus and A_s = shear area ($\approx 0.85\ A_{gross}$). In RC members responding in the inelastic range the flexural and shear deformations are strongly coupled and GA_s may grossly underestimate shear deformations. Experimental results from quasi-static cyclic tests have shown that the ratio of shear to flexural deformations remains approximately constant over a large range of inelastic deformations. The modelling approach that more accurately accounts for the interaction of shear and flexural deformations is the shell element model. Current state-of-the-practice beam element formulations do not successfully capture the coupling between flexural and shear flexibility, and therefore relatively crude approximations which consider flexural and shear deformations as independent mechanisms are required. ItShear flexibilities can be included through shear flexibility terms in the beam element formulation or shear springs at midheight of the storeys. It is recommended to compute the shear flexibilities corresponding to $\mu_\Delta = 1$ using Eq. (5) to estimate the ratio of shear to flexural displacement Δ_s/Δ_f (Beyer et al., 2014). The shear stiffness can be assumed to be distributed over the height of the wall in proportion to the flexural stiffness EI.

c) Moment capacity of RC walls with lap splices

The moment capacity of slender RC walls with shear spans ratios larger than approximately 2 can in general be determined using plane section analysis and the strain limits proposed in section 3.3.3. However, it should be checked that the lap splice is able to develop its full capacity; an approach was also presented in section 3.3.3. For more squat walls ideally shell element models should be employed but simpler models can give a first estimate of the displacement capacity.

d) Deformation capacity of RC walls with lap splices

Walls with unconfined lap splice at the wall base have in general a smaller deformation capacity than walls without lap splice. For the walls tested within the scope of this research project, the lap splice reduced the drift capacity by 50%.

Despite the advancement of numerical methods, predicting the deformation capacity of RC walls still poses significant challenges. In this study, three types of models were compared, i.e., plastic hinge models, beam element models and shell element models. The results showed that the predictions agreed well in terms of the global response in the elastic range and after the onset of yielding. However, as the inelastic deformations increase, the scatter given by the the different predictions also increased. This observation is greatly magnified if local deformation measures such as strains are compared. A case study that was based on the walls tested within this project showed that the difference in predicted strains for a given displacement demand can read several 100% (Almeida et al., 2014). One central reason for this difference is the distinct assumptions on which the considered methods and finite element formulations are based. Another reason lies in the lack of regularisation techniques for shell and beam element models (Almeida et al., 2014). Such methods are a matter of ongoing research efforts but have not yet found their way into most commercial or research codes.

This large difference in simulated strains from different analysis methods renders the recommendation of strain limits rather difficult. Recommendations can only be formulated for a particular method, type of finite element, and adopted meshing. Of all the previous methods, plastic hinge models are well suited for fast simulation purposes since they can be completely defined with relatively few equations.

However, since many walls within the considered buildings are relatively squat, the plastic hinge models reach their limit of applicability. Despite this concern, the plastic hinge model was used to predict the deformation capacity of the wall with lap splices. In this analysis, the plastic hinge length and shear deformations can be estimated as for walls without lap splices (Hannewald, 2013). The effect of a lap splice at the base of the wall needs to be considered when determining limit strains. In the following, the results of the comparison of analytical results with experimental results are summarised. It is stressed again that these recommendations are only valid for the plastic hinge model formulation described in section 3.3. For example, other equations for estimating the plastic hinge length could lead to different conclusions. It is further emphasized that the validation is limited to TW3. For this reason, the authors refrain from proposing new strain limits but only assess the applicability of previous strain limits proposed by other authors, which have been verified against larger sets of data:

- The lap splice failure should be assessed on the basis of a compressive and tensile strain limit. Addressing the lap splice failure on the basis of a compressive strain limit alone can lead to an overestimation of the deformation capacity (for TW3 this was the case when the flange was in compression).
- As a tensile limit, the limit proposed by Biskinis & Fardis (2010) led to a good estimate of the deformation capacity of TW3 for the positive loading direction (i.e., towards the flange).
- As a compressive limit, the strain limit by Priestley et al. (1996), which is also included in SIA 269/8 (2014), led to acceptable (even if slightly conservative) estimates of the deformation capacity of TW3 for the negative loading direction (i.e., towards the free web edge).

e) Shear strength

SIA 262 considers two shear failure modes of RC walls: Rupture of the transverse reinforcement and crushing of the compression diagonal. Shear strength of RC walls is in general critical if transverse reinforcement is low. Relying only on the strength of the shear reinforcement as SIA 262 (2004) proposes leads in this case to a rather conservative estimate of total shear strength. While such an approach is appropriate for new designs, more advanced models are required for the assessment of existing structures. Such models consider also the contribution of the concrete (i.e., the shear stress that can be transferred by aggregate interlock on the shear-flexure cracks) and the contribution of the axial force towards the shear strength. If the shear strength of RC walls is found to be critical, it is therefore recommended to use such advanced models for more accurate, less conservative, estimates. Several research groups have proposed such kind of proposals; for the RC walls herein considered the modified UCSD model is recommended. The model was proposed by Priestley and co-workers in 1990s and has been slightly updated in Priestley et al. (2007); the latter is reproduced in the following lines.

Priestley et al. (2007) compute the shear resistance as the sum of three components, i.e., the contribution of the concrete due to aggregate interlock V_C, the contribution of the shear reinforcement V_S and the contribution of the axial force V_P:

$$V_R = V_C + V_S + V_P \tag{25}$$

The concrete component accounts for aggregate interlock along the shear-flexure cracks. This contribution reduces as the crack widths increases. The strength is also dependent on the shear span ratio and on the longitudinal reinforcement content:

$$V_C = \alpha \cdot \beta \cdot \gamma \cdot \sqrt{f_c'} \cdot A_s \tag{26}$$

$$1.0 \leq \alpha = 3 - \frac{M}{V l_w} \leq 1.5 \tag{27}$$

$$\beta = 0.5 + 20\rho_l \leq 1.0 \tag{28}$$

where f_c' is the cylinder compressive strength of the concrete in MPa; A_s is the wall area that contributes to the shear resistance (A_e=0.8A_{gross}; for flanged walls A_{gross} should be computed disregarding the flange area); M and V are the moment and shear force at the wall base; l_w is the wall length; ρ_l is the total reinforcement longitudinal reinforcement content (ρ_l=$A_{s,long}$/A_{gross}). The shear stress γ is a function of the curvature ductility μ_ϕ at the wall base:

$$\mu_\phi \leq 1.0: \gamma = 0.29\ MPa \quad (29)$$

$$\mu_\phi \geq 13.0: \gamma = 0.05\ MPa \quad (30)$$

For μ_ϕ between 1.0 and 13.0 the shear stress γ can be linearly interpolated. This approach for computing the shear strength should only be used for assessment; if the wall is retrofitted with regard to the shear strength, its shear strength should be computed according to SIA 262 (2004).

4.3.2. Slabs

Slabs should be considered in the structural model and the building should not be analysed as a group of independent cantilever walls. In particular at instances where some walls have started to form plastic hinges at the base while others are still elastic, the walls have different displaced shapes, which can cause significant compatibility forces in the slabs (Beyer et al., 2014). These forces result from imposing equal displacements at each storey as a result of the inplane stiffness of the slab.

In general it is sufficient to consider only the in-plane stiffness of RC slabs and neglect the out-of-plane stiffness. If the slab is a solid RC slab and the span lengths of the slabs are relatively small, it can be assumed that the slab is infinitely rigid in plan. If this does not apply, the slab should be modelled as elastic with gross sectional properties. SIA 269/8 (2014) recommends that the in-plane slab flexibility should be considered, if the slab displacements relative to the ground increase by more than 20% when compared to the model with slab elements that are rigid in-plane. In this case, it should also be pondered whether the out-of-plane stiffness of the slab should be considered. This is necessary if the resulting change in axial force in a particular wall is significant and / or if the global overturning moment capacity of the building is significantly increased. For the former it is observed that a variation of axial force of ±5% $A_g f_c$ can be considered as significant. Such a change in axial force will have typically a significant effect on: (i) the moment capacity and therefore on the flexural stiffness of the cracked condition, (ii) the shear flexibility, and (iii) the deformation capacity.

4.3.3. Beams

If beams are present, they should be included in the model. Their flexural stiffness can be estimated using Eqs. (22) and (23) with a κ-coefficient of 1.70 for T-section beams (Priestley et al., 2007) or 2.1 for rectangular beams (SIA 269/8, 2014).

4.3.4. Columns

Columns in wall buildings typically do not contribute significantly to the lateral stiffness of the structure and their contribution to the lateral stiffness and strength can typically be neglected. It is, however, required that the slab-column connections are capable of maintaining their vertical load capacity when subjected to seismically induced deformations. A mechanical model for the assessment of punching failure of slab-column connections under seismically induced deformations is currently under development (Drakatos et al., 2014).

Figure 44. (a) Flat slabs on columns (Photo: T. Wenk); (b) Punching failure of slabs of a car park during the Christchurch earthquake (Photo: S. Sritharan).

4.4. Possible Measures for Improving the Seismic Behaviour

As outlined in the preface of this document, one of the main aims of this document was to develop and verify improved assessment methods that lead to more realistic (and less conservative) predictions of the seismic behaviour than what standard methods would do. Such an approach allows to preserve more buildings in their original configuration without exposing inhabitants to undue seismic risks. These approaches will also allow to single out those buildings whose performance in the event of a significant seismic event is clearly insufficient. For the type of buildings considered here, suitable retrofit methods could comprise (this list is far from exhaustive):

- If the deformation capacity of the walls is insufficient: Confinement of the lap splice by means of FRP wrapping; a concrete pedestal that moves the critical section above the lap splice.
- If the shear capacity is insufficient: External shear reinforcing; increasing the width of the wall (this should be done over several stories).
- Vertical irregularities due to non-continuous walls (soft-stories): At least some walls should be made continuous over the soft story.
- In-plane irregularities: Adding walls to make the building more regular in plan. Sometimes also the closure of dilation joints can lead to a more regular layout and a higher redundancy of the structural system.

Examples on retrofit projects that have been realised in Switzerland can be found in Wenk (2008).

5. CONCLUSIVE REMARKS

Although buildings in Switzerland were not designed for seismic loads before 1970, the present study showed that RC wall buildings constructed during the two previous decades have some characteristics that are in their favour. Amongst others, the often large number of walls and reasonable longitudinal *and* transverse reinforcement contents, as well as the flanges that help stabilizing the wall and reduce the detrimental effect of compressive strains. Other characteristics that were initially considered unfavourable, such as the placement of the transverse bars on the inside of the longitudinal bars, did not show a significant effect on the wall behaviour in the large-scale tests that were performed within the scope of this project. On the other hand, a clear shortcoming of these walls is the relatively short lap splices at the wall base. The lap splice significantly reduced the wall displacement capacity by up to 50%, which should be taken into account during the seismic evaluation of existing buildings (namely in the modelling phase), and in particular of important structures as cultural heritage ones. However, despite these shortcomings, the walls that were tested within this project reached their full force capacity and developed some inelastic deformations before failure, which indicates that the resulting deformation capacity might be often sufficient for regions of low seismicity.

The work conducted within the scope of this project aimed at improving the understanding of the expected seismic performance of RC walls that can be found in buildings constructed during the 1950-1970 in Switzerland. In this regard, the experimental results of two large-scale tests of such walls provided insights into critical aspects, which were outlined in detail in chapter 2 and summarised in section 4.1. Further important aspects with respect to structural modelling were discussed in chapter 3 and summarised in section 4.3.1. It is clear that the very large topic of seismic assessment of RC wall buildings cannot be completed conclusively with a single project. The interesting findings of this study triggered therefore further research in the same area, which has already started:

- Regularisation techniques for the numerical analysis of walls: The numerical analyses of the tested walls showed that the results vary significantly for larger values of inelasticity demands, particularly for the post-peak phase and with regard to the prediction of strains. This renders the formulation of failure criteria that are based on sound mechanics very difficult. Overcoming this current flaw calls for the development of regularisation strategies that will reduce the sensitivity of the model simulations to the finite element formulation and discretisation. Such regularisation techniques are currently under development but need further calibration against experimental results before they can be implemented in commercial codes.
- Effect of bi-directional loading: The loading protocols applied in this programme did not account for the effect of bi-directional loading. In order to study this issue a new wall specimen (TW4), geometrically and mechanically identical to wall TW2, was built and will be tested under a bidirectional loading. Although the out-of-plane stiffness and strength of the walls can be neglected when assessing the performance of an entire building, the effect of out-of-plane loading on the in-plane stiffness and strength cannot be disregarded, as it may very adversely affect the member behaviour. It is recalled that in a real earthquake the walls will be subjected to bi-directional loading and the out-of-plane component will therefore influence the in-plane behaviour. It is expected that it could affect in particular the stability of the very thin wall members (some walls in Swiss structures from 1950-1970 have wall thicknesses of 15 cm). As mentioned, both walls tested within the scope of this project did not develop out-of-plane stability problems. However, the behaviour of wall TW1, a 12 cm wall that was part of the same experimental program but represented a wall typical of the current construction practice in Colombia, was fundamentally controlled by instability issues.

New research results will be continuously published and are available on the laboratory's webpage (eesd.epfl.ch) or by contacting the authors of the report.

6. ACKNOWLEDGMENTS

The authors are appreciated for the time and availability shared by the following people (in alphabetical order): Angelica Rosso, Dr. Carlos Blandon, Danilo Tarquini, Prof. Hugo Bachmann, Hugues Vincent, Jean-Daniel Chavan, Joëlle Feihl, Jose Rave Arango, Matteo Campiche, Dr. Ovidiu Prodan, Prof. Pierino Lestuzzi (EPFL), and Dr. Thomas Wenk.

The financial support, without which the present study would not have been possible, of *Stiftung zur Förderung der Denkmalpflege* is deeply acknowledged.

7. REFERENCES

ACM. (2013). Archives de La Construction Moderne. École Polytechnique Fedérale de Lausanne. Retrieved from http://acm.epfl.ch/

Allenspach, C. (1999). *L'architecture Suisse - Bâtir aux XIXe et XXe* (p. 177). Pro Helvetia Fondation suisse pour la culture.

Almeida, J. P., Das, S., & Pinho, R. (2012). Adaptive force-based frame element for regularized softening response. *Computers & Structures*, *102-103*, 1–13. doi:10.1016/j.compstruc.2012.03.018

Almeida, J. P., Tarquini, D., & Beyer, K. (2014). Modelling Approaches for Inelastic Behaviour of RC Walls: Multi-level Assessment and Dependability of Results. *Archives of Computational Methods in Engineering (submitted)*.

Arbulu, A. G. B. (2006). *Plastic Hinge Length in High-Rise Concrete Shear Walls*. *The University of British Columbia*.

ASCE. (2006). *ASCE/SEI 41-06: Seismic Rehabilitation of Existing Buildings*. *American Society of Civil Engineers*. USA.

ASCE 7-02. (2002). *Minimum Design Loads for Buildings and Other Structures*. *ASCE Standard*.

ATC-3-06. (1978). *Tentative Provisions for the Development of Seismic Regulations for Buildings*. *Applied Technology Council*. California.

ATC-40. (1996). *Seismic Evaluation and Retrofit of Concrete Buildings*. *Applied Technology Council* (p. 334). Redwood City, CA.

AVL (2013). Archives de la Ville de Lausanne. Lausanne. Retrieved from http://www.lausanne.ch/archives

BABS (2004). Expertenbericht: Erdbeben und Kulturgüter. Bundesamt für Bevölkerungsschutz, Switzerland.

Bae, S., & Bayrak, O. (2008). Plastic Hinge Length of Reinforced Concrete Columns. *ACI Structural Journal*, *105*(3), 290–300.

Belletti, B., Damoni, C., & Gasperi, A. (2013). Modeling approaches suitable for pushover analyses of RC structural wall buildings. *Engineering Structures*, *57*, 327–338. doi:10.1016/j.engstruct.2013.09.023

Berry, M. P., Lehman, D. E., & Lowes, L. N. (2008). Lumped-plasticity models for performance simulation of bridge columns. *ACI Structural Journal*, *105*(3), 270–279.

Beyer, K., Dazio, A., & Priestley, M. J. N. (2007). *Seismic design of torsionally eccentric buildings with U-shaped RC Walls*. *European School for Advanced Studies in the Reduction of Seismic Risk* (p. 303).

Beyer, K., Dazio, A., & Priestley, M. J. N. (2008). Inelastic wide-column models for U-shaped reinforced concrete walls. *Journal of Earthquake Engineering*, *12*(sup1), 1–33. doi:10.1080/13632460801922571

Beyer, K., Dazio, A., & Priestley, M. J. N. (2011). Shear deformations of slender reinforced concrete walls under seismic loading. *ACI Structural Journal*, *108*(2), 167–177.

Beyer, K., Simonini, S., Constantin, R., & Rutenberg, A. (2014). Seismic shear distribution among interconnected cantilever walls of different lengths. *Earthquake Engineering and Structural Dynamics*.

Biskinis, D., & Fardis, M. N. (2010a). Deformations at flexural yielding of members with continuous or lap spliced bars. *Structural Concrete*, *11*(3).

Biskinis, D., & Fardis, M. N. (2010b). Flexure-controlled ultimate deformations of members with continuous or lap-spliced bars. *Structural Concrete*, *11*, 93–108.

Bozorgnia, Y., & Bertero, V. V. (2004). *Earthquake Engineering - From Engineering Seismology to Performance-Based Engineering*. *CRC Press* (p. 941).

Calabrese, A., Almeida, J. P., & Pinho, R. (2010). Numerical issues in distributed inelasticity modeling of RC frame elements for seismic analysis. *Journal of Earthquake Engineering*, *14*(S1), 38–68. doi:10.1080/13632469.2010.495681

Canbay, E., & Frosch, R. J. (2006). Bond Strength of Lap-Spliced Bars, (102).

Ceresa, P., Petrini, L., Pinho, R., & Sousa, R. (2009). A fibre flexure – shear model for seismic analysis of RC-framed structures. *Earthquake Engineering and Structural Dynamics*, *38*, 565–586. doi:10.1002/eqe

Coleman, J., & Spacone, E. (2001). Localization Issues In Force-Based Frame Elements. *Journal of Structural Engineering*, *127*(11), 1257–1265.

Computers and Structures Inc. (2013a). ETABS 2013: Integrated Analysis, Design and Drafting of Building Systems.

Computers and Structures Inc. (2013b). Perform-3D: Nonlinear Analysis and Performance Assessment for 3D Structures.

Crisfield, M. A. (1990). A consistent co-rotational formulation for non-linear, three-dimensional, beam-elements. *Computer Methods in Applied Mechanics and Engineering*, *81*(2), 131–150.

Cusson, D., & Paultre, P. (1994). High-strength concrete columns confined by rectangular ties. *Journal of Structural Engineering*, *120*(3), 783–804.

Cusson, D., & Paultre, P. (1995). Stress-strain model for confined high-strength concrete. *Journal of Structural Engineering*, *121*(3), 468–477.

Dazio, A., Beyer, K., & Bachmann, H. (2009). Quasi-static cyclic tests and plastic hinge analysis of RC structural walls. *Engineering Structures*, *31*(7), 1556–1571. doi:10.1016/j.engstruct.2009.02.018

De Veubeke, B. F. (1965). Displacement and equilibrium models in the finite element method. In *Stress Analysis* (O.C. Zienk., Vol. 52, pp. 145–197). John Wiley & Sons. doi:10.1002/nme.339

Drakatos, I. S., Muttoni, A. & Beyer, K. (2014). Mechanical model for flexural behaviour of slab-column connections under seismically induced deformations. *4th International fib Congress*, Mumbai, India.

EN1998-1. (2002). *Eurocode 8: Design of Structures for Earthquake Resistance. Part 1: General Rules, Seismic Actions and Rules for Buildings. Doc CEN/TC250/SC8/N306. European Committee for Standardization*.

EN1998-3. (2005). *Eurocode 8: Design of Structures for Earthquake Resistance. Part 3: Assessment and Retrofitting of Buildings. Doc CEN/TC250/SC8/N306. European Committee for Standardization*.

Fardis, M. N. (2009). *Seismic Design, Assessment and Retrofitting of Concrete Buildings*. *Springer* (p. 735).

FEMA. (2012a). *FEMA P-58-1: Seismic Performance Assessment of Buildings, Volume 1 - Methodology*. *Applied Technology Council, Federal Emergency Management Agency* (Vol. 1).

FEMA. (2012b). *FEMA P-58-2: Seismic Performance Assessment of Buildings, Volume 2 - Implementation Guide*. *Applied Technology Council, Federal Emergency Management Agency* (Vol. 2).

FEMA 356. (2000). *Prestandard and Commentary for the Seismic Rehabilitation of Buildings*. *U.S. Federal Emergency Management Agency*.

FEMA 368. (2001). *NEHRP Recommended Provisions for Seismic Regulations for New Buildings and Other Structures*. *U.S. Federal Emergency Management Agency*.

Filippou, F. C., Popov, E. P., & Bertero, V. V. (1983). *Effects of bond deterioration on hysteretic behavior of reinforced concrete joints* (p. 184). Berkeley, California, U.S.A.

Greifenhagen, C. (2006). *Seismic behavior of lightly reinforced concrete squat shear walls*. *École Polytechnique Fedérale de Lausanne - Département de Génie Civil*. École Polytechnique Fedérale de Lausanne.

Greifenhagen, C., & Lestuzzi, P. (2005). Static cyclic tests on lightly reinforced concrete shear walls. *Engineering Structures*, *27*(11), 1703–1712. doi:10.1016/j.engstruct.2005.06.008

Greifenhagen, C., Papas, D., & Lestuzzi, P. (2005). *Static-cyclic tests on reinforced concrete shear walls with low reinforcement ratios - Experimental Report*. *IMAC - Applied Computing and Mechanics Laboratory, Publication N4, École Polytechnique Fédérale de Lausanne* (p. 113).

Guedes, J., & Pinto, A. V. (1997). A numerical model for shear dominated bridge piers. In *2nd Italy-Japan Workshop on Seismic Design and Retrofit of Bridges*. Tsukuba, Japan.

Hagsten, L. G., Hestbech, L., & Fisker, J. (2011). Energiprincipper - del 3: Betonkonstruktioner, Teori, Lecture Notes.

Hannewald, P. (2013). *Seismic Behavior of Poorly Detailed RC Bridge Piers*. PhD thesis, Ecole Polytechnique Fédérale de Lausanne, Switzerland.

Hebdo (2007). Les glorieuses années 50. http://www.hebdo.ch/architecture_les_glorieuses_anneacutees_24899_.html

Hines, E. M. (2002). *Seismic Performance of Hollow Rectangular Reinforced Concrete Bridge Piers with Confined Corner Elements*. *University of California*.

Hines, E. M., Restrepo, J. I., & Seible, F. (2004). Force-displacement characterization of well-confined bridge piers. *ACI Structural Journal*, *101*(4), 537–548.

Ile, N., & Reynouard, J. M. (2005). Behaviour of U-shaped walls subjected to uniaxial and biaxial cyclic lateral loading. *Journal of Earthquake Engineering*, *9*(1), 67–94.

Imran, I., & Pantazopoulou, S. J. (1997). Experimental Study of Plain Concrete under Triaxial Stress. *ACI Structural Journal*, *93*(6), 589–601.

Kazaz, Í., Gulkan, P., & Yakut, A. (2012). Deformation limits for structural walls with confined boundaries. *Earthquake Spectra*, *28*(3), 1019–1046.

Kreslin, M., Fajfar, P. (2012). The extended N2 method considering higher mode effects in both plan and elevation. *Bulletin of Earthquake Engineering* 10:695-715.

Kölz, E., Schneider J. (2005). Beurteilung der Erdbebensicherheit bestehender Gebäude – der risikobasierte Ansatz des Schweizer Merkblatts SIA 2018. *Bautechnik* 82:8

Kowalsky, M. J. (2000). Deformation limit states for circular reinforced concrete bridge columns. *Journal of Structural Engineering*, *126*(8), 869–878.

Légeron, F., & Paultre, P. (2003). Uniaxial confinement model for normal- and high-strength concrete columns. *Journal of Structural Engineering*, *129*(2), 241–252.

Lodhi, M. S., & Sezen, H. (2012). Estimation of monotonic behavior of reinforced concrete columns considering shear-flexure-axial load interaction. *Earthquake Engineering and Structural Dynamics*. doi:10.1002/eqe

Lu, Y., & Panagiotou, M. (2012). *Three-dimensional nonlinear cyclic beam-truss model for non-planar reinforced concrete walls*. *Report No. UCB/SEMM-2012/01, Department of Civil and Environmental Engineering, University of California, Berkeley* (pp. 1–43).

Lu, Y., & Panagiotou, M. (2014). Three-dimensional cyclic beam-truss model for nonplanar reinforced concrete walls. *Journal of Structural Engineering*, *140*(3), 1–11. doi:10.1061/(ASCE)ST.1943-541X.0000852.

Mackie, K., & Stojadinovic, B. (2001). Seismic demands for performance-based design of bridges. In *PEER Annual Meeting*.

Mander, J. B., Priestley, M. J. N., & Park, R. (1988). Theoretical Stress-Strain Model for Confined Concrete. *Journal of Structural Engineering*, *114*(8), 1804–1826.

Marchand, B., Savoyat, M., Chenu, L., Girard, J.-C., Teysseire, E., & Buren, C. von. (2012). *Architecture du Canton de Vaud 1920-1975*. *Presses Polytechniques et Universitaires Romandes* (p. 419).

Marini, A., & Spacone, E. (2007). Analysis of reinforced concrete elements including shear effects. *ACI Structural Journal*, *103*(5), 645–655.

Martinelli, L. (2002). Numerical simulation of cyclic tests of R/C shear walls. In *12th European Conference on Earthquake Engineering* (Vol. 180). London, United Kingdom.

Mazars, J., Kotronis, P., Ragueneau, F., & Casaux, G. (2006). Using multifiber beams to account for shear and torsion. *Computer Methods in Applied Mechanics and Engineering*, *195*(52), 7264–7281. doi:10.1016/j.cma.2005.05.053

Menegotto, M., & Pinto, P. E. (1973). Method of analysis for cyclically loaded RC plane frames including changes in geometry and non-elastic behaviour of elements under combined normal force and bending. In *IABSE Symposium on resistance and ultimate deformability of structures acted on by well defined repeated loads - Final Report*.

Mergos, P. E., & Beyer, K. (2013). Modelling shear-flexure interaction in equivalent frame models of slender reinforced concrete walls. *The Structural Design of Tall and Special Buildings*. doi:10.1002/tal

Miki, T., & Niwa, J. (2004). Nonlinear analysis of RC structural members using 3D lattice model. *Journal of Advanced Concrete Technology*, *2*(3), 343–358. doi:10.3151/jact.2.343

Miranda, P. A., Calvi, G. M., Pinho, R., & Priestley, M. J. N. (2005). *Displacement-based Assessment of RC Columns with Limited Shear Resistance*. *IUSS Press - Istituto Universitario di Studi Superiori di Pavia* (p. 153).

Navarro Gregori, J., Miguel Sosa, P., Fernández Prada, M. a., & Filippou, F. C. (2007). A 3D numerical model for reinforced and prestressed concrete elements subjected to combined axial, bending, shear and torsion loading. *Engineering Structures*, *29*(12), 3404–3419. doi:10.1016/j.engstruct.2007.09.001

NDI. (2009). Optotrak Certus HD, Northern Digital Inc. Waterloo, Ontario, Canada.

Neuenhofer, A., & Filippou, F. C. (1997). Evaluation of nonlinear frame finite-element models. *Journal of Structural Engineering*, *123*(7), 958–966.

OpenSees. (2013). Open System for Earthquake Engineering Simulation - Version 2.4.3.

Orakcal, K., Massone, L. M., & Wallace, J. W. (2006). *Analytical Modeling of Reinforced Concrete Walls for Predicting Flexural and Coupled Shear-Flexural Responses*. *Pacific Earthquake Engineering Research Center* (p. 213). Los Angeles, California.

Palermo, D., & Vecchio, F. J. (2007). Simulation of cyclically loaded concrete structures based on the finite-element method. *Journal of Structural Engineering*, *133*(5), 728–738. doi:10.1061/(ASCE)0733-9445(2007)133:5(728)

Pam, H. J., & Ho, J. C. M. (2009). Length of critical region for confinement steel in limited ductility high-strength reinforced concrete columns. *Engineering Structures*, *31*(12), 2896–2908. doi:10.1016/j.engstruct.2009.07.015

Park, R., & Paulay, T. (1975). *Reinforced Concrete Structures*. *John Wiley & Sons* (p. 769).

Paulay, T., & Priestley, M. J. N. (1992). *Seismic Design of Reinforced Concrete and Masonry Buildings*. *John Wiley & Sons* (p. 744).

Paulay, T., & Priestley, M. J. N. (1993). Stability of ductile structural walls. *ACI Structural Journal*, *90*(4), 385–392.

Peter, B. K. (2000). *Erdbeden-Uberprufung bestehender Stahlbeton-Gebaude*. *École Polytechnique Fedérale de Lausanne - Département de Génie Civil*. École Polytechnique Fedérale de Lausanne.

Petrangeli, M. (1996). *Modelli numerici per strutture monodimensionali in cemento armato*. *PhD Thesis*. Università di Roma "La Sapienza."

Petrangeli, M., Pinto, P. E., & Ciampi, V. (1999). Fiber element for cyclic bending and shear of RC structures. I: Theory. *Journal of Engineering Mechanics*, *125*(9), 994–1001.

Popovics, S. (1973). A numerical approach to the complete stress-strain curve of concrete. *Cement and Concrete Research*, *3*(5), 583–599. doi:10.1016/0008-8846(73)90096-3

Priestley, M. J. N., Calvi, G. M., & Kowalsky, M. J. (2007). *Displacement-based Seismic Design of Structures*. *IUSS Press* (p. 721).

Priestley, M. J. N., Seible, F., & Calvi, G. M. (1996). *Seismic Design and Retrofit of Bridges*. *John Wiley & Sons* (p. 686).

Pugh, J. S., Lowes, L. N., & Lehman, D. E. (2014). Seismic design of concrete walled buildings. In *Second European Conference on Earthquake Engineering and Seismology*. Istanbul.

Ranzo, G., & Petrangeli, M. (1998). A fibre finite beam element with section shear modelling for seismic analysis of RC structures. *Journal of Earthquake Engineering*, *2*(3), 443–473.

Remino, M. (2004). *Starrylink Editrice Collana Tesi e Ricerca*. *PhD Thesis*. Università degli Studi di Brescia.

Richart, F. E., Brandtzaeg, A., & Brown, R. L. (1928). A study of the failure of concrete under combined compressive stresses. *University of Illinois Bulletin*, *XXVI*(12).

Romão, X., Delgado, R., & Costa, A. (2010). Practical aspects of demand and capacity evaluation of RC members in the context of EC8-3. *Earthquake Engineering and Structural Dynamics*, *39*, 473–499. doi:10.1002/eqe

Samani, A. K., & Attard, M. M. (2012). A stress–strain model for uniaxial and confined concrete under compression. *Engineering Structures*, *41*, 335–349. doi:10.1016/j.engstruct.2012.03.027

Scott, M. H., & Fenves, G. L. (2006). Plastic Hinge Integration Methods for Force-Based Beam-Column Elements. *Journal of Structural Engineering*, *132*(2), 244–252. doi:10.1061/(ASCE)0733-9445(2006)132:2(244)

SEAOC. (1959). *Recommended Lateral Force Requirements and Commentary*. *Seismology Committee, Structural Engineers Association of California* (First.).

SEAOC. (1980). *Recommended Lateral Force Requirements and Commentary*. *Seismology Committee, Structural Engineers Association of California* (Fourth.).

SEAOC. (1995). *Vision 2000 - Performance based seismic engineering of buildings*. *Structural Engineers Association of California*. Sacramento, California, USA.

SeismoSoft. (2013). SeismoStruct - A Computer Program for Static and Dynamic Nonlinear Analysis of Framed Structures.

Sheikh, S. A., & Uzumeri, S. M. (1982). Analytical model for concrete confinement in tied columns. *Journal of the Structural Division*, *108*(ST12), 2703–2722.

SIA (2003). Actions on structures. *Structural design standard SN 505 261*, Swiss Society of Engineers and Architects, Zürich, Switzerland.

SIA 261 (2004) Concrete structures. *Structural design standard SN 505 262*, Swiss Society of Engineers and Architects, Zürich, Switzerland.

SIA 269/8 (2014) Existing structures – earthquakes. *Pre-standard prSN 505 269/8*, Swiss Society of Engineers and Architects, Zürich, Switzerland.

Sittipunt, C., & Wood, S. L. (1993). *Finite Element Analysis of Reinforced Concrete Shear Walls*. *Department of Civil Engineering, University of Illinois at Urbana-Champaign* (p. 404). Urbana, Illinois.

Sritharan, S., Beyer, K., Henry, R. S., Chai, Y. H., Kowalsky, M., & Bull, D. (2014). Understanding poor seismic performance of concrete walls and design implications. *Earthquake Spectra*, *30*(1), 307–334. doi:10.1193/021713EQS036M

Steinmann, G. A. (1974). Bâtiments élevés en béton. *Bulletin Technique de La Suisse Romande*, *100*(2 (Special)), 88–103.

Vecchio, F. J. (2000). Disturbed stress field model for reinforced concrete: Formulation. *Journal of Structural Engineering*, *126*(9), 1070–1489.

Vecchio, F. J., & Collins, M. P. (1986). The modified compression-field theory for reinforced concrete elements subjected to shear. *ACI Journal*, *83*(2), 219–231.

Wenk, T. (2008). *Erbebenertüchtigung von Bauwerken*. *Bundesamt für Umwelt (BAFU), Switzerland*.

Wenk, T. (2014). Seismic assessment based on cost-benefit analysis. *Proceedings of the 2nd European Conference on Earthquake Engineering and Seismology*, Istanbul, Turkey.

Wenk, T., Beyer, K. (2014). Seismic conservation strategies for cultural heritage buildings in Switzerland. *Proceedings of the 2nd European Conference on Earthquake Engineering and Seismology*, Istanbul, Turkey.

Whittaker, A., Deierlein, G. G., Hooper, J., & Merovich, A. (2004). *ATC-58 Project Task Report: Engineering Demand Parameters for Structural Framing Systems*. *Applied Technology Council*.

Willam, K. J., & Warnke, E. P. (1974). Constitutive model for the triaxial behaviour of concrete. In *Seminar on "Concrete Structures Subjected fo Triaxial Stresses."* Bergamo, Italy.

Wong, P. S., Vecchio, F. J., & Trommels, H. (2013). *VecTor2 & FormWorks User's Manual*. *University of Toronto, Department of Civil Engineering* (p. 318).

Wong, P. S., Vecchio, F. J., & Trommels, H. (2014). VecTor2 - Nonlinear Analysis of Two-Dimensional Reinforced Concrete Membrane Structures.

Xu, S., & Zhang, J. (2011). Hysteretic shear–flexure interaction model of reinforced concrete columns for seismic response assessment of bridges. *Earthquake Engineering and Structural Dynamics*, *40*(3), 315–337. doi:10.1002/eqe

Yazgan, U., & Dazio, A. (2011). Simulating maximum and residual displacements of RC structures: I. Accuracy. *Earthquake Spectra*, *27*(4), 1187–1202. doi:10.1193/1.3650479

Zhang, J., Xu, S., & Tang, Y. (2011). Inelastic displacement demand of bridge columns considering shear – flexure interaction. *Earthquake Engineering and Structural Dynamics*, *40*, 731–748. doi:10.1002/eqe